Dissertation zur Erlangung des Doktorgrades

der Fakultät für Chemie und Pharmazie

der Ludwig-Maximilians-Universität München

Principles of RNA and Protein Quality Control at the Eukaryotic Ribosome

Timm Frank Nikolaus Hassemer

aus

Mainz

2017

Erklärung

Diese Dissertation wurde im Sinne von § 7 der Promotionsordnung vom 28. November 2011 von Herrn Prof. Dr. Franz-Ulrich Hartl betreut.

Eidesstattliche Versicherung

Diese Dissertation wurde eigenständig und ohne unerlaubte Hilfe erarbeitet.

München, den 18.08.2017

_____

Timm Hassemer

Dissertation eingereicht am: 18.08.2017

1. Gutachter: Prof. Dr. Franz-Ulrich Hartl

2. Gutachter: PD Dr. Dietmar Martin

Mündliche Prüfung am: 22.11.2017

Acknowledgements

First of all, I would like to thank Prof. Franz-Ulrich Hartl for the opportunity to conduct my PhD thesis in his research group at the Max Planck Institute of Biochemistry. The work described in this thesis would have not been possible without his invaluable scientific expertise, his experience, and his guidance in the last four years.

I am also very grateful to Dr. Sae-Hun Park and Dr. Young-Jun Choe for introducing me to yeast cell biology and countless biochemical methods. The quality of the results obtained during the course of my studies has benefited greatly from their scientific experience and support.

Furthermore, I would like to thank all members of the Hartl department for their support and the friendly and open-minded atmosphere in the lab, which always allowed for sophisticated discussions and mutual support.

I especially want to thank Emmanuel Burghardt, Albert Ries, Nadine Wischnewski, Anastasia Jungclaus and Romy Lange for their invaluable technical support, and Evelin Frey-Royston and Darija Pompino for their administrative support.

I am also very grateful to Dr. Roman Koerner for introducing me to proteomics and for measuring and analyzing countless samples.

I want to thank the member of my PhD committee PD Dr. Dietmar Martin for evaluating this thesis.

I would like to address special thanks to Dr. Thomas Hauser, Dr. Amit Gupta, Dr. Christian Loew, Dr. Tobias Neudegger, Dr. Robert Wilson, Leonhard Popilka, Dr. David Balchin, Dr. Gabriel Thieulin-Pardo, Martin Mueller and Michael Gropp for their friendship and support in the last four years.

Finally, my biggest thanks go to my parents and my sister. Without their unconditional love and support, it would have never been possible for me to achieve this goal. I am deeply grateful that you were always believing in me.

Table of contents

Summary

The translation of a messenger RNA (mRNA) into a polypeptide chain is a complex and tightly regulated process that requires the concerted action of a plethora of factors at the ribosome. Failure of this process, e.g. due to translation of damaged transcripts or insufficient translational fidelity, can result in inhibition of translation elongation or termination, an aberrant condition known as ribosomal stalling. This situation is further aggravated by the fact that erroneous translation leads to the production of faulty nascent polypeptides, which pose a serious threat to cellular protein homeostasis (proteostasis) as they typically lack function and tend to form potentially toxic aggregates. Thus, organisms from all kingdoms of life have evolved mechanisms to maximize translational fidelity, to recognize and rescue stalled ribosomes, and to rapidly degrade faulty mRNAs and their translation products.

In eukaryotes, the ribosomal quality control (RQC) complex recognizes 60S-peptidyl-tRNA complexes, an aberrant species generated by noncanonical splitting of stalled ribosomes. Following recognition of an exposed tRNA moiety in the ribosomal P-site by Rqc2p, recruitment of the RING E3 ubiquitin ligase Ltn1p to the 60S subunit allows for ubiquitination of the aberrant polypeptide. After extraction of the nascent chain by Cdc48p in an ATP-dependent manner, the polypeptide is targeted for proteasomal degradation. Failure of this process has been linked to neurodegeneration in mice. However, the cellular mechanisms underlying this phenotype remain unclear.

In this study, we systematically investigated the effects of RQC impairment on the proteostasis network in the baker's yeast *Saccharomyces cerevisiae* using a wide array of biochemical methods and recombinant reporter constructs. We found that deletion of *LTN1* leads to the formation of detergent-insoluble aggregates that sequester various key proteostasis factors, thus impairing general protein quality control mechanisms and exerting proteotoxic stress. We were also able to show that protein aggregation depends on an unexpected, Rqc2p-mediated modification of the nascent chain. Moreover, we could provide evidence that the ribosome

provides a central hub at which RNA and protein quality control pathways tightly cooperate in order to maintain proteostasis. Finally, we were able to propose a mechanism for aggregate formation and to identify several potential endogenous faulty polypeptide chains.

Our study not only provides novel insights into the molecular mechanisms of protein aggregation *in vivo*, but also suggests an explanation for pathological conditions such as neurodegeneration observed upon failure of the proteostasis network. These findings could help in understanding various incurable diseases that have been linked to protein aggregation and proteostasis imbalance. Moreover, due to the continuous increase in life expectancy during the last century, the importance of ageing as a risk factor for proteostasis imbalance has greatly increased, underlining the need to find ways to stop or at least delay the progressive decline of proteostasis network capacity. Our results might aid in finding novel therapeutic approaches that counteract the deleterious effects of disease-related proteostasis imbalance and help to preserve proteome integrity even at an advanced age.

I. Introduction

I.1 Protein folding and molecular chaperones

Proteins (from Greek "*proteios*", meaning "primary" or "of the first order") form the most versatile group of biomacromolecules and play an essential role in almost every cellular process. They are synthesized as linear chains of amino acids that are connected to each other via a peptide bond. The formation of this peptide bond is catalyzed by ribosomes, large assemblies of protein and RNA that read the nucleotide sequence of an input messenger RNA (mRNA) and translate this information into an amino acid sequence. As it emerges from the ribosome, the resulting nascent polypeptide chain needs to fold into a unique, three-dimensional structure in order to yield a functional protein (Dobson, Šali *et al.* 1998). The state under which a protein is functional is defined as its native fold and generally represents a thermodynamically stable condition, i.e. a state where it has a minimum of free energy (Anfinsen 1972). Anfinsen's experiments with ribonuclease A (RNase A), a small protein that can fold spontaneously *in vitro*, showed that all information that is necessary for a protein to fold into its native state is encoded in its primary structure, i.e. its amino acid sequence (Anfinsen 1972, Anfinsen 1973). Based on these results, it was suggested that the folding process is mainly driven by the sum of interactions between amino acid side chains and the polypeptide backbone. Hydrophobic side chains tend to collapse into a core region inside the folding protein, with hydrophilic residues exposed to the aqueous environment of the cell, a phenomenon called the hydrophobic effect (Dill, Bromberg *et al.* 1995, Daggett and Fersht 2003). This mechanism works well for polypeptides consisting of up to 100 amino acids, which can fold into their native state spontaneously within milliseconds and to full yield (Brockwell and Radford 2007); for larger proteins, however, the folding process is intrinsically error-prone. Since more than 90 % of the eukaryotic proteome consists of proteins longer than 100 amino acids, cells invest considerable resources in order to ensure productive protein folding (Balchin, Hayer-Hartl *et al.* 2016).

How do proteins ultimately find their native state? If we assume that a newly synthesized polypeptide chain randomly samples all possible conformations until it finds its native fold, then a small protein consisting of 100 amino acids would need more than 10^{70} years to fold, even if sampling would occur at picosecond rates; most proteins of that size, however, fold within milliseconds, a contradiction referred to as "Levinthal's Paradox". To resolve this paradox, it has been suggested that protein folding does not occur in a random manner, but by following defined pathways consisting of folding intermediates, thereby reducing the folding time to physiological timescales (Dill and Chan 1997). This model was later refined by the introduction of a rugged "folding funnel" concept (Fig. I.1), which accounts for the fact that progressive folding and burial of hydrophobic residues in folding intermediates further restrict the number of possible conformations (Dinner, Sali *et al.* 2000). In addition, this model is able to explain the slow or unproductive spontaneous folding of some large proteins: while navigating the free energy landscape, the folding polypeptide chain might encounter kinetic barriers and transiently populate partially folded or even misfolded states that correspond to local minima of free energy (Fig. I.1, green area). A hallmark of these kinetically trapped species is the exposure of "sticky", hydrophobic patches that would otherwise be buried inside the native protein structure due to the hydrophobic effect. Since a polypeptide chain can spend a considerable amount of time in such a partially folded state, kinetically trapped folding intermediates are especially vulnerable to unwanted intermolecular interactions that might result in the formation of potentially toxic oligomers, amorphous aggregates or amyloid fibrils (Jahn and Radford 2005, Hartl and Hayer-Hartl 2009) (Fig. I.1, red area).

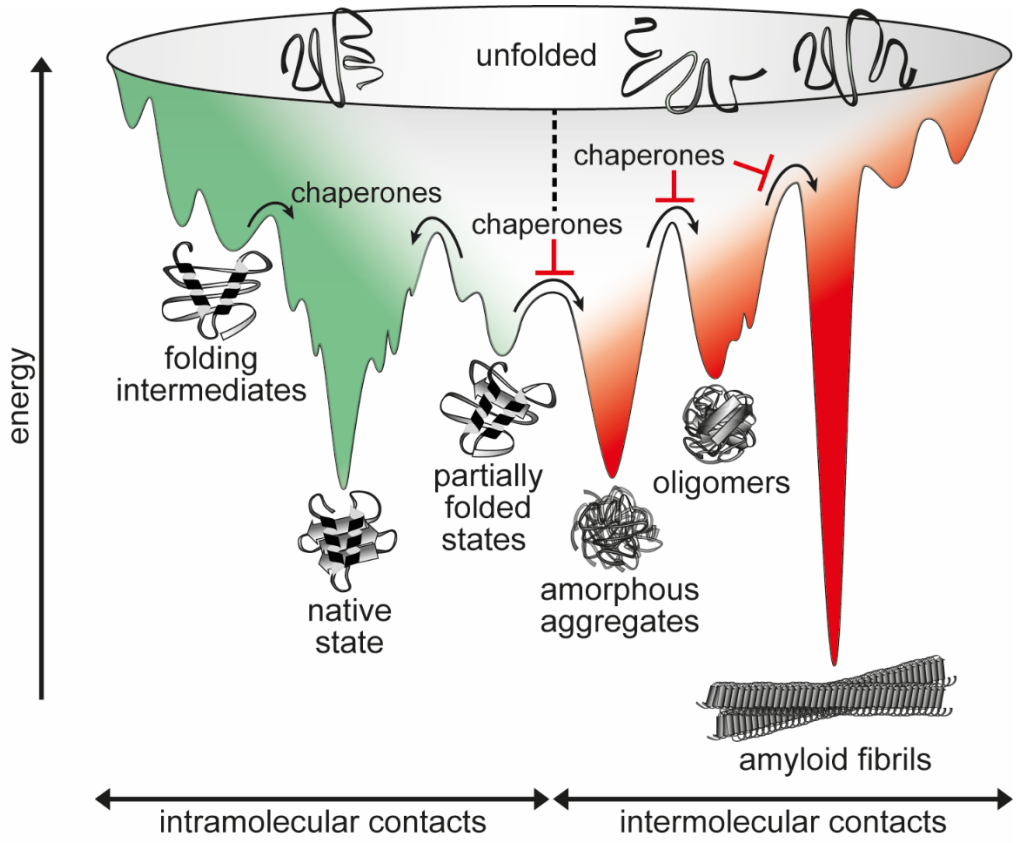

Fig. I.1: The rugged protein folding funnel concept. On their way down the free energy landscape, unfolded proteins sample various conformations such as folding intermediates or partially folded states until they finally reach their thermodynamically favored native state, a process that is driven by intramolecular interactions (green area). Partially folded states might correspond to local minima of free energy, leading to protein molecules being kinetically trapped and prone to aberrant intermolecular interactions, resulting in the formation of potentially toxic oligomers, aggregates or highly stable amyloid fibrils (red area). Molecular chaperones help in guiding protein molecules along a productive folding pathway by both reducing kinetic energy barriers and preventing unwanted intermolecular interactions. Figure adapted from (Balchin, Hayer-Hartl *et al.* 2016).

To overcome the energy barriers of kinetically trapped folding intermediates, cells have evolved a broad arsenal of molecular chaperones: highly conserved proteins that interact with the non-native states of other proteins, stabilize them, and help them to acquire their native state without being present in their final structure (Hartl 1996). Chaperones assist in protein folding by binding to newly synthesized polypeptide chains as well as to partially folded or misfolded states, thereby preventing aggregation and promoting both *de novo* protein folding and refolding

events. In addition, chaperones participate in the dissociation of protein aggregates and clearance of terminally misfolded proteins by cooperating with the proteasomal and autophagosomal degradation machinery (Fig. I.2) (Gamerdinger, Hajieva *et al.* 2009, Ciechanover and Kwon 2015, Mogk, Kummer *et al.* 2015).

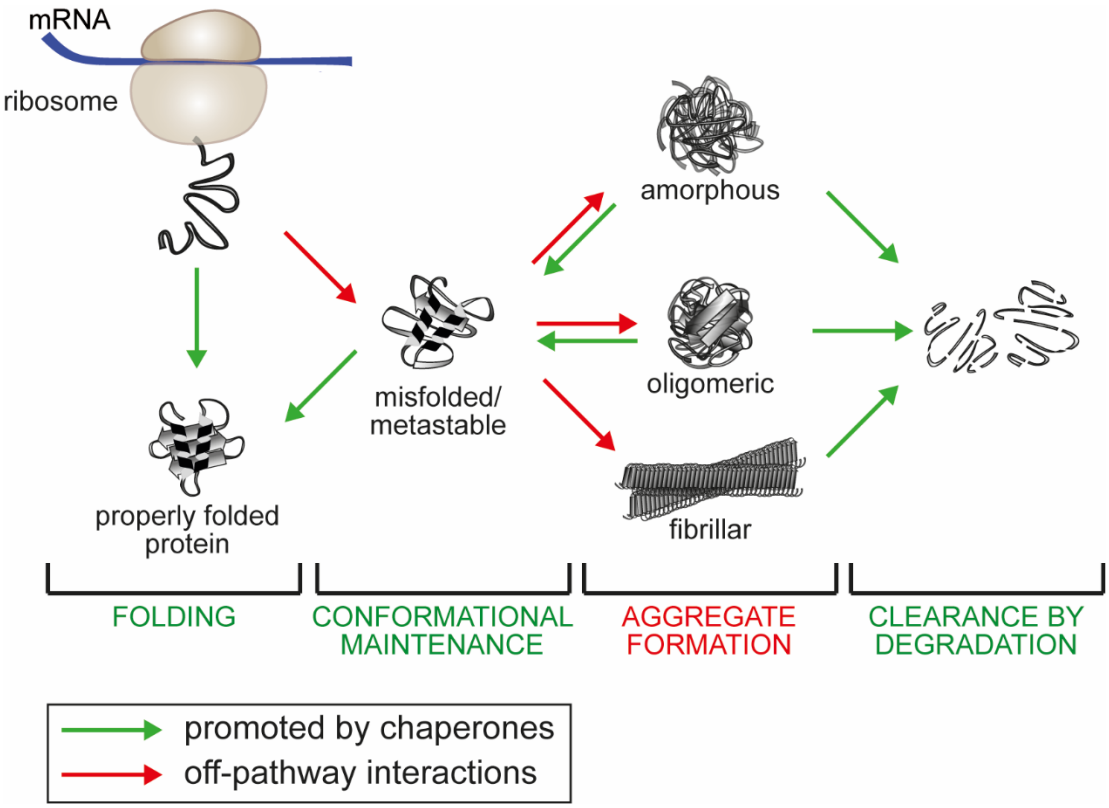

Fig. I.2: The roles of molecular chaperones in protein folding. Chaperones assist in protein folding by binding to newly synthesized polypeptide chains, to partially folded or misfolded states and to protein aggregates, thereby preventing their participation in unwanted off-pathway interactions and promoting both *de novo* folding and refolding events. Chaperones also cooperate with the cellular degradation machinery in order to target aberrant protein species for proteasomal or autophagosomal degradation. Figure adapted from (Balchin, Hayer-Hartl *et al.* 2016).

A subset of chaperones is usually referred to as "Heat Shock Proteins" (Hsps), because they were found to be strongly upregulated during conditions of conformational stress, e.g. heat stress. They are usually classified into six evolutionary conserved groups according to their

molecular weight: Hsp40s, Hsp60s, Hsp70s, Hsp90s, Hsp100s and the small Hsps. Small Hsps are almost exclusively stress-induced, and work as ATP-independent "holdases" that prevent aggregation by transiently binding to non-native protein species. In contrast, the members of the other chaperone families can be either constitutively expressed or stress-inducible, are ATP-dependent and participate more actively in the folding process as so-called "foldases" (Vabulas, Raychaudhuri *et al.* 2010, Kim, Hipp *et al.* 2013, Treweek, Meehan *et al.* 2015).

I.2 Protein aggregation *in vivo*

Folding of proteins *in vivo* differs substantially from the isolated and dilute *in vitro* conditions in which protein folding is studied. Due to the extremely high concentration of macromolecules such as proteins, carbohydrates and nucleic acids in the cell (up to 300-400 mg/mL total protein in the cytosol), the effective space in which a newly synthesized polypeptide chain can move and fold is greatly reduced, a phenomenon called macromolecular crowding, or the excluded volume effect (Ellis 2001, Ellis and Minton 2006). This crowding effect leads to extremely high effective concentrations of unfolded polypeptide chains, a condition which in turn promotes aberrant intermolecular interactions and therefore aggregation (Ellis and Minton 2006). This situation is further aggravated by the fact that translation, with an incorporation rate of only 4-20 amino acids per second, is a rather slow process. Folding cannot occur until the complete polypeptide chain (or at least a domain) has been synthesized, leaving the unfolded nascent chain exposed to the crowded cellular environment for up to several minutes in the case of a medium-sized protein (Etchells and Hartl 2004, Lu and Deutsch 2005). This leaves enough time for exposed hydrophobic patches to participate in unproductive intermolecular interactions, thereby further promoting aggregation of nascent polypeptides. In addition, protein aggregation *in vivo* can also be the result of stress-induced unfolding, or mutations that affect protein stability.

Protein aggregation has been linked to numerous progressive and late-onset neurodegenerative disorders including Huntington's disease (aggregated huntingtin protein), Alzheimer's disease (Aβ and tau protein), Parkinson's disease (α-synuclein), amyotrophic lateral sclerosis (TDP-43, FUS and SOD1) and Creutzfeldt-Jakob disease (prion protein). A hallmark of these diseases is the age-dependent accumulation of the respective protein in a non-native state and, subsequently, the formation of amyloid-like fibrils that form visible intra- or extracellular inclusions especially in the brain (Dobson 1999, Bucciantini, Calloni *et al.* 2004). Strikingly, despite having completely different chemical properties and functions in the cell, these proteins form highly stable amyloid fibrils consisting of β-sheet structures running perpendicular to the fibril axis, probably due to the fact that this state represents a thermodynamically favored condition for proteins that cannot fold into their native structure (Fandrich and Dobson 2002). Thus, the ability to form amyloid fibrils has been recognized as a generic feature of proteins, and extensive studies on the mechanism of fibril formation have been carried out using model proteins such as lysozyme or polyQ proteins (Booth, Sunde *et al.* 1997, Scherzinger, Lurz *et al.* 1997). A generic feature of fibril formation seems to be the thermodynamically unfavored, nonspecific oligomerization of partially unfolded or misfolded proteins. These soluble oligomers can serve as "aggregation nuclei" for the formation of protofilaments, which then rapidly assemble into fibrillary structures and form visible aggregate deposits (Buell, Dobson *et al.* 2014, Knowles, Vendruscolo *et al.* 2014). Since the occurrence of visible deposits in patients has been historically associated with disease, it was reasoned that amyloid fibrils have a cytotoxic effect on the cell. More recent studies, however, indicate that soluble oligomers might be the cytotoxic species due to their exposure of hydrophobic patches: in fact, the formation of amyloid fibrils and their storage in extracellular deposits might have a cytoprotective role (Arrasate, Mitra *et al.* 2004).

The toxicity of protein aggregation *in vivo* can be explained by two theories: the loss-of-function theory, which assumes that aggregation leads to depletion of functional protein and failure of essential cellular processes, and the gain-of-toxicity theory, which reasons that exposure of hydrophobic patches on the surface of protein aggregates leads to unwanted interactions with functional or newly synthesized polypeptides, or with cellular membranes. Oligomeric

aggregates provide a "sticky" surface due to the exposure of hydrophobic patches and unpaired β-strands, and can therefore participate in aberrant intermolecular interactions with newly synthesized polypeptides or metastable proteins. In fact, several studies have shown that common patterns of aggregation-mediated cytotoxicity are the sequestration of essential chaperones from the cytosol and interference with RNA homeostasis (Olzscha, Schermann *et al.* 2011, Park, Kukushkin *et al.* 2013, Choe, Park *et al.* 2016, Woerner, Frottin *et al.* 2016).

Cells have evolved numerous mechanisms to protect themselves from the deleterious effects of protein aggregation. First, chemical parameters such as pH, temperature and macromolecule concentration are tightly regulated in order to ensure an optimal environment for proteins to rapidly reach and maintain their native state. Second, evolution has optimized the primary structure of proteins to favor folding over aggregation, for example by avoiding the repetition of motifs that promote formation of β-strands (Dobson 2004, DePristo, Weinreich *et al.* 2005). Third, cells have developed an extensive network of chaperones and other factors that monitor protein synthesis, target aberrant polypeptides for degradation, and actively promote both *de novo* folding of newly synthesized proteins and refolding of misfolded polypeptides. Furthermore, chaperones interfere at different steps of the aggregation process and actively promote disaggregation, thereby preventing or at least slowing down the formation of amyloid fibrils (Schaffar, Breuer *et al.* 2004, Knowles, Waudby *et al.* 2009, Cohen, Arosio *et al.* 2015).

I.3 The protein homeostasis network

A healthy and intact proteome is an absolute prerequisite for the survival of any living structure from a single cell to a complex multicellular organism. Protein homeostasis ("proteostasis") is defined as a state in which there is a tightly regulated equilibrium between protein synthesis and degradation. The corresponding concept of the "proteostasis network" describes an integrated network of quality control factors that ensures proteome integrity by maintaining this

equilibrium (Balch, Morimoto *et al.* 2008). This complex network includes the cellular chaperone machinery as well as the ubiquitin-proteasome system (UPS) and components of the autophagy pathway. Its main tasks are to preserve the balance between protein synthesis and degradation, to recognize and remove misfolded or aggregated proteins, and to respond to external or endogenous stressors (Powers, Morimoto *et al.* 2009, Brehme, Voisine *et al.* 2014, Hipp, Park *et al.* 2014). A decline in proteostasis network capacity has been linked to a variety of protein folding and aggregation-related diseases as well as to the process of aging, with increasing proteostasis imbalance being both the result and cause of this decline (Taylor and Dillin 2011, Labbadia and Morimoto 2015) (Fig. I.3).

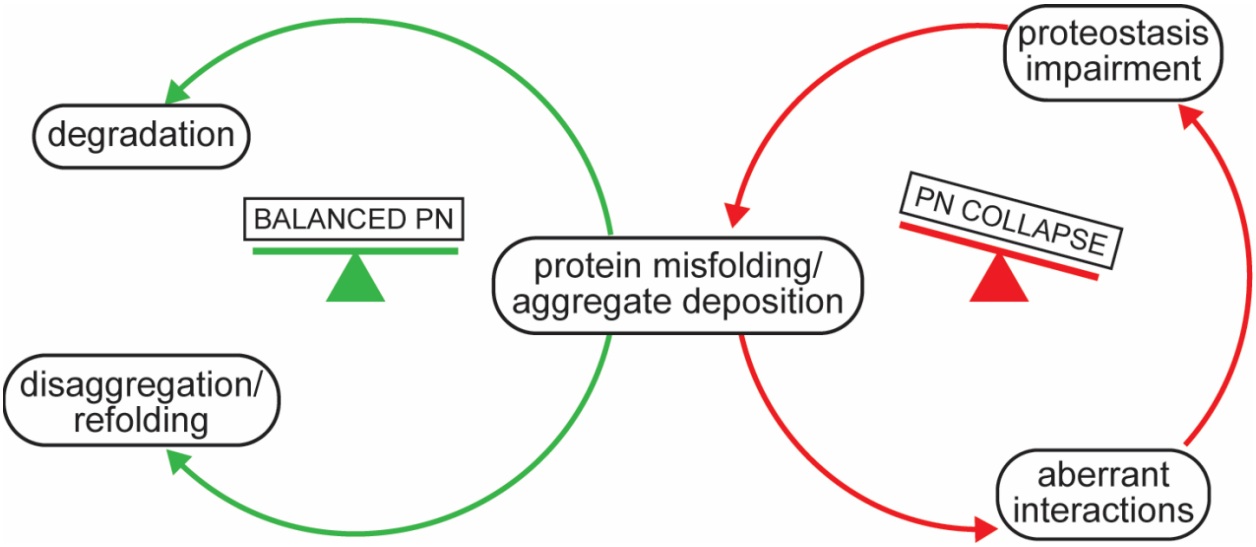

Fig. I.3: The cellular responses to protein misfolding under balanced versus imbalanced PN conditions. A healthy cell copes with aberrant protein species by the induction of PN factors that ultimately lead to their degradation or refolding (green arrows). Conversely, a collapsed PN leads to the accumulation of even more misfolded proteins participating in unwanted intermolecular interactions, thereby inducing a vicious cycle that ultimately results in cell death (red arrows). Figure adapted from (Balchin, Hayer-Hartl *et al.* 2016).

I.3.1 Protein synthesis and folding in the cytosol

The productive folding of newly synthesized proteins is crucial for a healthy proteome. Hence, quality control mechanisms have evolved that monitor proteome integrity already at the level of translation. Protein translation is slow compared to folding, suggesting that folding can occur cotranslationally. Except for α-helices and some small domains that can fold inside the exit tunnel, the C-terminal 30-40 amino acids of the nascent chain are largely excluded from intramolecular interactions due to the architecture of the ribosomal exit channel (approximately 100 Å long and 10-20 Å wide) (Wilson and Beckmann 2011, Balchin, Hayer-Hartl *et al.* 2016). This makes *de novo* folding of the nascent polypeptide especially challenging, as the sequence information that can be used for proper folding is continuously changing and incomplete until the end of translation. Recent studies, however, have shown that the expanded vestibule at the very end of the ribosomal exit tunnel might provide enough space for very small proteins or domains of up to 70 amino acids to reach their native structure or to fold almost to completion before release of the nascent chain from the ribosome (O'Brien, Christodoulou *et al.* 2011, Nilsson, Hedman *et al.* 2015). In addition, the ribosome itself might actively modulate protein folding by surface effects and by translational pausing, allowing the nascent chain to explore local conformations and to fold into initial subdomain structures that can assemble into larger domains upon nascent chain release (Kaiser, Goldman *et al.* 2011, O'Brien, Christodoulou *et al.* 2011). Finally, it has also been shown that the distance between nascent polypeptide chains emerging from ribosomes is maximized by the arrangement of translating polyribosomes, thereby minimizing the chance of unwanted intermolecular contacts (Brandt, Carlson *et al.* 2010).

Besides the active and passive roles of the translating ribosome in protein folding, cells have also evolved a subset of ribosome-associated chaperones that shield nascent chains from unwanted intra- or intermolecular interactions and to prevent protein misfolding and aggregation. In bacteria, the chaperone trigger factor (TF) binds in close proximity to the ribosomal exit channel and interacts with hydrophobic residues of the nascent chain, thereby preventing premature chain collapse and preparing the nascent polypeptide for interactions with the downstream Hsp70/40 systems (Kaiser, Chang *et al.* 2006, Kim, Hipp *et al.* 2013). In eukaryotes,

two systems have evolved that play a role similar to that of TF in protein folding: the ribosome-associated complex that interacts with the Hsp70 Ssb (RAC-Ssb) and the nascent chain-associated complex (NAC). The yeast RAC consists of the Hsp70 Ssz1 and its cochaperone, the Hsp40 Zuotin, and cooperates with the ribosome-binding Hsp70s, Ssb1 and Ssb2. NAC is a heterodimeric complex that is highly conserved from yeast to mammals and is required for intracellular protein sorting (del Alamo, Hogan *et al.* 2011, Preissler and Deuerling 2012, Willmund, Del Alamo *et al.* 2013). Newly synthesized proteins that cannot be folded by any of the ribosome-associated chaperone systems (more than 30 % of the proteome) are recognized by the cytosolic Hsp70 system. The C-terminal substrate binding domain of Hsp70 recognizes exposed hydrophobic stretches of five to seven amino acids of client proteins (Mayer 2013). Protein folding is then achieved by repeated, ATP-dependent cycles of substrate binding and release, thereby eliminating aberrant interactions between client residues, and allowing the substrate to explore alternative conformations (Sharma, De Los Rios *et al.* 2010). Hsp70 activity can be modulated by a variety of Hsp40 cochaperones that deliver substrates to Hsp70 and stimulate ATP hydrolysis, and Hsp110 nucleotide exchange factors that facilitate ADP release and binding of a new molecule of ATP (Mayer 2013, Zhuravleva and Gierasch 2015). At the same time, the Hsp70 system acts as a central hub that directs nascent chains to more specific chaperone systems such as the Hsp90 or Hsp60 systems (Hartl and Hayer-Hartl 2002, Calloni, Chen *et al.* 2012). In addition, the hexameric chaperone Prefoldin, which is present in archaea and eukaryotes, recognizes nascent polypeptides and facilitates transfer to the chaperonin TRiC/CCT (Hartl and Hayer-Hartl 2002).

The bacterial GroEL/GroES chaperonin system and its eukaryotic counterpart TRiC/CCT are large, cylindrical complexes with lid-shaped structures that allow a single unfolded polypeptide chain to undergo repeated, ATP-dependent cycles of folding in the isolated environment of their inner cavities (Leitner, Joachimiak *et al.* 2012, Lopez, Dalton *et al.* 2015, Hayer-Hartl, Bracher *et al.* 2016). Both bacterial and eukaryotic chaperonins are responsible for the folding of approximately 10 % of their respective proteomes, with GroEL mainly targeting aggregation-prone substrates of up to 60 kDa in size and TRiC being especially important for the

folding of cytoskeleton proteins such as actin and tubulin (Fujiwara, Ishihama *et al.* 2010, Gupta, Haldar *et al.* 2014, Lopez, Dalton *et al.* 2015, Hayer-Hartl, Bracher *et al.* 2016).

Besides its role in *de novo* folding of substrates, the Hsp90 system is responsible for the conformational maintenance of a number of clients involved in signaling pathways, for example kinases, transcription factors and steroid hormone receptors (Taipale, Krykbaeva *et al.* 2012, Röhl, Rohrberg *et al.* 2013). Strikingly, Hsp90 is able to recognize exposed hydrophobic patches of client proteins independent of their folding state and to stabilize the native state of metastable proteins such as the protooncogenic v-Src kinase, thereby explaining why inhibition of this chaperone system might be a promising target for cancer therapy (Boczek, Reefschläger *et al.* 2015, Karagöz and Rüdiger 2015). However, the precise mode of substrate recognition and client folding by Hsp90, remains largely unknown.

I.3.2 Degradation of proteins

A prerequisite for cells to maintain proteome integrity is a mechanism for the rapid and efficient clearance of aberrantly folded proteins and protein aggregates. Cells have evolved two major mechanisms for protein degradation: the ubiquitin proteasome system (UPS) and autophagy. Prerequisites for proteasomal degradation by the UPS are ubiquitination of the substrate by an E3 ubiquitin ligase, and delivery of the ubiquitinated polypeptide to the proteasome in a non-aggregated state (Finley 2009). To this end, cells have evolved a canonical pathway for ubiquitination that is conserved throughout all kingdoms of life. First, ubiquitin is activated by conjugation of its C-terminal carboxyl group to a cysteine residue of the E1 ubiquitin-activating enzyme in an ATP-dependent manner. In the second step, the activated ubiquitin is transferred to a cysteine residue of the E2 ubiquitin-conjugating enzyme. Finally, the E2-ubiquitin conjugate forms a ternary complex with a specific E3 ubiquitin ligase and the client protein, and an isopeptide bond is formed between the C-terminal carboxyl group of the ubiquitin moiety and the ε-amino group of a lysine residue of the client protein. Client proteins are usually marked for proteasomal degradation by conjugation with several ubiquitin molecules in a process called polyubiquitination, where the lysine residue K48 of ubiquitin serves as the ε-amino group donor

for the next round of ubiquitination (Hershko and Ciechanover 1992). Ubiquitination does not only target proteins for proteasomal degradation. Linkage through the lysine K63 of ubiquitin has been associated with lysosomal degradation, and modification with a single ubiquitin molecule on one or several lysine residues of the client protein may modulate its subcellular localization and activity rather than its stability (Polo, Sigismund *et al.* 2002, Flick, Ouni *et al.* 2004, Barriere, Nemes *et al.* 2007). Due to the sequential nature of the ubiquitination cascade, organisms evolved to possess only one or two E1 and up to 35 E2 enzymes, but a comparatively large set of E3 ligases (> 600 in mammals) that allows the ubiquitination system to target a broad array of substrate proteins with high specificity (Li, Bengtson *et al.* 2008). The cochaperone CHIP, which is also an E3 ligase, can bind to Hsc70 and Hsp90 and ubiquitinate their clients to target them for proteasomal degradation, thereby providing a link between the chaperone and UPS machineries (Kettern, Dreiseidler *et al.* 2010). Protein aggregates are first dissociated in an ATP-dependent manner either by the Hsp70 system or the Hsp100 disaggregase in bacteria and fungi, ubiquitinated by cytosolic E3 ligases (e.g. Ubr1p in yeast) and then delivered to the proteasome in a soluble state for degradation (Prakash and Matouschek 2004, Rampelt, Kirstein-Miles *et al.* 2012, Escusa-Toret, Vonk *et al.* 2013, Mogk, Kummer *et al.* 2015). Alternatively, misfolded substrates might also be transported to the nucleus in a chaperone-bound state, ubiquitinated by nuclear E3 ligases (e.g. San1p in yeast), and degraded by nuclear proteasomes (Amm, Sommer *et al.* 2014). Being a key player of the UPS, the 26S proteasome complex is located both in the cytosol and the nucleus, making the latter a compartment that is subject to protein quality control. In fact, several terminally misfolded proteins were described that are subject to proteasomal degradation and require chaperones for delivery to the nucleus (Heck, Cheung *et al.* 2010, Park, Kukushkin *et al.* 2013). The cellular disaggregase machinery, however, sometimes fails to dissociate protein aggregates, e.g. when the aggregate is too large in size or is in the extremely stable amyloid conformation. In this case, cells exploit the autophagy machinery to selectively degrade these aggregates. The E3 ligase CHIP recognizes and ubiquitinates aggregate structures that are bound to Hsp70. Subsequently, the Hsp70 cofactor Bag-3 mediates macroautophagy either via the autophagic ubiquitin adaptor p62 or in an ubiquitin-independent manner (Arndt, Dick *et al.* 2010, Gamerdinger, Kaya *et al.* 2011). Notably, cells promote concentration of aggregates in specific

compartments often termed "aggresomes" or "JUNQ" (JUxtaNuclear Quality control compartment), presumably to facilitate degradation and to keep aberrant proteins in a nontoxic state until degradation occurs (Kopito 2000, Kaganovich, Kopito *et al.* 2008, Sontag, Vonk *et al.* 2014). Finally, Hsp70 can also directly target its misfolded clients for lysosomal degradation by using the highly abundant KFERQ peptide motif as a signal sequence, a pathway called chaperone-mediated autophagy (CMA) (Arias and Cuervo 2011).

Besides the canonical UPS pathway for damaged or terminally misfolded proteins, a considerable number of newly synthesized nascent polypeptide chains are subject to cotranslational ubiquitination. Whereas earlier studies suggested that more than 30 % of newly synthesized nascent chains are ubiquitinated, more recent findings questioned the significance of ubiquitination at the ribosome for degradation and indicated a much lower number of 1-5 % (Schubert, Anton *et al.* 2000, Vabulas and Hartl 2005, Duttler, Pechmann *et al.* 2013). This might at least in part be due to the fact that translation is much faster than folding and that newly synthesized polypeptide chains are unable to fold until a complete domain has emerged from the ribosome, making nascent chains vulnerable to cellular quality control systems. However, the exact mechanisms and the importance of cotranslational ubiquitination *in vivo* remain largely unknown. Experiments with reporters with N-terminal ubiquitination signals have shown that the propensity of newly synthesized polypeptide chains to become ubiquitinated correlates with their size (Turner and Varshavsky 2000). Conversely, a mutant variant of actin that is unable to fold can only be ubiquitinated after release from the ribosome (Frydman and Hartl 1996). Furthermore, not all nascent chains are ubiquitinated to the same extent; instead, a small subset consisting of large, aggregation-prone polypeptides with high translation rates and inefficient spontaneous folding seems to be the preferential target of cotranslational ubiquitination (Duttler, Pechmann *et al.* 2013). Ribosome-associated chaperones such as NAC may counteract this quality control system by shielding newly synthesized nascent chains, thereby protecting them from ubiquitination (Duttler, Pechmann *et al.* 2013). The ribosomal quality control (RQC) pathway, which also involves cotranslational ubiquitination of nascent polypeptide chains, represents a

crucial pathway for the clearance of aberrant protein species and will be discussed in detail in section I.4.

I.3.3 The cellular stress response

All organisms need to adequately respond to exogenous and endogenous stressors in order to protect core biological processes such as DNA repair, protein folding, clearance of misfolded proteins and aggregation prevention, and ultimately to preserve proteome integrity. Examples of such stressors include elevated temperatures, nutrient starvation or the presence of toxic agents such as heavy metals or reactive oxygen species, all posing severe challenges to the proteostasis network as they can promote the accumulation of potentially toxic misfolded protein species. Cells have evolved several pathways, e.g. the cytosolic heat shock response (HSR) and the unfolded protein response (UPR) in organelles such as the endoplasmic reticulum (ER) and mitochondria, with the common goal of a rapid and robust upregulation of Hsps to prevent further protein damage (Morimoto 2008, Anckar and Sistonen 2011, Walter and Ron 2011, Schulz and Haynes 2015). Although Hsps are highly abundant and ubiquitously expressed, their concentration is often closely titrated to the requirements of the cell to prevent the accumulation of aberrant protein species, one of the hallmarks of proteostasis imbalance. Thus, the cellular stress response needs to be tightly regulated in order to rapidly adapt the proteostasis network to the particular requirements of the cell. The expression of Hsps is proportional to the intensity and duration of the respective stress condition (Gasch, Spellman *et al.* 2000).

Heat shock factor 1 (Hsf1p) is the central hub for activation, attenuation and regulation of the cytosolic HSR. Whereas Hsf1p is conserved from yeast to humans, three additional isoforms (Hsf2-4p) have evolved in vertebrates that exhibit various functions during development and stress and are also involved in longevity (Akerfelt, Morimoto *et al.* 2010). The overall Hsf1p architecture consists of an N-terminal DNA binding domain for binding to heat shock elements (HSE) upstream of heat shock genes, followed by hydrophobic heptad repeats (HR-A/B/C) responsible for the formation of active Hsf1p homotrimers, and a C-terminal transcription activation domain that ultimately leads to the stimulation of the RNA polymerase II complex and

subsequent high-level transcription of stress-inducible genes (Anckar and Sistonen 2011, Neudegger, Verghese *et al.* 2016). The conversion from monomeric Hsf1p to its homotrimeric form, its accumulation in the nucleus and the subsequent binding to HSEs of heat shock genes represent the key steps in Hsf1p activation. A prerequisite for the formation of active Hsf1p trimers is the conversion from intramolecular contacts between HR-A/B and HR-C domains to solely intermolecular interactions between the HR-A/B domains, resulting in the formation of an unusual, triple-stranded coiled coil and the derepression of the transcriptional activation domain (Sorger and Nelson 1989). In addition, the sudden appearance of non-native protein species leads to sequestration of cytosolic Hsp40, Hsp70 and Hsp90, thereby releasing monomeric Hsf1p from its inactive, chaperone-bound state and making it available for trimerization (Shi, Mosser *et al.* 1998). After trimerization, Hsf1p activity is modulated mainly by posttranslational modifications (PTMs) such as phosphorylation, sumoylation and acetylation, and by inactivation through binding to chaperones (Wu 1995, Shi, Mosser *et al.* 1998). Interestingly, activation of Hsf1p not only leads to upregulated transcription of chaperones, but also of genes involved in protein degradation, DNA repair, signal transduction and metabolism, with 3 % of all known yeast genomic loci showing binding of Hsf1p upon heat stress (Gasch, Spellman *et al.* 2000, Trinklein, Murray *et al.* 2004). Conversely, studies have shown that especially neurons – presumably owing to their postmitotic state – might be partially or even completely HSR-deficient, making this cell type especially vulnerable to proteotoxic stress (Mathur, Sistonen *et al.* 1994, Marcuccilli, Mathur *et al.* 1996).

In the ER and mitochondria, a set of gene expression programs termed the UPR ensures proteome integrity by responding to insufficient folding capacities in the respective organelle. In case of the ER, activation of the UPR leads to an expansion of the ER membrane and the induction of ER-resident chaperones (Schuck, Prinz *et al.* 2009). Since prolonged UPR activation can trigger the induction of apoptosis and therefore cell death, it is vital for cells to rapidly and efficiently target misfolded proteins for proteasomal degradation, a process called ER-associated degradation (ERAD) (Smith, Ploegh *et al.* 2011, Tabas and Ron 2011). Therefore, cells have evolved three pathways in order to detect the accumulation of misfolded proteins in the ER lumen: the

ATF6 branch, the PERK branch and the IRE1 branch (Walter and Ron 2011). ATF6 is an ER-resident transmembrane protein with a large N-terminal cytosolic portion that is delivered to the Golgi and subject to limited proteolysis upon UPR induction, resulting in nuclear localization of the N-terminal fragment and subsequent induction of UPR target genes such as the ER Hsp70 BiP and Hsp90 GRP94. In contrast, the PERK pathway involves oligomerization of the PERK kinase and phosphorylation of eIF2α, thereby attenuating translation and reducing protein flux into the ER. Additionally, upregulation of the transcription factor ATF4 leads to the induction of several UPR target genes, including genes involved in apoptosis. Finally, IRE1 is a bifunctional kinase and endoribonuclease that oligomerizes and splices an mRNA coding for the transcription factor XBP1, which, in its active form, induces the expression of proteins involved in lipid biosynthesis and ERAD. All three branches rely on sensors that reliably and specifically detect non-native proteins. However, it remains unclear how misfolded proteins are exactly recognized by the respective sensors and how aberrant species can be distinguished from newly synthesized and unfolded proteins that have just been translocated to the ER. Whereas earlier work suggested a transient interaction of the sensors with ER-resident chaperones that is lost upon accumulation of misfolded proteins and allows the sensors to oligomerize, recent work implies more direct modes of interaction (Walter and Ron 2011).

I.3.4 Endoplasmic reticulum-associated degradation

As described in the previous section, cells need to rely on efficient degradation of misfolded proteins in the ER to prevent unnecessary cell death by UPR-mediated apoptosis. Since the ER is lacking proteasomes, misfolded ER-resident proteins need to be dislocated to the cytosol for proteasomal degradation to occur (Claessen, Kundrat *et al.* 2011). The main factors that determine if a protein is subjected to ERAD are its size and hydrophobicity, folding rate, and precise location within the ER. This means that proteins that spend an extended amount of time folding might be targeted by ERAD and degraded although they would be functional, a kinetic control that becomes deleterious in cases where mutations produce proteins with mild folding defects, e.g. during cystic fibrosis (Drumm, Wilkinson *et al.* 1991).

Multiprotein ER transmembrane complexes with core E3 RING finger domain ubiquitin ligases are the central hubs of the ERAD machinery (Carvalho, Goder *et al.* 2006). In yeast, the two known ER membrane-associated E3 ligases are Hrd1p and Doa10p, whereas mammals show a much higher diversity in ERAD-associated E3 ligases (Gardner, Swarbrick *et al.* 2000, Swanson, Locher *et al.* 2001). Hrd1p alone is able to ubiquitinate soluble ER substrates, but a plethora of adaptor proteins is needed to ensure substrate specificity and to facilitate delivery to the E3 ligase complex (Carvalho, Stanley *et al.* 2010). Adaptor proteins typically consist of one transmembrane domain and an ER-luminal tetratricopeptide repeat (TPR) domain for interactions with misfolded clients (Gauss, Jarosch *et al.* 2006). Cytosolic and ER-resident chaperones such as Hsp70 might also serve as adaptors by delivering unfolded or partially folded polypeptides to ERAD-associated E3 ligases (Hosokawa, Wada *et al.* 2008, Nakatsukasa, Huyer *et al.* 2008). ERAD activity itself largely depends on the activity of the underlying E3 ligases, which is in turn regulated by autoubiquitination, oligomerization status, and the levels of adaptor proteins and other ERAD components (Gardner, Swarbrick *et al.* 2000, Carvalho, Stanley *et al.* 2010). The delivery of substrates to E3 ligase complexes is a complex process with various underlying mechanisms and pathways, with some of them being exploited by pathogens such as the human cytomegalovirus (hCMV) and toxins like ricin or cholera toxin (Lord, Roberts *et al.* 2006). One possibility for regulated delivery is the recognition of small peptide motifs serving as ERAD-associated "degrons" or simply the constitutive ubiquitination of substrates (Shearer and Hampton 2005, Mbonye, Wada *et al.* 2006). Proteins in a particularly compact misfolded state or non-native oligomers may require dismantling by disulfide isomerases or peptidyl-prolyl isomerases prior to dislocation into the cytosol (Ushioda, Hoseki *et al.* 2008, Bernasconi, Soldà *et al.* 2010). Besides that, the glycosylation status can also play a role since proteins undergo repeated cycles of de- and re-glycosylation after the initial cotranslational modification of specific asparagines with branched high-mannose glycans. Consequently, these proteins are repeatedly bound by the chaperone lectins calnexin (CNX) and calreticulin (CRT) in order to promote folding (Helenius and Aebi 2004). Mannosidases progressively deglycosylate these folding intermediates on their way to the native state, thereby reducing the chance of entry into further folding cycles, but also exposing an α1,6-linked mannose that is necessary for ERAD (Oda, Hosokawa *et al.* 2003). Finally,

ER-resident chaperones such as Hsp70 might directly deliver their unfolded or partially folded clients to the E3 ligase complexes (Okuda-Shimizu and Hendershot 2007).

After ubiquitination, substrates need to be extracted from the ER membrane for subsequent proteasomal degradation, an ATP-dependent process driven by the AAA+ ATPase activities of Cdc48p or the proteasome lid (Lee, Liu *et al.* 2004). In the case of glycosylated proteins, a cytosolic peptide *N*-glycanase (PNGase) deglycosylates the substrate prior to proteasomal degradation (Hirsch, Blom *et al.* 2003). Transmembrane proteins with misfolded cytosolic domains residing in the ER membrane are recognized and ubiquitinated by Doa10p in yeast, a process that involves no adaptor proteins. Substrate recognition might be driven by direct interactions between the E3 ligase and hydrophobic patches of misfolded proteins, explaining the broad substrate specificity of Doa10p and its ability to ubiquitinate even soluble cytosolic proteins (Swanson, Locher *et al.* 2001, Ravid, Kreft *et al.* 2006).

I.3.5 The proteostasis network in disease and aging

In order to be able to respond to multiple conditions of environmental and cellular stresses, the proteostasis network shows a high degree of redundancy – approximately 1400 components are known in mammals, and only 55 of the 332 chaperones that are expressed in human K562 leukemia cells are essential (Taipale, Tucker *et al.* 2014, Wang, Birsoy *et al.* 2015). However, during aging, the proteostasis network capacity declines, thereby facilitating the occurrence of various protein misfolding diseases such as type II diabetes, certain types of cancer, and especially neurodegenerative diseases (Taylor and Dillin 2011, Labbadia and Morimoto 2015). This inevitable collapse is accelerated if the proteostasis network is constantly challenged by aggregation-prone proteins, as is the case in certain hereditary types of neurodegenerative diseases or single nucleotide polymorphisms (SNPs) that lead to the expression of metastable proteins (Ben-Zvi, Miller *et al.* 2009, Sahni, Yi *et al.* 2015). The accumulation of aggregates of disease-related proteins in turn further perturbates proteome integrity, thereby initiating a vicious cycle that ultimately leads to a complete collapse of the proteostasis network and cell death. Although hereditary forms of protein misfolding diseases such as Huntington's disease or

ALS pose a serious threat to proteome integrity and are essentially incurable, they have a very low prevalence, with the result of aging being the major risk factor for the collapse of the proteostasis network. In fact, numerous studies have shown that during evolution, the propagation of a healthy and intact germline during early adulthood has evolved to be more important for higher organisms than to achieve immortality by long-term maintenance of the somatic proteome, a phenomenon that led to the theory of the "disposable soma" (Kirkwood 1977).

Nevertheless, multiple components of the proteostasis network including chaperones have been identified as targets for small molecules in the last decades, with the common goal of modulating the proteostasis network in a way that it can buffer the detrimental effects of aggregation-prone proteins and eventually suppress or at least postpone the manifestation of protein misfolding and age-related diseases. In theory, both boosting the proteostasis network capacity and inhibiting specific components might be effective in achieving this goal (Powers, Morimoto *et al.* 2009, Pratt, Gestwicki *et al.* 2015). Screening with low molecular weight compounds, for example, has led to the identification of potential drugs that activate the heat shock response and therefore induce the upregulation of chaperones, and that enhance the clearance of misfolded proteins by stimulating proteasome activity (Lee, Lee *et al.* 2010, Calamini, Silva *et al.* 2012). Conversely, the drug Guanabenz has been shown to attenuate translation, thereby reducing the amount of unfolded and potentially aggregation-prone nascent chains that the cellular folding machinery has to cope with (Tsaytler, Harding *et al.* 2011). Finally, the Hsp90 inhibitor Geldanamycin represents a promising candidate for cancer therapy, as Hsp90 is known to be involved in the folding of various proto-oncogenic proteins (Goetz, Toft *et al.* 2003).

I.4 The ribosomal quality control pathway

The reliable and faithful translation of genomic information is absolutely crucial for maintaining proteostasis and cell survival. Thus, cells have evolved multiple quality control pathways that recognize aberrant mRNAs, their translation products and even defective ribosomes, and target them for degradation (LaRiviere, Cole *et al.* 2006, Van Hoof and Wagner 2011). Defects in the translational machinery have been linked to a plethora of pathological conditions including neurodegenerative diseases, thereby underlining the importance of translational fidelity (Lee, Beebe *et al.* 2006, Scheper, Van Der Knaap *et al.* 2007, Ishimura, Nagy *et al.* 2014). Therefore, the recognition and degradation of aberrant mRNAs and their translation products contributes to prevent their accumulation and, as a result, proteome damage (Gregersen, Bross *et al.* 2006, Anckar and Sistonen 2011).

I.4.1 Ribosomal stalling

The phenomenon of ribosomal stalling is defined as a state in which either elongation of the nascent chain or translation termination is irreversibly blocked as a result of the ribosome trying to translate a faulty mRNA (Shoemaker and Green 2012). Translation of aberrant transcripts leads to truncated proteins that are not only partially or completely nonfunctional, but also potentially prone to aggregation and thus need to be eliminated rapidly in order to prevent the accumulation of toxic aggregates. Strikingly, all surveillance mechanisms targeting defective mRNAs and their translation products rely on ribosomal stalling as an activation signal, which is why a defective mRNA needs to be translated at least once in order to be recognized as corrupted (Van Hoof and Wagner 2011, Shoemaker and Green 2012).

During the complex and naturally error-prone process of RNA maturation in eukaryotic cells, incorrect splicing events or polyadenylation within the open reading frame (ORF) can result in the generation of so-called “non-stop (NS) mRNAs”, i.e. truncated transcripts or mRNAs lacking an in-frame stop codon (Fig. I.4 (B)) (Frischmeyer, van Hoof *et al.* 2002, van Hoof,

Frischmeyer *et al.* 2002, Meaux and Van Hoof 2006, Ozsolak, Kapranov *et al.* 2010). Translation of a truncated mRNA leads to ribosomal stalling at the 3' end of the mRNA, leaving the aminoacyl (A) site of the translating ribosome empty and rendering the stalled 80S ribosome inaccessible for the canonical translation elongation and termination machineries (Inada 2016). The *HAC1* mRNA is an example for an endogenous NS-mRNA as it is subject to frequent erroneous splicing in the cytosol, resulting in considerable amounts of truncated transcripts (Guydosh and Green 2014). In case of mRNA lacking an in-frame stop codon, translation of the 3' untranslated region (UTR) and the poly(A) tail lead to C-terminal extension of the nascent chain and a poly-lysine stretch that is added as a result of the poly(A) tail being interpreted as a series of lysine-encoding AAA codons. In addition to stalling at the 3' end of the mRNA, translation of the poly(A) tail itself was shown to induce a translational arrest and to cause ribosomal stalling, presumably due to electrostatic interactions between the positively charged poly-lysine stretch and the negatively charged ribosomal exit channel (Lu and Deutsch 2005, Ito-Harashima, Kuroha *et al.* 2007, Lu, Kobertz *et al.* 2007). More recent studies, however, could demonstrate that deletion of the 40S subunit protein Asc1p (RACK1 in mammals) or the ribosome-associated E3 ubiquitin ligase Hel2p (presumably ZNF598 in mammals) strongly enhances read-through of sequences encoding polybasic tracts, thereby questioning the relevance of electrostatic interactions in the ribosomal exit channel for stalling (Brandman, Stewart-Ornstein *et al.* 2012, Letzring, Wolf *et al.* 2013, Juszkiewicz and Hegde 2016). Moreover, codon usage was also found to play a role, as an internal poly(AAA) stretch induced ribosomal stalling and translational repression much more efficiently than a synonymous poly(AAG) stretch in mammals, indicating that the poly(A) tail might represent a strong endogenous stalling sequence to repress translation of faulty NS-mRNAs (Inada and Aiba 2005, Arthur, Pavlovic-Djuranovic *et al.* 2015). Interestingly, a recent study found that the introduction of defined poly(A) stretches into an ORF can be used to fine tune protein expression levels independent of promoter strength, thereby facilitating the generation of hypomorphic mutants (Arthur, Chung *et al.* 2017). Ribosomal stalling can also be induced in the absence of polybasic sequences by a lack of suitable and charged aminoacyl-tRNAs, a condition that might be the result of amino acid depletion and/or the repeated occurrence of rare codons such as the arginine-encoding CGA codon (Fig. I.4 (C)) (Letzring, Dean *et al.* 2010, Letzring, Wolf

et al. 2013, Wolf and Grayhack 2015). In this context, it is important to distinguish between ribosomal stalling, which represents a terminal state that is the result of faulty mRNA translation, and ribosomal pausing, which might use stalling sequences such as polybasic stretches or rare codons to modulate local translation speeds in order to ensure efficient folding or translocation of the nascent chain (Pechmann and Frydman 2013, Pechmann, Chartron *et al.* 2014). Consistently, synonymous codon changes have been found to alter various properties of the corresponding translation product and can even lead to disease in the case of silent SNPs in patients (Sauna and Kimchi-Sarfaty 2011, Zhou, Guo *et al.* 2013, Buhr, Jha *et al.* 2016). In addition, mRNAs might also show the tendency to form strong secondary structures that block the ribosome during translation and prevent further elongation of the nascent chain, thereby also leading to ribosomal stalling (Fig. I.4 (D)) (Doma and Parker 2006).

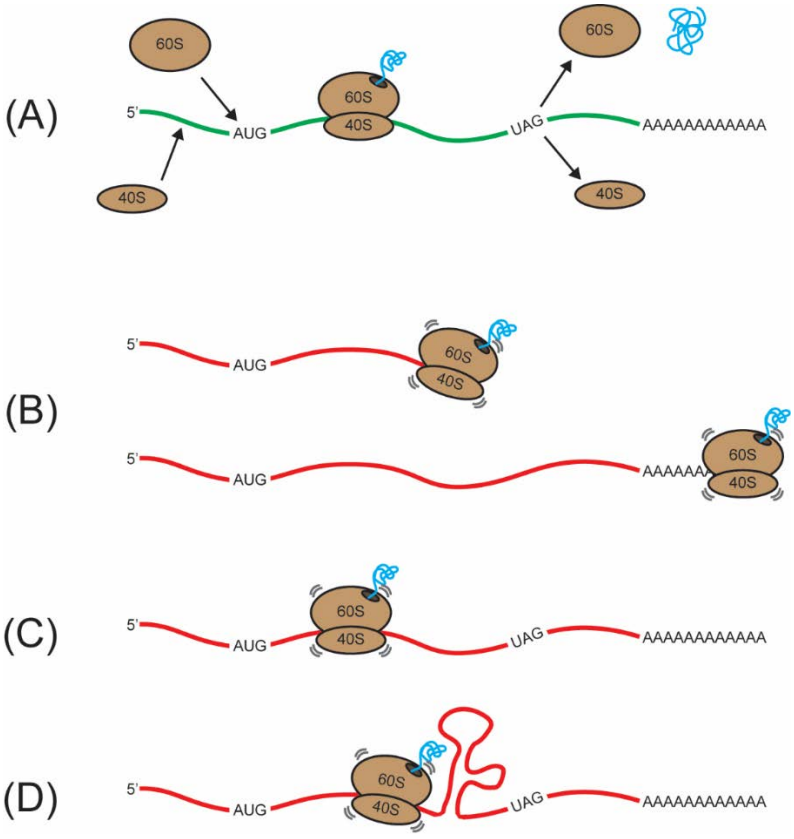

Fig. I.4: Types of ribosomal stalling. (A) Canonical transcription usually involves assembly of the translationally active 80S ribosome at the initation (AUG) codon, followed by translation of the ORF,

dissociation of the ribosome at the stop (UAG) codon and release of the newly synthesized polypeptide chain. (B) NS-mRNAs such as truncated transcripts or mRNAs lacking an in-frame stop codon lead to ribosomal stalling at the 3′ end of the transcript. (C) Amino acid insufficiency or stalling features such as repeats of rare codons within the ORF lead to internal stalling of the ribosome. (D) mRNA secondary structures within the ORF can block the ribosome during translation and also induce stalling.

I.4.2 Recognition and dissociation of stalled ribosomes

Since ribosomal stalling can be the result of translation of different aberrant mRNA species, the topology and conformation of stalled ribosomes can vary significantly. A hallmark of ribosomes that stall due to translation of a NS-mRNA is the absence of a codon in the ribosomal A-site, making it impossible for canonical translation elongation or termination factors to bind since they require the presence of a sense or stop codon, respectively. In the case of internal stalling events, e.g. as a result of rare codons, the A-site is occupied with a sense codon, but delivery of an appropriate aminoacyl-tRNA fails due to tRNA insufficiency. Thus, cells evolved a pathway for noncanonical ribosome dissociation that acts specifically on stalled ribosomes and consists of the proteins Dom34p (Pelota in mammals), Hbs1p (hHbs1 in mammals) and the canonical ribosome dissociation factor Rli1p (ABCE1 in mammals) (Shoemaker, Eyler *et al.* 2010, Pisareva, Skabkin *et al.* 2011, Brandman and Hegde 2016).

In short, this pathway involves binding of the Dom34p/Hbs1p-GTP complex at the stalled ribosome, followed by GTP hydrolysis and positioning of Dom34p in the ribosomal A-site, recruitment of Rli1p, and subsequent dissociation of the ribosome by Rli1p in an ATP-dependent manner (Fig.I.5 (b)) (Shoemaker, Eyler *et al.* 2010, Becker, Armache *et al.* 2011, Shoemaker and Green 2011). Unlike the canonical translation termination machinery, which also uses the AAA+ ATPase Rli1p for the dissociation of ribosomes that reached a stop codon, the Dom34p/Hbs1p pathway does not depend on the presence of a codon in the A-site, indicating that ribosomes that stalled during translation of NS-mRNAs might be the primary target of this complex (Fig. I.5 (a), (b)). Strikingly, *in vitro* experiments with purified stalled ribosomes have shown that the Dom34p/Hbs1p complex can recognize and dissociate stalled ribosomes independent of the presence or absence of a codon in the A-site, suggesting a role as a general splitting pathway for

the rescue of stalled ribosomes (Shoemaker, Eyler *et al.* 2010, Becker, Armache *et al.* 2011, Pisareva, Skabkin *et al.* 2011, Shoemaker and Green 2011). Although these findings suggest a role as a general ribosome splitting pathway, other mechanisms might exist *in vivo* for the dissociation of stalled ribosomes with an occupied A-site. Dom34p/Hbs1p shows a low affinity for ribosomes in the GTP-bound state, indicating that during the time of GTP hydrolysis, Dom34p/Hbs1p might compete with the translation elongation and termination machinery or other factors for ribosome binding until the irreversible decision to split the ribosome is made (Brandman and Hegde 2016).

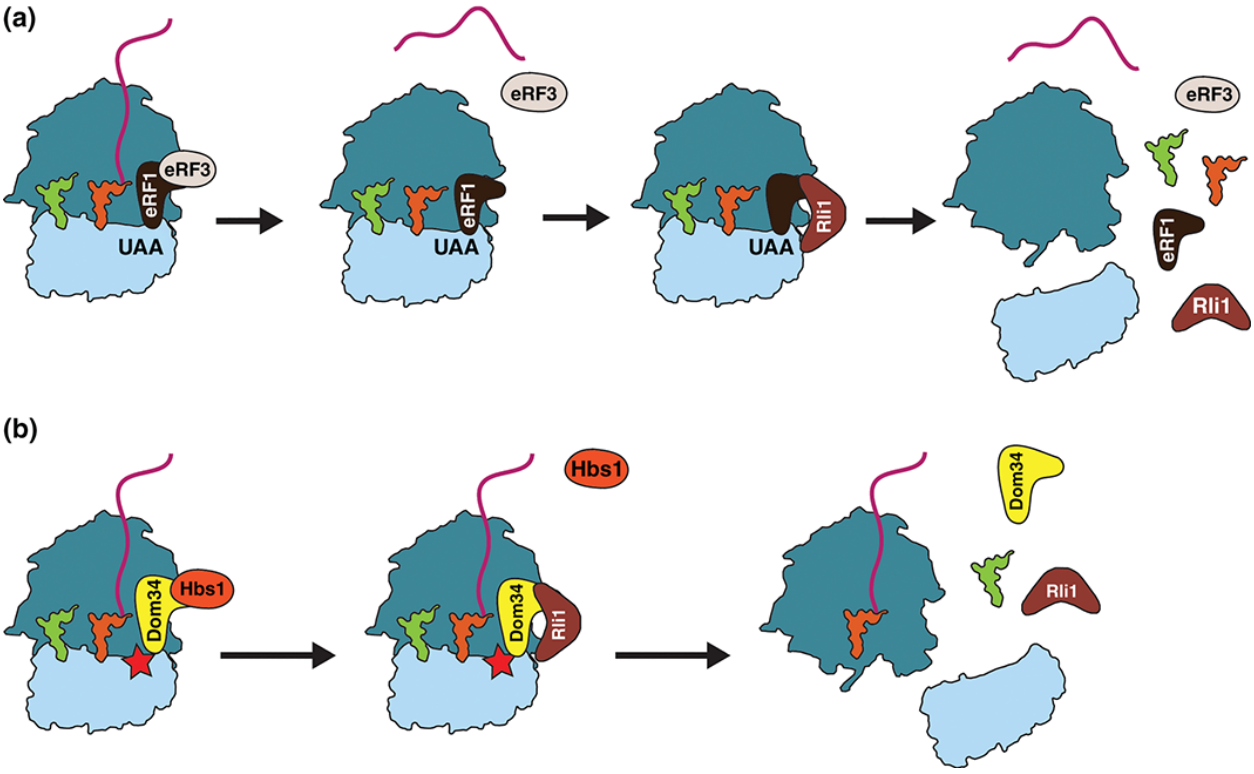

Fig. I.5: Canonical translation termination and dissociation of stalled ribosomes. (a) At the end of translation under normal conditions, a stop codon in the A site leads to binding of a ternary eRF1-eRF3-GTP complex. Upon GTP hydrolysis, eRF3 dissociates and eRF1 undergoes conformational changes that lead to hydrolysis of the peptidyl-tRNA bond and release of the nascent chain. The AAA+ ATPase Rli1p then binds to eRF1 and dissociates the 80S ribosome in an ATP-dependent manner. (b) Upon ribosomal stalling (indicated by a star in the ribosomal A site), the ternary Dom34p/Hbs1p-GTP complex, which is homologous to the eRF1-eRF3-GTP termination complex, binds close to the A site. Following GTP hydrolysis and Hbs1p release, Dom34p provides a binding platform for Rli1p to allow for ribosome dissociation without releasing the nascent chain. Figure adapted from (Simms, Thomas *et al.* 2017).

Dom34p is a homolog of the eukaryotic release factor 1 (eRF1), with whom it shares structural similarity to a tRNA molecule, thereby allowing it to bind to the ribosomal A-site (Chen, Muhlrad *et al.* 2010). The β3- β4 loops of the N-terminal domain of Dom34p were shown to directly interact with the decoding site of the 40S subunit, thereby making the presence of a sense or stop codon in the A-site dispensable for binding (Kobayashi, Kikuno *et al.* 2010). After binding of the ternary Dom34p/Hbs1p-GTP complex to the GTPase center close to the A-site of the ribosome, positioning of Dom34p in the ribosomal A-site is accomplished upon GTP hydrolysis by Hbs1p, a translational GTPase with similarity to eukaryotic elongation factor 1A (eEF1A) and eukaryotic release factor 3 (eRF3) (Shoemaker, Eyler *et al.* 2010, Becker, Armache *et al.* 2011). Dom34p can then recruit the canonical ribosome splitting factor Rli1p, which dissociates the ribosome in an ATP-dependent, yet largely unknown mechanism. In addition, binding of Dom34p/Hbs1p to the ribosome *per se* might facilitate dissociation by weakening the codon-anticodon interactions at the peptidyl (P)-site of the ribosome (Kobayashi, Kikuno *et al.* 2010). Furthermore, the Dom34p/Hbs1p complex was also shown to mediate the release of stalled nascent chains that were targeted for the ER or mitochondria into the lumen of the respective organelle (Izawa, Tsuboi *et al.* 2012).

I.4.3 Degradation of aberrant polypeptides

Following dissociation of the stalled ribosome and release of both the defective mRNA and the 40S subunit, the cell is faced with a complex consisting of the 60S subunit and a peptidyl-tRNA molecule, i.e. the stalled nascent chain that is located in the ribosomal exit channel and linked to a tRNA moiety in the ribosomal P-site. This complex represents an aberrant species that requires a specific machinery for its recognition and disassembly, as canonical translation termination typically results in a released nascent chain and free 60S and 40S subunits. In eukaryotic cells, the ribosomal quality control (RQC) pathway is responsible for the degradation of stalled nascent chains, its main role being to ubiquitinate the aberrant polypeptide, to extract it from the 60S subunit and to deliver it to the proteasome for degradation (Bengtson and Joazeiro 2010, Brandman, Stewart-Ornstein *et al.* 2012, Defenouillere, Yao *et al.* 2013). Interestingly,

ubiquitination of faulty nascent chains occurs independent of the type of stalling and stringently requires ribosome dissociation, indicating that the RQC pathway might represent a general cotranslational quality control mechanism for the recognition of 60S-peptidyl-tRNA complexes and degradation of aberrant polypeptides (Shao, von der Malsburg *et al.* 2013, Shao and Hegde 2014). Moreover, failure of the RQC pathway in yeast leads to the formation of SDS-resistant cytosolic aggregates that sequester various essential chaperones, thereby leading to proteotoxic stress (Choe, Park *et al.* 2016, Defenouillere, Zhang *et al.* 2016, Yonashiro, Tahara *et al.* 2016).

A mutation in the *LISTERIN* gene encoding a E3 ubiquitin ligase has been linked to a neurodegenerative phenotype in mice, including impairment of rear leg movement, reduced life span, and neuronal cell death (Chu, Hong *et al.* 2009). Deletion of the yeast homolog of Listerin, Ltn1p, was identified in a screen as a suppressor of the phenotype caused by a non-stop mutation (Wilson, Meaux *et al.* 2007). This E3 ligase was later found to be involved in the ubiquitination of non-stop proteins at the ribosome, indicating a central role in cotranslational protein quality control (Bengtson and Joazeiro 2010). In two comprehensive studies in yeast screening for activators of Hsf1 and proteins being functionally linked to SKI complex-mediated RNA degradation, two genetic interactors of Ltn1p, Rqc1p and Tae2p (now termed Rqc2p), were identified that, together with Ltn1p, form a 60S-associated complex that interacts with the AAA+ ATPase Cdc48p and its cofactors Npl4p and Ufd1p (Brandman, Stewart-Ornstein *et al.* 2012, Defenouillere, Yao *et al.* 2013). Whereas the main role of Rqc2p remained unclear, it was found that Rqc1p is required for the recruitment of Cdc48p, and that the latter mediates extraction of the ubiquitinated nascent polypeptide chain from the 60S subunit and delivery to the proteasome in an ATP-dependent manner (Brandman, Stewart-Ornstein *et al.* 2012, Defenouillere, Yao *et al.* 2013, Verma, Oania *et al.* 2013). However, the exact mechanism of peptidyl-tRNA hydrolysis prior to nascent chain extraction still remains unclear, although recent findings suggest that the empty ribosomal A-site of the 60S subunit might be involved, e.g. via noncanonical binding of eRF1 (Shao, Brown *et al.* 2015, Brandman and Hegde 2016). Rqc2p and its mammalian homolog Nuclear Export Mediation Factor (NEMF) were later found to specifically bind to 60S-peptidyl-tRNA complexes by recognizing the exposed tRNA moiety in the P-site with its N- and C-terminal lobes

and by making interactions between its middle domain and the sarcin-ricin loop (SRL) and the P stalk of the 60S subunit (Fig. I.6b, c) (Lyumkis, Oliveira dos Passos *et al.* 2014, Shao, Brown *et al.* 2015, Shen, Park *et al.* 2015). This extensive network not only allows for specific recognition of these aberrant ribosomal species and provides a binding platform for Ltn1, but also prevents reassociation with the 40S subunit by occupying a large parts of the subunit interface (Fig. I.6a) (Shao, Brown *et al.* 2015). The N-terminal domain of Ltn1p then interacts with both the middle domain of Rqc2p and the 60S subunit, thereby ensuring specificity for stalled 60S-peptidyl-tRNA complexes (Fig. I.6b, c) (Shao, Brown *et al.* 2015). Due to the HEAT repeats in its middle domain that confer enhanced flexibility and an elongated shape by forming an extended superhelical structure, Ltn1p is able to wrap around the 60S subunit and to position its C-terminal RING domain close to the vestibule of the ribosomal exit channel for ubiquitination of the nascent polypeptide (Fig. I.6c) (Lyumkis, Doamekpor *et al.* 2013, Shao, Brown *et al.* 2015).

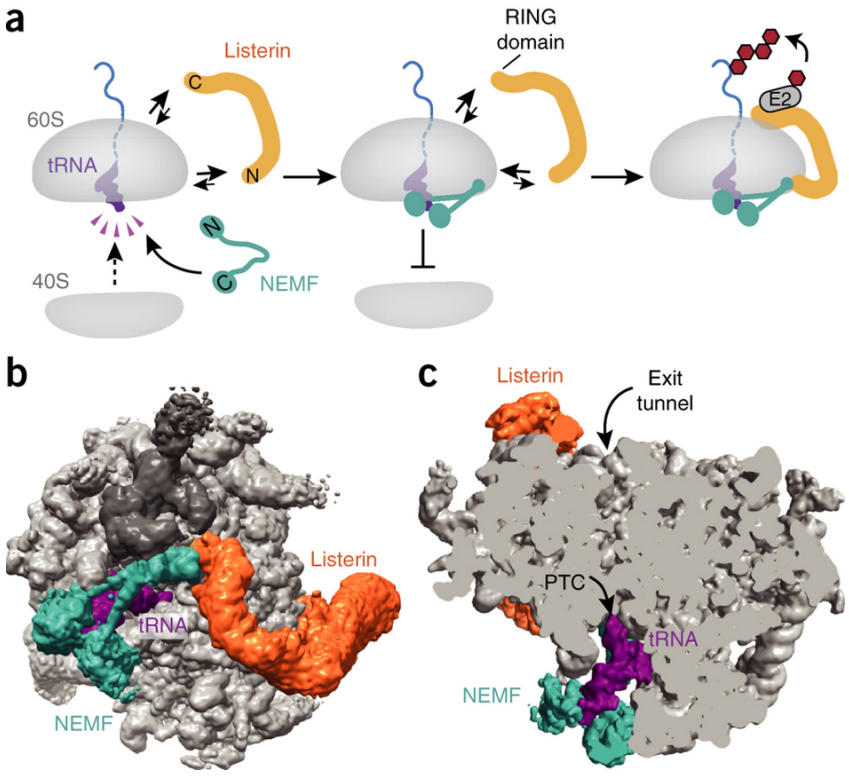

Fig. I.6: Mechanism and structure of the RQC complex. (a) Following dissociation of the stalled ribosome, the cell is faced with an aberrant 60S-peptidyl-tRNA complex. NEMF (Rqc2p in yeast) interacts with both

the exposed tRNA moiety and the subunit interface, thereby preventing reassociation with the 40S subunit and providing a binding platform for Listerin (Ltn1p in yeast). The N-terminal domain of Listerin then interacts with Rqc2p and the 60S subunit, and positions its C-terminal RING finger domain in close proximity to the ribosomal exit channel by using its elongated shape to wrap around the 60S subunit. The nascent chain is then ubiquitinated in a Listerin-dependent manner, allowing for extraction by VCP (Cdc48p in yeast) and proteasomal degradation. (b) + (c) Cryo-EM structure of the mammalian 60S-peptidyl-tRNA-RQC complex. Teal, NEMF; orange, Listerin; purple, P-site tRNA; gray, 60S subunit. PTC, peptidyl transferase center. Figure adapted from (Brandman and Hegde 2016).

Strikingly, whereas deletion of *LTN1* or *RQC1* leads to activation of the cytosolic heat shock response, deletion of *RQC2* alone or in combination with *LTN1* or *RQC1* resulted in suppression of Hsf1p induction, indicating a central role of Rqc2p in activation of the cellular stress response (Brandman, Stewart-Ornstein *et al.* 2012). In a recent study, cryo-EM and mass spectrometry analyses of 60S-RQC complexes revealed the presence of tRNAs in ribosomal A-sites and a C-terminal extension of the stalled nascent chain with alanine and threonine residues, respectively (Shen, Park *et al.* 2015). Elongation of nascent polypeptides with these so-called C-terminal alanine and threonine (CAT) tails was shown to be mediated by Rqc2p in a noncanonical, 40S- and mRNA-independent manner (Shen, Park *et al.* 2015). It was suggested that specificity for tRNAs carrying alanine and threonine residues might be the result of recognition by Rqc2p due to similarities in their anticodon loops (Gerber and Keller 1999). Notably, CAT tails seem to be heterogeneous in both length and sequence: extensions of up to 20 amino acids consisting of roughly equal amounts of alanine and threonine have been described that seem to lack a clear sequence (Shen, Park *et al.* 2015). A mutant version of Rqc2p was identified that can still recognize stalled 60S-peptidyl-tRNA complexes and provides a binding platform for Ltn1p, but lacks the ability to generate CAT tails (Shen, Park *et al.* 2015). Strikingly, suppression of CAT tail formation in *LTN1* and *RQC1* deletion backgrounds not only abolished Hsf1p induction, but also prevented the formation of proteotoxic SDS-resistant aggregates (Shen, Park *et al.* 2015, Choe, Park *et al.* 2016, Yonashiro, Tahara *et al.* 2016). Thus, it was reasoned that the Rqc2p-dependent activation of the heat shock response might either be a direct result of CAT tail recognition by Hsf1p or due to CAT tail-mediated aggregation of aberrant nascent chains (Choe, Park *et al.* 2016, Yonashiro, Tahara *et al.* 2016). Besides that, the precise role of CAT tails remains unclear. It was

suggested that a C-terminal extension of the stalled nascent polypeptide might serve as a spacer to resolve stalling due to electrostatic interactions between polybasic stretches of the nascent chain and the ribosomal exit channel, and to bring these stretches, which are potentially attractive targets for Ltn1p-mediated ubiquitination due to their high lysine content, out of the exit tunnel (Brandman and Hegde 2016). Another hypothesis is that CAT tails might have a protective role by promoting aggregation of aberrant nascent chains, thereby facilitating both sequestration into less toxic inclusions that can be targeted for vacuolar degradation and activation of the heat shock response in order to restore proteostasis (Yonashiro, Tahara *et al.* 2016). In fact, it has previously been shown that homopolymers of alanine form aggregates, and that activation of the heat shock response results in a global attenuation of translation, thereby facilitating degradation of potentially aggregation-prone nascent chains and mRNAs that are in the process of translation (Forood, Perez-Paya *et al.* 1995, Shalgi, Hurt *et al.* 2013, Merret, Nagarajan *et al.* 2015).

I.4.4 mRNA quality control pathways

Since aberrant mRNAs might participate in iterative rounds of translation and subsequent ribosomal stalling, they pose a considerable threat to the translation machinery and proteostasis in general. Thus, cells have evolved several cotranslational quality control pathways that allow for selective and rapid degradation of transcripts containing potential stalling sequences such as NS-mRNAs or transcripts with strong secondary structure elements or rare codons (Shoemaker and Green 2012, Inada 2013).

In general, eukaryotic cells can degrade mRNAs in two ways: from the 5′ end or the 3′ end. In both cases, the typical features of an mRNA, the 5′ cap and the 3′ poly(A) tail, need to be removed prior to degradation (Parker 2012). Whereas removal of the 5′ cap structure is mediated by the decapping enzymes Dcp1p and Dcp2p, the Pan2p-Pan3p and Ccr4p-Not complexes are responsible for deadenylation of the transcript (Parker 2012). Following deadenylation, most mRNAs are subject to degradation from their 3′ end by the exosome, a complex consisting of 9 subunits and the RNase Rrp44p that is present in both the cytosol and the nucleus (Klauer and van Hoof 2012). Degradation of mRNAs by the cytosolic exosome complex requires the SKI

complex, which consists of a helicase (Ski2p), two copies of a regulatory WD-repeat protein (Ski8p) and a scaffold protein (Ski3p), and that facilitates mRNA degradation by binding to the exosome complex and threading target mRNAs to the active site of Rrp44p (Klauer and van Hoof 2012, Schmidt, Kowalinski *et al.* 2016). The protein Ski7p, which is only present in a subset of fungi, mediates contact between the SKI complex and the exosome via its N-terminal domain, whereas the C-terminal domain shows structural similarity to translational GTPases like eRF3 and Hbs1p, but has no detectable GTPase activity due to several mutations in its active site (Kowalinski, Schuller *et al.* 2015). As an alternative to exosome-dependent degradation, mRNAs might also be degraded from the 5′ end by the exonuclease Xrn1p after decapping.

Three major RNA quality control mechanisms have been identified in eukaryotic cells: nonsense-mediated decay (NMD), which mediates degradation of transcripts with a premature stop codon, non-stop decay (NSD), which targets NS-mRNAs that lead to ribosomal stalling at their 3′ end, and no-go decay (NGD), which is responsible for the degradation of transcripts with features that result in internal stalling (Losson and Lacroute 1979, Doma and Parker 2006, Klauer and van Hoof 2012, Lykke-Andersen and Jensen 2015). The NSD pathway was originally found to be involved in the degradation of mRNAs that were subject to erroneous splicing events or premature polyadenylation and therefore lack an in-frame stop codon (Frischmeyer, van Hoof *et al.* 2002, van Hoof, Frischmeyer *et al.* 2002, Ozsolak, Kapranov *et al.* 2010). Translation of these aberrant transcripts leads to stalling of the ribosome at the 3′ end of the mRNA, leaving the ribosomal A-site empty. This configuration triggers dissociation of the ribosome by the Dom34p/Hbs1p complex and RQC-dependent degradation of the nascent chain (Bengtson and Joazeiro 2010, Shoemaker, Eyler *et al.* 2010, Brandman, Stewart-Ornstein *et al.* 2012, Lyumkis, Oliveira dos Passos *et al.* 2014). The released mRNA is then degraded from the 3′ end by the cytosolic exosome machinery (Fig. I.7 (A)) (Tsuboi, Kuroha *et al.* 2012). Interestingly, Ski7p seems to be essential for degradation of NS-mRNAs, but the exact mechanism of NS-mRNA recognition remains unknown (Frischmeyer, van Hoof *et al.* 2002, van Hoof, Frischmeyer *et al.* 2002, Meaux and Van Hoof 2006). Rescue and dissociation of ribosomes that stalled during translation of mRNAs with internal stalling features such as rare codons or secondary structures, however, is

more complex as the ribosomal A-site is still occupied with a sense codon, thereby making the ribosome an unfavorable target for dissociation by the Dom34p/Hbs1p complex (Doma and Parker 2006, Chen, Muhlrad *et al.* 2010). In this case, stalling leads to cleavage of the mRNA in close vicinity and upstream of the stalled ribosome by a yet to be identified endonuclease, resulting in the generation of two fragments: a 5′ fragment that resembles a truncated mRNA, and a 3′ fragment with the stalled ribosome close to the 5′ end of this fragment (Tsuboi, Kuroha *et al.* 2012, Inada 2016). Whereas the 5′ fragment can be targeted for exosome-mediated degradation via the NSD pathway, the 3′ fragment is subject to Xrn1p-dependent degradation from the 5′ end (Fig.I.7 (B)). However, the exact mechanism of ribosome dissociation in the latter case remains unsolved.

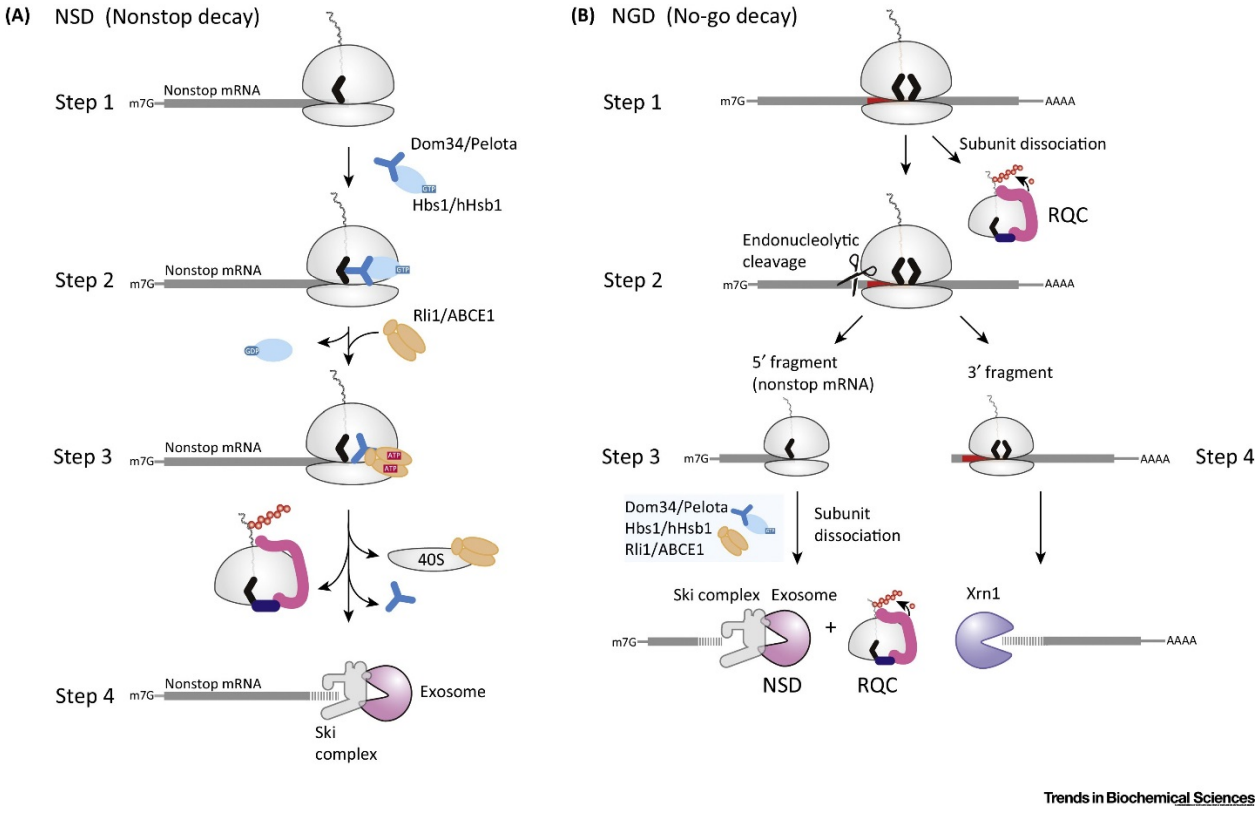

Fig. I.7: Mechanisms of NSD and NGD. (A) Translation of NS-mRNA leads to ribosomal stalling at the 3′ end of the aberrant transcript. Following dissociation of the stalled ribosome by the Dom34p/Hbs1p complex and RQC-dependent degradation of the nascent chain, the NS-mRNA is degraded from the 3′ end by the cytosolic SKI complex/exosome machinery. (B) Aberrant transcripts with internal stalling features

lead to stalled ribosomes with an occupied A-site, thereby disfavoring Dom34p/Hbs1p-dependent dissociation. Ribosomal stalling induces cleavage of the mRNA upstream of the ribosome, generating a 5′ fragment that is subject to NSD, and a 3′ fragment, which is degraded from the 5′ end via Xrn1p. Figure adapted from (Inada 2016).

I.5 Aim of the study

The intrinsically error-prone process of mRNA maturation in higher eukaryotes can lead to the generation of defective transcripts, e.g. truncated mRNAs or transcripts lacking an in-frame stop codon. Furthermore, mRNAs can contain stretches of nonoptimal codons or form strong secondary structures due to sequence-specific internal base pairing. Translation of these faulty transcripts leads to ribosomal stalling, i.e. an irreversible block of the elongation process. Truncated polypeptide chains, which are produced during translation of these defective mRNAs, pose a serious threat to proteome integrity as they are nonfunctional and typically prone to aggregation. Besides that, stalled ribosomes are not recognized and recycled by the canonical translation termination machinery, hence they are not available for subsequent rounds of translation. Thus, a network of quality control pathways has evolved in all kingdoms of life, its main tasks being to recognize and rescue stalled ribosomes and to degrade faulty mRNAs and their potentially harmful translation products. Failure of this process has previously been linked to pathological conditions, e.g. the development of neurodegenerative disorders. However, the mechanisms by which impairment of ribosome-associated RNA and protein quality control leads to toxicity remain elusive.

The goal of the present study was to dissect the molecular mechanisms of the RQC pathway in the yeast *Saccharomyces cerevisiae* and to find possible explanations for the neurodegenerative phenotype observed in RQC-deficient mice. To this end, a set of reporter constructs with distinct stalling features was expressed in RQC-deficient yeast to determine the critical features that are necessary for aggregation of faulty translation products. Furthermore, a mass spectrometric approach was used to determine the interactome of a recombinantly

expressed NS-protein. The influence of RQC deficiency on general protein quality control was also analyzed in order to reveal the toxicity of endogenous aberrant polypeptides that are the result of translation of faulty mRNAs. Since these faulty transcripts are normally subject to rapid degradation via one of the mRNA quality control pathways, the role of mRNA surveillance in the aggregation of aberrant nascent chains was investigated. Strikingly, cells seem to be constantly challenged by aberrant polypeptides, but the reasons for ribosomal stalling under normal conditions as well as the identity of endogenous faulty mRNAs and their translation products remain unknown. Thus, a mass spectrometric approach was used in order to determine the identity of endogenous stalled nascent chains and to possibly identify the features that are responsible for the majority of stalling events *in vivo*. Finally, *in vitro* aggregation experiments with purified proteins resembling translation products of faulty mRNAs were performed in order to characterize the aggregation process of aberrant polypeptides.

II. Materials & Methods

II.1 Chemicals

Name	Vendor
100 mM dNTP Mix	Bioline
LE Agarose	Biozym
[$^{13}C_6$, $^{15}N_2$]L-lysine	Cambridge Isotope Laboratories
L-lysine D4	Cambridge Isotope Laboratories
Bacto Agar	Difco
Bacto Peptone	Difco
Bacto Tryptone	Difco
Bacto Yeast Extract	Difco
Yeast Nitrogen Base without amino acids	Difco
InstantBlue Protein Stain	expedeon
Formic acid	Fluka
L-Serine	Fluka
ECL Western Blotting Detection Reagent	GE Healthcare
Ammonium chloride	Merck
Calcium chloride dihydrate	Merck
D-Sorbitol	Merck
Ethylenediamine tetraacetate disodium salt	Merck
Glycerol anhydrous	Merck
L-Leucine	Merck

Magnesium acetate tetrahydrate	Merck
Sodium dihydrogen phosphate monohydrate	Merck
Sodium hydroxide	Merck
Sucrose	Merck
Trifluoroacetic acid	Merck
Tris(hydroxymethyl)aminomethane	Merck
CutSmart Buffer (10x)	NEB
1,4-Dithiothreitol	Roche
cOmplete Mini, EDTA-free protease inhibitor cocktail	Roche
Acetonitrile	Roth
Di-potassium hydrogen phosphate trihydrate	Roth
Di-sodium hydrogen phosphate	Roth
Ethanol p.a.	Roth
Glycine	Roth
Guanidine hydrochloride	Roth
Isopropyl β-D-1-thiogalactopyranoside	Roth
Methanol	Roth
Potassium acetate	Roth
Potassium chloride	Roth
Potassium dihydrogen phosphate	Roth
Milk powder	Saliter
Dimethyl sulfoxide	Serva
Sodium dodecyl sulfate	Serva
α-D-Raffinose	Serva
2-Propanol	Sigma

3-(N-morpholino)propanesulfonic acid	Sigma
Acetic acid	Sigma
Acetone	Sigma
Adenine hemisulfate	Sigma
Ampicillin sodium salt	Sigma
Bis-Tris	Sigma
Bromophenol blue sodium salt	Sigma
Chloramphenicol	Sigma
Cycloheximide	Sigma
D-Galactose	Sigma
D-Glucose	Sigma
Iodoacetamide	Sigma
L-Alanine	Sigma
L-Arginine	Sigma
L-Asparagine	Sigma
L-Aspartic acid sodium salt	Sigma
L-Cysteine hydrochloride monohydrate	Sigma
L-Glutamic acid sodium salt	Sigma
L-Glutamine	Sigma
L-Histidine	Sigma
L-Isoleucine	Sigma
Lithium acetate dihydrate	Sigma
L-Lysine	Sigma
L-Methionine	Sigma
L-Phenylalanine	Sigma

L-Proline	Sigma
L-Threonine	Sigma
L-Tryptophane	Sigma
L-Tyrosine	Sigma
L-Valine	Sigma
Magnesium chloride hexahydrate	Sigma
Myo-inositol	Sigma
Para-aminobenzoic acid	Sigma
Polyethylene glycol 3,350	Sigma
Rubidium chloride	Sigma
Sodium azide	Sigma
Sodium deoxycholate	Sigma
Trichloroacetic acid	Sigma
Triton X-100	Sigma
Tween 20	Sigma
Uracil	Sigma
Urea	Sigma
β-mercaptoethanol	Sigma
DNA Gel Loading Dye (6x)	Thermo Fisher Scientific
Herring Sperm DNA Solution	Thermo Fisher Scientific
PageRuler Prestained Protein Ladder	Thermo Fisher Scientific
SYBR Safe DNA Gel Stain	Thermo Fisher Scientific
Nonidet P40	USB
Hydrochloric acid	VWR
Sodium chloride	VWR

II.2 Enzymes and antibodies

II.2.1 Enzymes

Name	Vendor
Herculase II Fusion DNA Polymerase	Agilent
PreScission Protease	GE Healthcare
Benzonase	Millipore
AgeI-HF	NEB
BamHI-HF	NEB
EcoRI	NEB
HindIII-HF	NEB
SpeI-HF	NEB
T4 DNA Polymerase	NEB
XbaI	NEB
XhoI	NEB
RNase A	Qiagen
Lysozyme	Sigma
Lysyl Endopeptidase, MS Grade	Wako

II.2.2 Antibodies

Immunogen	Host	Vendor	Working dilution
GFP	Mouse monoclonal	Roche	1:1,000
Pgk1p	Mouse monoclonal	Invitrogen	1:1,000
mCherry	Mouse monoclonal	Clontech	1:1,000

Rpl3p	Mouse monoclonal	Developmental Studies Hybridoma Bank	1:500
β-galactosidase	Mouse polyclonal	Sigma	1:1,000
Sis1p	Rabbit polyclonal	cosmobio	1:5,000
FLAG	Rabbit polyclonal	Sigma	1:1,000
Hsp104p	Rabbit polyclonal	abcam	1:4,000
Hsp42p	Rabbit polyclonal	Johannes Buchner lab	1:4,000
Hsp26p	Rabbit polyclonal	Johannes Buchner lab	1:4,000
HA	Rat monoclonal	Roche	1:1,000
Ubiquitin	Mouse monoclonal	Santa Cruz	1:500
Mouse IgG	Goat polyclonal	Dako	1:1,000
Rabbit IgG	Goat polyclonal	Sigma	1:10,000
Rat IgG	Goat polyclonal	Sigma	1:5,000

II.3 Strains

II.3.1 Bacterial strains

Name	**Genotype**	**Source**
DH5α	F⁻ *endA1 glnV44 thi-1 recA1 relA1 gyrA96 deoR nupG purB20* ϕ80d*lacZ*ΔM15 Δ(*lacZYA-argF*)U169, hsdR17(r_{K}^{-} m_{K}^{+}), λ^{-}	Invitrogen
Rosetta 2 (DE3) pLysS	F⁻ *ompT gal dcm lon*? *hsdS*$_{B}$($r_{B}^{-}m_{B}^{-}$) λ(DE3 [*lacI lacUV5-T7p07 ind1 sam7 nin5*]) [*malB*$^{+}$]$_{K\text{-}12}$(λ^{S}) pLysSRARE[*T7p20 ileX argU thrU tyrU glyT thrT argW metT leuW proL ori*$_{p15A}$](Cm^{R})	Novagen

II.3.2 Yeast strains

Name	Genotype	Source
BY4741	*MATα his3Δ1 leu2Δ0 met15Δ0 ura3Δ0*	EUROSCARF
ltn1Δ	*BY4741 ltn1Δ::KanMX*	EUROSCARF
rqc1Δ	*BY4741 rqc1Δ::KanMX*	EUROSCARF
rqc2Δ	*BY4741 rqc2Δ::KanMX*	EUROSCARF
ltn1Δrqc2Δ	*BY4741 ltn1Δ::KanMX rqc2Δ::LEU2(K. lactis)*	(Choe, Park *et al.* 2016)
rqc1Δrqc2Δ	*BY4741 rqc1Δ::KanMX rqc2Δ::LEU2(K. lactis)*	(Choe, Park *et al.* 2016)
ltn1Δhel2Δ	*BY4741 ltn1Δ::KanMX hel2Δ::loxP*	(Choe, Park *et al.* 2016)
ltn1Δski7Δ	*BY4741 ltn1Δ::KanMX ski7Δ::LEU2(K. lactis)*	Young-Jun Choe
ltn1Δski2Δ	*BY4741 ltn1Δ::KanMX ski2Δ::LEU2(K. lactis)*	Timm Hassemer
ltn1Δski3Δ	*BY4741 ltn1Δ::KanMX ski3Δ::LEU2(K. lactis)*	Young-Jun Choe
ltn1Δski8Δ	*BY4741 ltn1Δ::KanMX ski8Δ::LEU2(K. lactis)*	Young-Jun Choe
ltn1Δxrn1Δ	*BY4741 ltn1Δ::KanMX xrn1Δ::LEU2(K. lactis)*	Timm Hassemer
ltn1Δski7Δdom34Δ	*BY4741 ltn1Δ::KanMX ski7Δ::LEU2(K. lactis) dom34Δ::HIS3MX(S. pombe)*	Young-Jun Choe
ltn1Δski7Δhbs1Δ	*BY4741 ltn1Δ::KanMX ski7Δ::LEU2(K. lactis) hbs1Δ::HIS3MX(S.pombe)*	Young-Jun Choe
SIS1-GFP	*BY4741 sis1Δ::SIS1-GFP-HIS3*	(Huh, Falvo *et al.* 2003)
ltn1Δ SIS1-GFP	*SIS1-GFP ltn1Δ::HphMX*	(Choe, Park *et al.* 2016)
SIS1-HA	*BY4741 sis1Δ::SIS1-HA-HphMX*	(Choe, Park *et al.* 2016)
ltn1Δ SIS1-HA	*SIS1-HA ltn1Δ::KanMX*	(Choe, Park *et al.* 2016)
ltn1Δski7Δ SIS1-HA	*SIS1-HA ltn1Δ::KanMX ski7Δ::LEU2(K. lactis)*	Young-Jun Choe

II.4 Plasmids

Vector	Source
pRS413	(Sikorski and Hieter 1989)
pRS413GAL-Δss-CPY*-GFP	(Park, Kukushkin *et al.* 2013)
pRS413GAL-Δss-CPY*-mCherry	(Park, Kukushkin *et al.* 2013)
pRS413RQC2-RQC2	(Choe, Park *et al.* 2016)
pRS413RQC2-rqc2$_{aaa}$	(Choe, Park *et al.* 2016)
pRS415-P$_{HSE}$-lacz	Dennis Thiele lab
pRS415GAL-HA-SIS1	(Park, Kukushkin *et al.* 2013)
pRS416	(Sikorski and Hieter 1989)
pRS416GAL-2xmyc-Luc	(Choe, Park *et al.* 2016)
pRS416GAL-2xmyc-NS-Luc	(Choe, Park *et al.* 2016)
pRS416GAL-GFP-s	(Choe, Park *et al.* 2016)
pRS416GAL-GFP-s-K$_{12}$	(Choe, Park *et al.* 2016)
pRS416GAL-GFP-s-K$_{20}$	(Choe, Park *et al.* 2016)
pRS416GAL-GFP-s*	(Choe, Park *et al.* 2016)
pRS416GAL-GFP-s*-K$_{20}$	(Choe, Park *et al.* 2016)
pRS416GAL-GFP-s-mCherry	(Choe, Park *et al.* 2016)
pRS416GAL-GFP-s-K$_{20}$-mCherry	(Choe, Park *et al.* 2016)
pRS416GAL-GFP-s-R3$_{RARE}$	Timm Hassemer
pRS416GAL-GFP-s-R4$_{RARE}$-mCherry	(Choe, Park *et al.* 2016)
pRS416GAL-GFP-s-R20$_{RARE}$-mCherry	(Choe, Park *et al.* 2016)
pRS416GAL-GFP-s-R20$_{FREQ}$-mCherry	(Choe, Park *et al.* 2016)
pRS416GAL-GFP-s-R20$_{FREQ}$-R4$_{RARE}$-mCherry	(Choe, Park *et al.* 2016)

pRS416GAL-GFP-s-$(AT)_6$	(Choe, Park *et al.* 2016)
pRS416GAL-GFP-s-K_{20}-$(AT)_6$	(Choe, Park *et al.* 2016)
pRS416GAL-GFP-s-K_{20}-$(GS)_6$	(Choe, Park *et al.* 2016)
pRS416GAL-RQC2-2xFLAG	Young-Jun Choe
pRS416GAL-$rqc2_{aaa}$-2xFLAG	Young-Jun Choe
pRS316CUP-RNQ1-GFP	(Choe, Park *et al.* 2016)
YEplac181CUP-His_6-ubiquitin	(Scazzari, Amm *et al.* 2015)
pGEX-6P-1-GFP-s	Timm Hassemer
pGEX-6P-1-GFP-s-K_{20}	Timm Hassemer
pGEX-6P-1-GFP-s-$(AT)_{10}$	Timm Hassemer
pGEX-6P-1-GFP-s-K_{20}-$(AT)_{10}$	Timm Hassemer

II.5 Media and buffers

II.5.1 Media

Medium	Composition	Comment
LB	1 % (w/v) tryptone 0.5 % (w/v) yeast extract 170 mM NaCl	Standard medium for bacterial growth
SOB	2 % (w/v) tryptone 0.5 % (w/v) yeast extract 10 mM NaCl 2.5 mM KCl 10 mM $MgCl_2$ (add after autoclaving) 10 mM $MgSO_4$ (add after autoclaving)	Improved bacterial growth medium for preparation of chemocompetent cells
TB	1.2 % (w/v) tryptone 2.4 % (w/v) yeast extract 0.5 % (v/v) glycerol 90 mM K-phosphate pH 7.5 (add after autoclaving)	Rich bacterical growth medium for expression and purification of recombinant proteins
YPD	2 % (w/v) peptone 1 % (w/v) yeast extract 2 % (w/v) glucose (add after autoclaving)	Standard medium for yeast growth

SC	0.67 % (w/v) yeast nitrogen base w/o amino acids 0.2 % (w/v) amino acid dropout mix	Defined medium for yeast growth and expression of recombinant proteins
	If required (add after autoclaving): 55.3 mg/L adenine 22.4 mg/L uracil 219 mg/L leucine 62.85 mg/L histidine 180.26 mg/L lysine 82 mg/L tryptophane	Supplements added as required by presence or absence of auxotrophic markers
	2 % (w/v) glucose or 2 % (w/v) raffinose or 2 % (w/v) raffinose 3 % (w/v) galactose	Repression of P_{GAL1} Derepression of P_{GAL1} Induction of P_{GAL1}
Amino acid dropout mix	5 g of each of the following L-amino acids: alanine, arginine, asparagine, aspartic acid, cysteine, glutamine, glutamic acid, glycine, isoleucine, methionine, phenylalanine, proline, serine, threonine, tryptophane, tyrosine 5 g myo-inositol 0.5 g p-aminobenzoic acid	Grind to homogeneity in a mortar and store at room temperature

II.5.2 Buffers

Buffer	**Composition**		
Yeast Alkaline Lysis Buffer	1.85	M	NaOH
(freshly prepared)	1	M	β-mercaptoethanol
Yeast IP Lysis Buffer	25	mM	Tris-HCl pH 7.4
	150	mM	NaCl
	1	mM	EDTA
	5	% (v/v)	Glycerol
	cOmplete protease inhibitor (freshly added)		
Yeast IP Wash Buffer	25	mM	Tris-HCl pH 7.4
	150	mM	NaCl
	1	mM	EDTA
	5	% (v/v)	Glycerol
	0.5	% (v/v)	NP40
Yeast Sucrose Gradient Lysis Buffer	10	mM	Tris-HCl pH 7.5
	100	mM	NaCl
	30	mM	$MgCl_2$
	1	mM	DTT (freshly added)
	100	µg/ml	CHX (freshly added)
	cOmplete protease inhibitor (freshly added)		

7 % Sucrose Gradient Solution	40	mM	Tris-acetate pH 7.0
	50	mM	NH_4Cl
	12	mM	$MgCl_2$
	7	% (w/v)	Sucrose
	1	mM	DTT (freshly added)
	100	µg/ml	CHX (freshly added)
47 % Sucrose Gradient Solution	40	mM	Tris-acetate pH 7.0
	50	mM	NH_4Cl
	12	mM	$MgCl_2$
	47	% (w/v)	Sucrose
	1	mM	DTT (freshly added)
	100	µg/ml	CHX (freshly added)
HU Buffer	200	mM	Tris-HCl pH 6.8
	8	M	Urea
	5	% (w/v)	SDS
	1	mM	EDTA
	100	mM	DTT (freshly added)
	0.01	% (w/v)	Bromophenol blue

MOPS-SDS Running Buffer for SDS-PAGE	50	mM	Tris-base
	50	mM	MOPS
	0.1	% (w/v)	SDS
	1	mM	EDTA
Towbin Transfer Buffer	50	mM	Tris-base
	192	mM	Glycine
	0.1	% (w/v)	SDS
	20	% (v/v)	Methanol
5x SDD-AGE Sample Buffer	250	mM	Tris-HCl pH 6.8
	10	% (w/v)	SDS
	50	% (v/v)	Glycerol
	0.5	% (w/v)	Bromophenol blue
SDD-AGE Running Buffer	40	mM	Tris-base
	20	mM	Acetic acid
	1	mM	EDTA
	0.1	% (w/v)	SDS
SDD-AGE Transfer Buffer	50	mM	Tris-HCl pH 7.5
	150	mM	NaCl

PBS-T	25	mM	Na-phosphate pH 7.4
	150	mM	NaCl
	0.05	% (v/v)	Tween 20
Blocking Buffer	25	mM	Na-phosphate pH 7.4
	150	mM	NaCl
	0.05	% (v/v)	Tween 20
	5	% (w/v)	Milk powder
Stripping Buffer	62.5	mM	Tris-HCl pH 6.8
	100	mM	β-mercaptoethanol
	2	% (w/v)	SDS
TAE	40	mM	Tris-base
	20	mM	Acetic acid
	1	mM	EDTA
TfB I	30	mM	K-acetate pH 7.5
	100	mM	$RbCl_2$
	50	mM	$MnCl_2$
	10	mM	$CaCl_2$
	15	% (v/v)	Glycerol

TfB II	10	mM	MOPS-NaOH pH 6.8
	10	mM	$RbCl_2$
	75	mM	$CaCl_2$
	15	% (v/v)	Glycerol
TE Buffer	10	mM	Tris-HCl pH 7.5
	1	mM	EDTA
TEL Buffer	10	mM	Tris-HCl pH 7.5
	1	mM	EDTA
	100	mM	Lithium acetate
PLATE Solution	10	mM	Tris-HCl pH 7.5
	1	mM	EDTA
	100	mM	Lithium acetate
	40	% (w/v)	PEG 3,350
Yeast DNA Isolation Buffer	10	mM	Tris-HCl pH 8.0
	100	mM	NaCl
	1	mM	EDTA
	1	% (w/v)	SDS
	2	% (v/v)	Triton X-100

Bacterial Lysis Buffer	50	mM	Na-phosphate pH 8.0
	100	mM	NaCl
	10	% (v/v)	Glycerol
	1	mM	DTT (freshly added)
	2	mg/mL	Lysozyme (freshly added)
	5	U/mL	Benzonase (freshly added)
	1	% (w/v)	Triton X-100
	cOmplete protease inhibitor (freshly added)		
Bacterial Wash Buffer 1	50	mM	Na-phosphate pH 8.0
	1	M	NaCl
	10	% (v/v)	Glycerol
	1	mM	DTT (freshly added)
	1	% (w/v)	Triton X-100
Bacterial Wash Buffer 2	50	mM	Na-phosphate pH 8.0
	100	mM	NaCl
	10	% (v/v)	Glycerol
	1	mM	DTT (freshly added)
	1	% (w/v)	Triton X-100

Bacterial Elution Buffer	50	mM	Na-phosphate pH 8.0
	100	mM	NaCl
	10	% (v/v)	Glycerol
	1	mM	DTT (freshly added)
	1	% (w/v)	Triton X-100
	20	mM	Reduced glutathione (freshly added)
Dialysis Buffer	20	mM	Tris-HCl pH 8.0
	150	mM	KCl
	100	µM	EDTA
	10	% (v/v)	Glycerol
	100	µM	DTT (freshly added)

II.6 Materials and instruments

II.6.1 Kits and consumables

Name	Vendor
β-Galactosidase Assay Kit	Agilent
Pierce Coomassie Plus (Bradford) Protein Assay Kit	Invitrogen
Pierce BCA Protein Assay Kit	Invitrogen
μMACS GFP/HA Isolation Kit	Miltenyi Biotec
Q5 Site-Directed Mutagenesis Kit	NEB
Wizard SV Gel and PCR Clean-up System	Promega
QIAprep Spin Miniprep Kit	Qiagen
Rapid DNA Ligation Kit	Roche
Pierce High pH Reversed-Phase Peptide Fractionation Kit	Thermo Fisher Scientific

II.6.2 Instruments

Name	Vendor
51708TS Fridge	AEG
Sonorex RK100 ultrasonic bath	Bandelin
Allegra X-15R Centrifuge + SX4750 rotor	Beckman Coulter
Avanti J-25I Centrifuge + JA-14 rotor	Beckman Coulter
J6-MI Centrifuge + JS 4.2 rotor	Beckman Coulter
Optima L-90K Ultracentrifuge + SW41 rotor	Beckman Coulter
Optima MAX-XP Ultracentrifuge + TLA 120.2 rotor	Beckman Coulter
Gradient Master	Biocomp
PGF ip Piston Gradient Fractionator	Biocomp

T3 Thermocycler	Biometra
(Wide) Mini-Sub Cell GT Cell DNA electrophoresis system	Bio-Rad
ChemiDoc XRS Imaging system	Bio-Rad
Econo UV Monitor	Bio-Rad
Mini Trans-Blot Cell	Bio-Rad
PowerPac 300 power supply	Bio-Rad
PipetAid XP	Drummond Scientific
Sky Line Shaker DRS-12	Elmi
BioSpectrometer kinetic	eppendorf
Centrifuge 5424/5415 R	eppendorf
Research (2.5/10/20/100/200/1000 µL) and Research Plus multi-channel (10 µL) pipettes	eppendorf
Thermomixer comfort	eppendorf
biostep ViewPix 700 Gel Scanner	Epson
LAS-3000 Imaging System	Fujifilm
FC203B Fraction Collector	Gilson
LaminAir HA2448GS sterile hood	Heraeus
Genie Blotter	Idea Scientific
RCT basic magnetic stirrer	IKA
Fireboy	Integra
SafeImager 2.0	Invitrogen
Type B Waterbath	LAUDA
Wavedom Microwave	LG Electronics
Premium NoFrost Freezer	Liebherr
AB265-5/FACT precision scale	Mettler Toldeo
M200L ice machine	Microcubes

Reference A+ Milli-Q Water Dispenser	Millipore
Magnetic rack	Miltenyi Biotec
Sonicator Ultrasonic Processor XL	Misonix
FastPrep-24 bead beater	MP Biomedicals
innova 40 incubator shaker series	New Brunswick Scientific
U570 Ultra-Low Temperature High Efficiency Freezer	New Brunswick Scientific
MC6 Centrifuge	Sarstedt
CP3202 P scale	Sartorius
Vortex Genie 2	Scientific Industries
Rotator SB3	Stuart
See-saw rocker SSL4	Stuart
EASY-nLC 1000 nano liquid chromatography system	Thermo Fisher Scientific
NanoDrop One Spectrophotometer	Thermo Fisher Scientific
Q-Exactive orbitrap mass spectrometer	Thermo Fisher Scientific
Savant SPD-121P SpeedVac Concentrator	Thermo Fisher Scientific
XCell SureLock Mini-Cell Electrophoresis System	Thermo Fisher Scientific
Lourmat Quantum Imaging System	Vilber
inoLab pH meter	WTW Series
Axiovert 200M Inverted Fluorescence Microscope	Zeiss

II.7 Molecular biology

II.7.1 DNA quantification

Concentration and purity of DNA samples were measured by UV spectroscopy at a wavelength of 260 nm under the assumption that one absorption unit corresponds to 50 ng/µL dsDNA. Nuclease-free water or elution buffer (Qiagen) served as a reference. The A_{260}/A_{280} ratio was also measured to check for protein contaminants in the sample, where a value of 1.85 or higher indicated negligible contamination.

II.7.2 Agarose gel electrophoresis

1.2 % (w/v) agarose gels were prepared by melting agarose in TAE buffer until the agarose was completely dissolved. SYBR Safe DNA gel stain was added at a final dilution of 1:10,000 to visualize DNA bands. For analytical agarose gels, 5 µL of DNA sample were mixed with 1 µL 6x DNA loading dye and 5 µL were loaded on the gel. For preparative agarose gels, the whole PCR or restriction digest mixture (typically 50 µL) was mixed with 10 µL 6x DNA loading dye and the whole sample was loaded on the gel. Gel electrophoresis was performed at a constant voltage of 110 V in TAE buffer until the lower dye front had migrated approximately 60 % towards the bottom end of the gel.

II.7.3 DNA sequencing

DNA sequencing was performed by eurofins Genomics (Ebersberg, Germany). Premixed samples containing 1 µg purified plasmid DNA and 20 pmol of the respective primer in a total volume of 17 µL were prepared and submitted for sequencing.

II.7.4 Purification of DNA fragments and plasmid DNA

For purification of linear dsDNA fragments from PCR amplifications or out of excised agarose gel bands, the Wizard SV Gel and PCR Clean-Up Kit was used according to the manufacturer's instructions.

For purification of plasmid DNA, 5 mL LB medium supplied with 100 µg/mL Ampicillin were inoculated with *E. coli* DH5α cells harboring the respective plasmid and the culture was grown overnight at 37 °C with shaking. The next morning, cells were harvested by centrifugation at 4,000 x g for 10 minutes and plasmid DNA was isolated using the QIAprep Spin Miniprep Kit according to the manufacturer's instructions.

II.7.5 Polymerase chain reaction

PCR was used for the amplification of defined DNA fragments. To this end, the Herculase II Fusion DNA Polymerase was used according to the manufacturer's instructions for all PCR-based applications. A comprehensive list of primers can be found in section VI. Typically, a PCR reaction consisted of 30 repetitive cycles of denaturation, primer annealing and elongation. The annealing temperature was calculated by subtracting 5 °C from the primer melting temperature, which was in turn calculated using Thermo Fisher Scientific's "Multiple Primer Analyzer" online tool. Primers were designed with melting temperatures in between 52 – 58 °C and with a maximum difference of 3 °C.

II.7.6 Restriction digest and DNA ligation

For enzymatic digestion of plasmid DNA or PCR fragments, typically 5 µg of purified plasmid DNA or PCR product were used. The DNA was incubated with 10 U of the respective restriction enzyme(s) in 1X CutSmart buffer in a total reaction volume of 50 µL at 37 °C for 2 hours. After digestion, the reaction was subjected to agarose gel electrophoresis, the corresponding band was cut out and the DNA fragment was isolated by using the Wizard SV Gel and PCR Clean-Up Kit.

For DNA ligation, the Rapid DNA ligation kit was used according to the manufacturer's instructions with minor modifications. Briefly, 50 ng of vector DNA was mixed with insert DNA at a molar ratio of 1:5 in a total volume of 10 µL. An equal amount of 2X ligation buffer and 1 µL of DNA ligase were added and the reaction was incubated at room temperature for 15 minutes. 2 µL of the ligation reaction were transformed into chemocompetent *E. coli* DH5α cells.

II.7.7 Sequence- and ligation-independent cloning

For the construction of bacterial expression vectors, the method of sequence- and ligation-independent cloning was used, which exploits the exonucleolytic activity of T4 DNA Polymerase in the absence of dNTPs (Li and Elledge 2007).To this end, the gene of interest was amplified by PCR using primers with 20 bp homology to the regions flanking the insertion site in the target bacterial expression vector. Meanwhile, the target vector was digested with a conventional restriction enzyme cutting at the insertion site. After purification of both linearized vector and insert DNA, 1 µg of each fragment was treated with 0.5 U T4 DNA polymerase at 22 °C for 30 minutes in a total reaction volume of 20 µL. The reaction was stopped by adding dCTP to a final concentration of 1 mM. 100 ng of vector and the respective amount of insert DNA were mixed in a molar ratio of 1:2 in 1X ligation buffer and incubated at 37 °C for 30 minutes in a total reaction volume of 10 µL. 5 µL of the ligation reaction were transformed into chemocompetent *E. coli* DH5α cells.

II.7.8 Site-directed mutagenesis

To introduce mutations or to delete or substitute specific regions within a construct, the Q5 site-directed mutagenesis kit was used according to the manufacturer's instructions. Briefly, appropriate primers were designed using the "NEBaseChanger" online tool and a PCR was performed using the respective template DNA and the Q5 High Fidelity Polymerase Master Mix. Then, digestion of methylated template DNA, 5'-phosphorylation, and ligation of the amplified

DNA fragment were carried out in a single step using the provided KLD reagent. The reaction was then transformed into chemocompetent *E. coli* DH5α cells.

II.7.9 Preparation and transformation of chemocompetent *E. coli* cells

Chemocompetent *E. coli* DH5α and SURE cells were prepared using the RbCl method (Hanahan 1983). Briefly, cells were grown to mid-log phase (OD_{600} ≈ 0.5) in SOB medium, chilled on ice for 15 minutes and then harvested by centrifugation at 4,000 x g for 15 minutes at 4 °C. The cell pellet was resuspended in 16 mL TfB 1 buffer, chilled on ice for 15 minutes and centrifuged again at 4,000 x g for 15 minutes at 4 °C. Cells were resuspended in 4 mL TfB 2 buffer, chilled on ice for 15 minutes and 100 µL aliquots were prepared on dry ice in prechilled Eppendorf tubes. Cells were immediately frozen at -80 °C until further use.

For transformation, aliquots of competent cells were thawed on ice. Approximately 100 ng of plasmid DNA or 2 µL of ligation reaction were added and the cell suspension was gently mixed with the pipette tip. Cells were incubated on ice for 20 minutes, followed by a heat shock at 42 °C in a waterbath for exactly 45 seconds and incubation on ice for 2 minutes. 300 µL LB medium were added to the cell suspension, the mixture was incubated at 37 °C for 45 minutes and then plated on LB agar plates containing the appropriate antibiotic.

II.7.10 Preparation and transformation of chemocompetent *S. cerevisiae* cells

Chemocompetent *S. cerevisiae* cells were prepared freshly at the day of transformation using the LiOAc/single-stranded carrier DNA/PEG method (Gietz and Woods 2002). Briefly, yeast cells were grown to mid-log phase (OD_{600} ≈ 0.8) in YPD medium at 30 °C with shaking and 2.5 OD_{600} of cells were harvested per transformation reaction by centrifugation at 4,000 x g for 5 minutes. Cells were washed once with 1 mL of TE buffer and then resuspended in 100 µL of TEL buffer. In the meantime, single stranded Herring Sperm DNA was boiled at 95 °C for 10 minutes and immediately put on ice. 5 µL of the denatured Herring Sperm DNA and 1 – 5 µg of plasmid DNA or PCR product were added to the yeast cell suspension. Next, 700 µL of PLATE solution were

added and the sample was thoroughly mixed by vortexing. Samples were then incubated at 30 °C for 1 hour, followed by a heat shock at 42 °C for 20 minutes in waterbaths, respectively. Cells were pelleted by centrifugation at 16,000 x g for 2 minutes, the supernatant was discarded and the cell pellet was resuspended in 100 µL nuclease-free water. Cells were plated on appropriate selective medium agar plates and incubated at 30 °C for 2 – 3 days.

II.7.11 Construction of mutant *S. cerevisiae* strains

For the generation of mutant yeast knockout strains that were not available through the EUROSCARF yeast deletion library, a method was used that is based on the integration of PCR-amplified selective marker cassettes into the yeast genome by homologous recombination (Baudin, Ozier-Kalogeropoulos *et al.* 1993)**.** To this end, the appropriate marker cassette was amplified by PCR using a plasmid carrying the respective marker as a template. By using respective primers, the final PCR product also carried short flanking sequences of 45 bp that were homologous to the flanking regions of the gene that was to be deleted. After purification, the PCR product was transformed into chemocompetent yeast cells and the transformed cells were plated on agar plates with the appropriate selective medium. After 4 - 5 days of incubation, several big colonies were picked, genomic DNA was isolated and the correct integration of the marker cassette was verified by PCR using primers that were specific for the flanking regions of the deleted gene and for the marker cassette.

II.7.12 Isolation of genomic DNA from *S. cerevisiae*

For isolation of genomic DNA from yeast cells, 10 mL YPD medium were inoculated with BY4741 cells and grown to saturation at 30 °C with shaking. Cells were harvested by centrifugation at 4,000 x g for 10 minutes and washed once with water. Cells were then resuspended in 300 µL yeast DNA isolation buffer. 300 µL of a mixture of phenol, chloroform and isoamyl alcohol (25:24:1) and 300 µL glass beads were added and cells were lysed using a bead beater (3 cycles of 60 seconds each on intensity level 6.5 with 60 seconds incubation on ice between two cycles).

200 µL TE buffer were added and the sample was vortexed for 15 seconds, followed by centrifugation at 16,000 x g for 5 minutes. The top aqueous layer was transferred to a new tube and 1 mL ethanol p.a. was added to the sample. After thorough mixing by inversion, the sample was incubated at -20 °C for 30 minutes and then centrifuged at 16,000 x g for 10 minutes. The supernatant was discarded and the pellet resuspended in 400 µL TE with 75 ng/ µL RNase A, followed by incubation at 37 °C for 15 minutes to degrade RNA contaminants. DNA was precipitated by adding 10 µL 3 M sodium acetate pH 5.2 and 1 mL ethanol p.a. and mixing the sample by inverting the tube several times. After centrifugation at 16,000 x g for 10 minutes, the supernatant was discarded, the pellet was air dried, washed once with 70 % (v/v) ethanol, air dried again and resuspended in 50 µL TE buffer.

II.8 Expression and purification of proteins

II.8.1 Expression of proteins in *E. coli*

Recombinant GST fusion proteins were expressed in *E. coli* Rosetta 2 (DE3) pLysS cells by induction of the *lac* operon. These cells are harboring an additional plasmid coding for several tRNAs that are rarely used in bacteria, which makes them suitable for the expression of eukaryotic proteins.

For each construct, 1 L of TB medium supplied with 100 µg/mL Ampicillin and 34 µg/mL Chloramphenicol was inoculated with cells from an overnight culture to an optical density of $OD_{600} \approx 0.02$. Cultures were incubated at 37 °C with shaking until an optical density of $OD_{600} \approx 0.7$ was reached. Protein expression was induced by the addition of IPTG to a final concentration of 0.5 mM, the incubation temperature was shifted to 30 °C and cultures were kept shaking for 3 more hours. Cells were then harvested by centrifugation at 4,000 x g for 15 minutes at 4 °C and cell pellets were stored at -80 °C.

II.8.2 Purification of proteins expressed in *E. coli*

Cells were resuspended in 25 mL bacterial lysis buffer, incubated for 30 minutes at 4 °C on a rotator, and lysed by sonication (10 % amplitude, 5 cycles of 2.5 minutes and intervals of 30 seconds). The resulting lysate was cleared by centrifugation at 30,000 x g for 30 minutes at 4 °C and the supernatant was incubated with 2.5 mL of preequilibrated glutathione-agarose beads for 30 minutes at 4 °C on a rotator. The slurry was filled into disposable gravity flow columns and the agarose beads were washed 4 times with 20 mL bacterial wash buffer 1, followed by a washing step with 10 mL of bacterial wash buffer 2. GST fusion proteins were then eluted with 20 mL of bacterial elution buffer. 2 mL fractions were collected and analyzed by SDS-PAGE. Fractions containing detectable amounts of the GST fusion proteins were pooled and dialyzed overnight in 2 L dialysis buffer per construct at 4 °C. The next day, the buffer was replaced with 2 L of fresh dialysis buffer, samples were dialyzed for 8 more hours, the buffer was again replaced and the samples again dialyzed overnight. The next day, the protein concentration of the purified GST fusion proteins was determined using the Pierce BCA Protein Assay Kit according to the manufacturer's instructions. Samples were diluted to a concentration of 2 µM, aliquots of 100 µL were prepared, flash-frozen in liquid nitrogen and stored at -80 °C.

II.8.3 Expression of proteins in *S. cerevisiae*

Proteins were overexpressed in *S. cerevisiae* under control of the regulatable *GAL1* promoter, which allows for tight repression or strong induction of protein expression depending on the presence or absence of glucose or galactose in the growth medium, respectively. Typically, a fresh colony was picked from a plate, resuspended in 3 mL of the respective dropout medium containing 2 % (w/v) glucose and the culture was grown to saturation overnight at 30 °C with shaking. The next day, 20-50 µL of the culture were used to inoculate 3 mL of dropout medium supplied with 2 % (w/v) raffinose, and the culture was again grown to saturation. Finally, 50-100 mL of dropout medium containing 2 % (w/v) raffinose and 3 % (w/v) galactose were inoculated with cells from the raffinose culture to produce an initial optical density of $OD_{600} \approx 0.02$ and to induce protein expression. Cultures were then incubated at 30 °C with shaking for

approximately 16-18 hours until cells reached mid-log phase, which corresponds to an optical density of ≈ 0.8. Cells were harvested by centrifugation at 4,000 x g for 10 minutes at 4 °C, cell pellets were washed once with 1 mL of cold 30 mM NaN_3, flash-frozen in liquid nitrogen and stored at -80 °C until lysis.

For SILAC experiments, 30 mL of dropout medium containing 2 % (w/v) raffinose and either light, medium or heavy lysine were inoculated with cells from a raffinose culture that was grown to saturation to produce an initial optical density of OD_{600} ≈ 0.02. Cultures were then incubated at 30 °C with shaking for approximately 16-18 hours until cells reached an optical density of ≈ 0.8. 15 OD_{600} of cells were harvested by gentle centrifugation at 1,000 x g for 10 minutes, resuspended in 60 mL of fresh dropout medium, and incubated at 30 °C with shaking for 90 minutes to allow for recovery. Overexpression of Rqc2p under control of the *GAL1* promoter was then induced by the addition of galactose to a final concentration of 3 % (w/v), cultures were incubated for 3 more hours at 30 °C with shaking, and cells were harvested as described above.

II.9 Protein analytics

II.9.1 Preparation of yeast lysates

Yeast lysates were prepared by disrupting the yeast cell wall and membranous structures with glass beads. Typically, approximately 500 µL of 0.5 mm acid washed glass beads and 500 µL of the respective yeast lysis buffer were added to a frozen yeast cell pellet. Cells were then disrupted using a FastPrep-24 bead beater with a CoolPrep adaptor (3 cycles of 60 seconds with intensity 6.5, 60 seconds incubation on ice between each cycle). Unbroken cells, glass beads and cellular debris were removed by centrifugation at 400 x g for 5 minutes and 4 °C. The supernatant was then transferred into a new tube and centrifuged twice at 2,000 x g for 5 minutes at 4 °C to yield the final lysate.

II.9.2 Protein quantification

To determine the total protein concentration of a precleared lysate or of purified GST fusion proteins, the Pierce Coomassie Plus (Bradford) Assay Kit or the Pierce BCA Protein Assay Kit were used according to the manufacturer's instructions, respectively. A dilution series of BSA in the respective buffer was used to generate a calibration curve. Typically, 30 µL of a 1:100 dilution of lysate were mixed with 1 mL of the Bradford reagent and samples were incubated for 10 minutes at room temperature before measuring the absorbance at 595 nm. In case of the BCA protein assay kit, 50 µL of the purified protein sample were mixed with 1 mL of the BCA reagent and samples were incubated for 30 minutes at 37 °C before measuring the absorbance at 562 nm.

II.9.3 Trichloroacetic acid precipitation

In order to concentrate proteins from a dilute solution for subsequent SDS-PAGE analysis, a TCA precipitation was performed. Briefly, protein samples were incubated on ice for 15 minutes after addition of sodium deoxycholate to a final concentration of 0.02 % (w/v). Subsequently, TCA was added to a final concentration of 10 % (v/v) and samples were further incubated on ice for 60 minutes. Precipitated proteins were then sedimented by centrifugation at 16,000 x g for 30 minutes at 4 °C. The supernatant was discarded, the pellet was washed once with 1 mL of -20 °C acetone and the sample was again centrifuged at 16,000 x g for 5 minutes at 4 °C. The supernatant was aspirated, the pellet was air dried and dissolved in HU buffer by incubation at 70 °C for 10 minutes with shaking.

II.9.4 Sodium dodecyl sulfate polyacrylamide gel electrophoresis

To separate proteins based on their molecular weight, NuPAGE 4-12 % Bis-Tris gradient gels with 1X MOPS-SDS running buffer were used. Typically, 30 µg protein sample were loaded and electrophoresis was performed at a constant voltage of 180 V until the dye front reached the bottom of the gel.

II.9.5 Semidenaturing-detergent agarose gel electrophoresis

In order to resolve SDS-resistant high molecular weight aggregates that might get trapped in the wells of a polyacrylamide gel, the SDD-AGE method was used with minor modifications (Kryndushkin, Alexandrov *et al.* 2003). Briefly, a 1.5 % (w/v/) agarose gel was prepared with 1X SDD-AGE running buffer. Samples were prepared by mixing lysates with 5X SDD-AGE sample buffer and subsequent incubation of the samples for 10 minutes at room temperature. Typically, 30 µg protein sample were loaded and electrophoresis was performed for 3 hours at a constant voltage of 75 V at 4 °C and with prechilled 1X SDD-AGE running buffer.

II.9.6 Transfer of proteins onto nitrocellulose membranes

After SDS-PAGE, proteins were transferred onto nitrocellulose membranes for subsequent detection via immunoblotting. Transfer was performed at a constant voltage of 70 V for 60 minutes with a cooling pack to prevent overheating. Proteins resolved by SDD-AGE were transferred at a constant voltage of 7 V overnight at 4 °C.

II.9.7 Western blotting

Membranes were first blocked by incubation in blocking buffer for 45 minutes at room temperature to prevent unspecific binding of primary or secondary antibodies. Membranes were then incubated in blocking buffer containing the primary antibody for 60 minutes at room temperature or overnight at 4 °C using the working dilutions described in section II.2.2. Membranes were then washed twice with PBS-T for 15 minutes and subsequently incubated in blocking buffer containing the respective secondary antibody for 60 minutes at room temperature. Membranes were then washed once with blocking buffer and twice with PBS-T for 10 minutes each and developed using the ECL Western Blotting detection reagent and the LAS-3000 imaging system.

II.9.8 Mass spectrometry analysis of protein samples

II.9.8.1 Isotopic labeling of proteins

For isotopic labeling of proteins for subsequent SILAC analysis, cells were grown as described in section II.7.3 in the respective dropout medium supplied with either normal L-lysine, [4,4,5,5-D4]L-lysine or [$^{13}C_6$,$^{15}N_2$]L-lysine at a final concentration of 150 µg/mL. Typically, the control was labeled with normal, light (L) L-lysine, [4,4,5,5-D4]L-lysine served as medium (M) lysine and produced a mass shift of 4 Da, and [$^{13}C_6$, $^{15}N_2$]L-lysine served as heavy (H) lysine, generating a mass shift of 8 Da. During each experiment, 10 µg of each labeled lysate were kept aside, processed as described in section II.8.13.3 without mixing, and separately analyzed to check for efficient incorporation of the labeled amino acids.

II.9.8.2 In-gel digestion

Following immunoprecipitation of genomically tagged Sis1-HA, eluates containing light-, medium- and heavy-labeled proteins were mixed 1:1:1 and 100 µL of the mixture were resolved by SDS-PAGE. Gels were stained in 0.1 % (w/v) Coomassie R250, 10 % (v/v) acetic acid for 20 minutes, fixed in 30 % (v/v) methanol, 10 % (v/v) acetic acid for 30 minutes and then destained in 8.5 % (v/v) acetic acid. The region between the sample well and the 170 kDa marker band containing SDS-resistant aggregates was cut out with a clean scalpel blade, transferred to Protein LoBind tubes and cut into cubes of 1 mm side length. Reduction, alkylation and digestion of proteins in the gel pieces was carried out as described in (Shevchenko, Wilm *et al.* 1996). After extraction, peptides were dried in a vacuum concentrator, dissolved in 100 µL 0.1 % (v/v) trifluoroacetic acid and subjected to desalting using Bond Elut OMIX C_{18} pipette tips according to the manufacturer's instructions. Peptides were eluted in 100 µL 0.1 % (v/v) trifluoroacetic acid, 70 % (v/v) acetonitrile, dried in a vacuum concentrator and stored at -20 °C until analysis.

II.9.8.3 Filter-aided sample preparation

For total protein analysis, protein lysates labeled with light, medium or heavy L-lysine were reduced and denatured by adding DTT and SDS to final concentrations of 1 mM and 2 % (w/v), respectively. Samples were then boiled for 5 minutes at 95 °C and mixed 1:1:1. Protein reduction, alkylation and digestion was then carried out in Vivacon 10 kDa ultrafiltration devices as described in (Wisniewski, Zielinska *et al.* 2011). Peptides were dried in a vacuum concentrator after extraction, dissolved in 300 µL 0.1 % (v/v) trifluoroacetic acid, and fractionated using the Pierce High pH Reversed-Phase Peptide Fractionation Kit to reduce sample complexity. After fractionation, peptides were again dried in a vacuum concentrator and stored at -20 °C until analysis.

II.9.8.4 LC-MS/MS analysis of peptides

All peptides were analyzed using an EASY-nLC 1000 nano liquid chromatography system with a home-made 25 cm silica reversed-phase capillary column packed with 1.9 µm ReproSil-Pur C_{18}-AQ coupled to a Q-Exactive orbitrap mass spectrometer. To this end, peptides were dissolved in 6 µL of 5 % (v/v) formic acid, sonicated for 5 minutes and loaded on the column by using a nLC autosampler at a flow rate of 0.5 µL/min. Peptides were separated by a stepwise 120-minute gradient of 0-95 % between 0.2 % (v/v) formic acid in H_2O and 0.2 % (v/v) formic acid in acetonitrile at a flow rate of 0.25 µL/min. MS/MS analysis was performed with standard settings using cycles of 1 high resolution (70,000 full width at half maximum (FWHM) setting) MS scan followed by MS/MS scans of the 10 most intense ions with charge states of +2 or higher at a resolution setting of 17,500 FWHM. Protein identification and SILAC based quantitation was performed with MaxQuant (version 1.3.0.5) using default settings. The UNIPROT *S. cerevisiae* database (version 2013-12-05) was used for protein identification. MaxQuant uses a decoy version of the specified UNIPROT database to adjust the false discovery rates for proteins and peptides to below 1%. Proteins that were enriched ≥ 2-fold in at least two out of three independent experiments were defined as interactors.

II.10 Functional *in vivo* and *in vitro* assays

II.10.1 Protein expression analysis

For determination of the steady-state level of a protein, yeast lysates were prepared in yeast IP lysis buffer and normalized to a total protein concentration of 20 mg/mL. 5 µL of lysate were mixed with 45 µL HU buffer, samples were incubated for 10 minutes at 70 °C and 15 µL resolved by SDS-PAGE. After transfer of proteins onto a membrane, proteins of interest were detected by immunoblotting. Immunoblotting against Pgk1p served as a loading control. Band intensities were quantified densitometrically with correction for background and loading control signals.

II.10.2 Immunoprecipitation

For immunoprecipitation of reporter constructs or tagged proteins from crude lysates, the epitope-tagged protein isolation kit was used according to the manufacturer's instructions with minor modifications. Yeast lysates were prepared in yeast IP lysis buffer, 100 µg total protein were mixed with HU buffer to a final volume of 50 µL, and DTT was added to a final concentration of 100 mM. Samples were incubated for 10 minutes at 70 °C with shaking, and kept aside as an input control. Lysis buffer was added to 2 mg total protein to a final volume of 950 µL, and NP40 was added to a final concentration of 0.5 % (v/v). 50 µL of the respective microbeads were added, and samples were incubated for 60-90 minutes at 4 °C on a rotator. The sample was subsequently loaded on a µMACS column equilibrated with 200 µL yeast IP wash buffer, followed by washing the column 4 times with 200 µL yeast IP lysis buffer and once with 100 µL 25 mM Tris-HCl pH 7.4. Bound proteins were eluted by first applying 20 µL of preheated HU buffer without DTT, waiting for 5 minutes and then applying 50 µL of preheated HU buffer without DTT while collecting the eluate in a fresh tube. DTT was added to the eluate to a final concentration of 100 mM, the sample was incubated for 5 more minutes at 70 °C with shaking and 10 µL were resolved by SDS-PAGE.

II.10.3 Protein stability analysis

To test the half-life of a reporter protein in living yeast cells, a cycloheximide chase assay was performed. Yeast cells were grown to mid-log phase, 10 OD_{600} of cells were centrifuged at 4,000 x g for 5 minutes at room temperature and resuspended in 2 mL of fresh dropout medium containing 2 % (w/v) Raffinose, 3 % (w/v) Galactose and 500 µg/mL cycloheximide. 400 µL of the culture were immediately taken and mixed with 500 µL ice-cold 30 mM NaN_3 and incubated on ice for 5 minutes. The cells were then pelleted by centrifugation at 16,000 x g for 2 minutes at room temperature, the supernatant was aspirated and the cells flash-frozen in liquid nitrogen. The culture was meanwhile incubated at 30 °C with shaking and further samples of 400 µL each were taken at the indicated timepoints. Cell pellets were resuspended in 1 mL distilled H2O and 150 µL yeast alkaline lysis buffer and lysed by incubation on ice for 15 minutes with vigorous vortexing for 30 seconds every 5 minutes. The resulting lysates were then subjected to TCA precipitation. The protein pellet was dissolved in 100 µL HU buffer and 15 µL were resolved by SDS-PAGE. Band intensities were quantified densitometrically.

II.10.4 Sucrose density gradient centrifugation

To analyze the sedimentation behavior of a protein in a sucrose density gradient, cells were grown to mid-log phase in the respective dropout medium. Cycloheximide was added to a final concentration of 100 µg/mL, cultures were incubated for 15 more minutes at 30 °C with shaking and then harvested. Lysates were prepared in yeast sucrose gradient lysis buffer and an amount of lysate corresponding to 40 OD_{260} was carefully layered upon a precooled 7-47% sucrose density gradient that had previously been prepared using a Biocomp Gradient Master. Sucrose gradients were centrifuged at 40,000 x rpm (corresponding to an average of 200,000 x g) for 2 hours at 4 °C without braking down the rotor after the run. Gradients were then fractionated into 13 fractions while recording the UV trace at a wavelength of 260 nm using a Biocomp Piston Gradient Fractionator, and 500 µL of every fraction was diluted with an equal volume of distilled H_2O. Subsequently, proteins were TCA precipitated, the protein pellet was dissolved in 50 µL HU buffer and 15 µL of every sample was resolved by SDS-PAGE.

II.10.5 β-Galactosidase assay

To determine the influence of protein overexpression on the cellular heat shock response, a β-Galactosidase assay was performed according to the manufacturer's instructions with minor modifications. Briefly, 400 µg of yeast lysate were mixed with 900 µL of the supplied buffer and brought to a volume of 1 mL with sterile, distilled H_2O. 200 µL of ONPG solution were added and samples were incubated at 37 °C in a waterbath until all samples developed a clear yellow color. Reactions were stopped by adding 500 µL of stop solution and the exact time of incubation was recorded. Subsequently, the absorbance at a wavelength of 420 nm was measured and used to calculate the specific β-Galactosidase activity in each sample, which in turn was a direct measure of the cellular heat shock response.

II.10.6 Yeast growth assay

To reveal cytotoxic effects induced by overexpression of proteins, growth assays were performed. Yeast cells were grown to an optical density of ≈ 0.5 in the respective dropout medium containing 2 % (w/v) Raffinose. An amount of cells corresponding to 0.1 OD_{600} were taken and fresh Raffinose medium was added to a final volume of 1 mL. Five serial 1:5 dilutions of this culture were prepared in sterile, distilled H_2O, 4 µL of every dilution were spotted on the respective dropout medium agar plates containing either 2 % (w/v) Glucose or 2 % (w/v) Raffinose and 3 % (w/v) Galactose, and plates were incubated for 2-3 days at 30 °C or 37 °C.

II.10.7 Live cell fluorescence microscopy

To visualize inclusion bodies in living cells, a Zeiss Axiovert 200M inverted fluorescence microscope was used. Yeast cells were grown to mid-log phase in the respective dropout medium, 2 µL were spotted on a glass microscope slide and covered with a cover slide without trapping any air bubbles in between. A drop of immersion oil was put on the cover slide, the sample was mounted on the microscope and images were acquired.

II.10.8 *In vitro* aggregation of purified GST fusion proteins

To evaluate the aggregation propensity of purified fusion proteins after removal of the highly soluble Glutathion-(S)-Transferase (GST) domain, 3.75 µL of dialysis buffer or 7.5 U of PreScission protease were added to 150 µL of 1.5 µM purified protein and the samples were incubated for 16 hours at 30 °C with shaking at 300 rpm. The next day, samples were mixed with an equal volume of 4 % (w/v) SDS, 100 mM DTT and boiled for 5 minutes at 95 °C. Sample volumes corresponding to 5-75 pmol of purified protein were applied into the wells of a slot blot apparatus with a 0.2 µm cellulose acetate membrane that has been equilibrated in 0.1 % (w/v) SDS. All wells were washed 3 times with 200 µL 0.1 % (w/v) SDS and the membrane was processed as described in section II.8.7 for immunodetection.

III. Results

III.1 Properties of non-stop proteins

In order to determine the consequences of RQC impairment on the aggregation state of NS-proteins, two RQC model substrates were designed by deletion of the canonical stop codon as well as all in-frame stop codons in the 3′ UTR: non-stop green fluorescent protein (NS-GFP) and non-stop firefly luciferase (NS-Luc). These NS-proteins and their respective wild-type (WT) counterparts (GFP and Luc) were expressed in WT-yeast and in yeast lacking Ltn1p. Both NS-GFP and NS-Luc were barely detectable in WT yeast cells, indicating that NS-proteins are subject to rapid degradation (Fig. III.1a, c). In contrast, NS-GFP and NS-Luc strongly accumulated in the absence of Ltn1p and formed SDS-resistant high molecular weight species that were detectable as smears at the upper part of the gel (Fig. III.1a, c). In addition, NS-GFP also formed visible inclusions when expressed in *ltn1*Δ cells, indicating that considerable amounts of at least partially folded NS-protein accumulate in the cytosol upon impairment of the RQC pathway (Fig. III.1b).

To rule out the possibility that the observed high molecular weight species represent a ubiquitinated or otherwise posttranslationally modified form of NS-proteins, NS-GFP was treated with formic acid after immunoprecipitation in order to specifically dissolve aggregates without harming covalently linked modifiers such as ubiquitin. Indeed, the smear observed with NS-GFP disappeared after formic acid treatment, indicating that the high molecular weight species does not represent a ubiquitinated form of NS-GFP (Fig. III.2a). This hypothesis was further supported by the fact that polyubiquitinated NS-Luc was detected in a different region of the gel and only in WT cells, consistent with Ltn1p being the major E3 ligase responsible for ubiquitination of NS-proteins in yeast (Fig. III.2b).

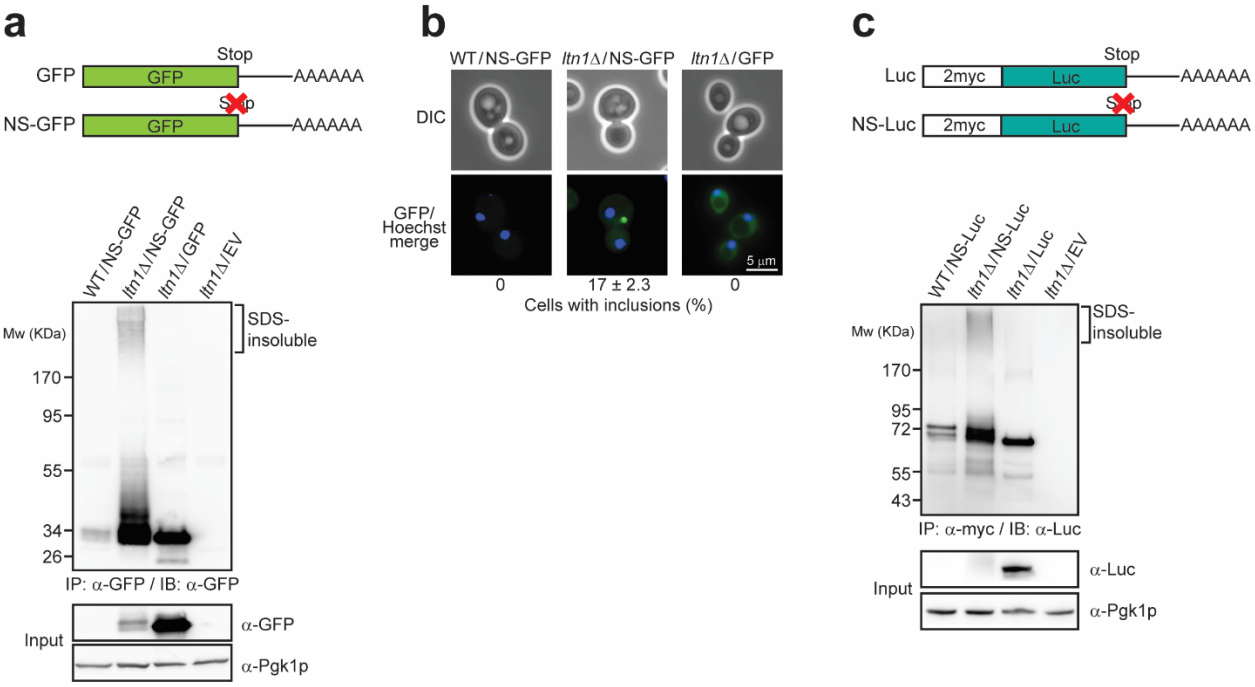

Fig. III.1: NS-proteins form SDS-resistant aggregates and visible inclusions upon deletion of *LTN1*. (a) NS-GFP or GFP were expressed in WT and *ltn1*Δ cells, immunoprecipitated, and detected by immunoblotting against GFP. Pgk1p served as a loading control. EV = empty vector. (b) Cells expressing NS-GFP or GFP were analyzed by fluorescence microscopy, and cells containing visible fluorescent inclusions were counted and expressed as a fraction of total (standard deviation from 3 independent experiments). Nuclei were stained with Hoechst 33342. Exposure time was adjusted for *ltn1*Δ cells expressing GFP to prevent overexposure. Scale bar, 5 μm. (c) Myc-tagged Luc or NS-Luc were expressed in WT and *ltn1*Δ cells, immunoprecipitated, and detected by immunoblotting against Luc. Pgk1p served as a loading control. EV = empty vector. Figure modified from (Choe, Park *et al.* 2016).

Since cells fail to efficiently ubiquitinate NS-proteins when RQC is defective, and given that extraction of the faulty nascent chain by Cdc48p relies on ubiquitination, we reasoned that a substantial fraction of NS-proteins might still be bound to the ribosome while aggregating in the absence of Ltn1p. Surprisingly, sucrose density gradient centrifugation revealed that, despite inefficient ubiquitylation, NS-GFP is still released from the ribosome (Fig. III.3). Furthermore, the SDS-resistant high molecular weight species is substantially smaller in size than ribosomes, indicating that the observed smear represents SDS-resistant oligomers that coexist with visible inclusions (Fig. III.1b, Fig. III.3).

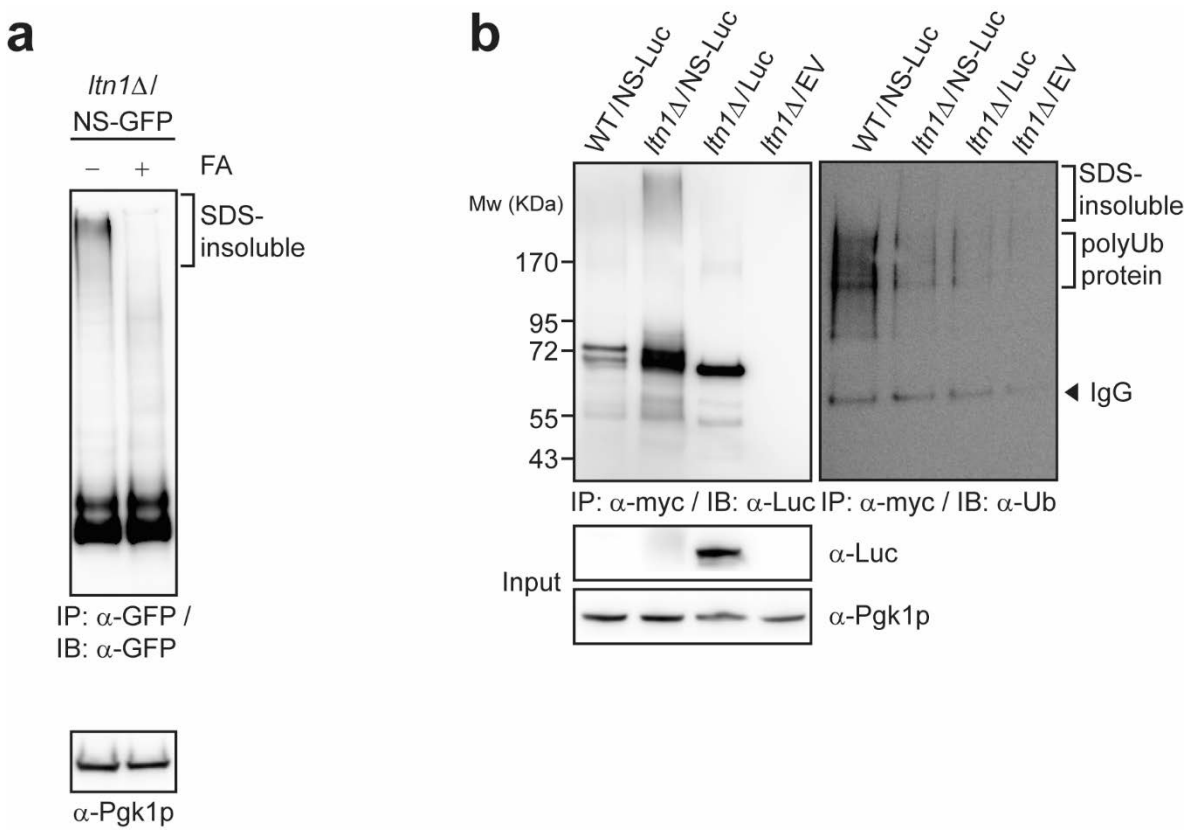

Fig. III.2: High molecular weight species of NS-proteins do not represent ubiquitinated protein. (a) NS-GFP expressed in *ltn1*Δ cells was immunoprecipitated and subjected to formic acid treatment. Pgk1p served as a loading control. (b) NS-Luc or Luc were immunoprecipitated from WT or *ltn1*Δ cells and detected by immunoblotting against Luc or Ubiquitin. Pgk1p served as a loading control. EV = empty vector. Figure modified from (Choe, Park *et al.* 2016).

To rule out that inclusion body formation in *ltn1*Δ cells is dependent on the *RNQ* prion status of the cell, Rnq1 was expressed in *ltn1*Δ cells in the [*RNQ*$^{+}$] state or in an isogenic strain that has been cured from this state by growth on medium supplied with 3 mM guanidinium chloride. Notably, the ability of Rnq1p to form inclusions is abolished in *ltn1*Δ cells with the [*rnq*$^{-}$] state, proving that deletion of *LTN1 per se* does not lead to the formation of visible inclusions (Fig. III.4a). Moreover, formation of SDS-resistant high molecular weight species of NS-GFP is independent of the prion state of *ltn1*Δ cells, thereby showing that NS-GFP aggregation does not rely on the presence of preexisting inclusions (Fig. III.4b).

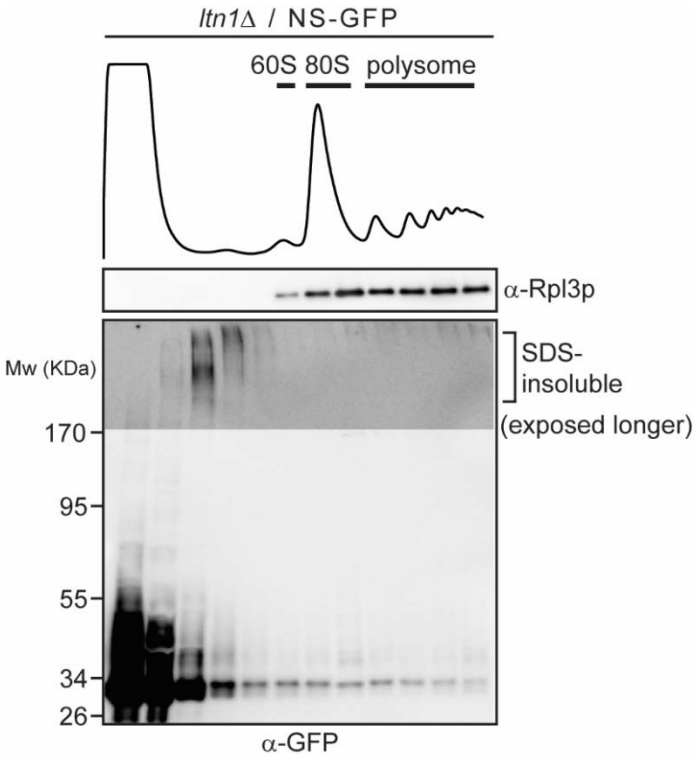

Fig. III.3: NS-proteins are efficiently released from the ribosome in the absence of Ltn1p. NS-GFP was expressed in *ltn1*Δ cells and clarified lysate was subjected to sucrose density gradient centrifugation. After centrifugation, the gradient was fractionated while continuously monitoring UV absorbance at 254 nm, and equal amounts of every fraction were analyzed by immunoblotting against GFP. Rpl3p served as a marker for the 60S subunit, 80S ribosomes and polysomes. The top part of the blot was overexposed to visualize SDS-resistant aggregates. Figure modified from (Choe, Park *et al.* 2016).

Taken together, the results show that artificial NS-proteins are not ubiquitinated in the absence of Ltn1p, but are still efficiently released from the ribosome. Furthermore, NS-proteins form both SDS-resistant aggregates and visible inclusions in *ltn1*Δ cells, thereby proving that efficient degradation of the reporter constructs indeed relies on a functional RQC.

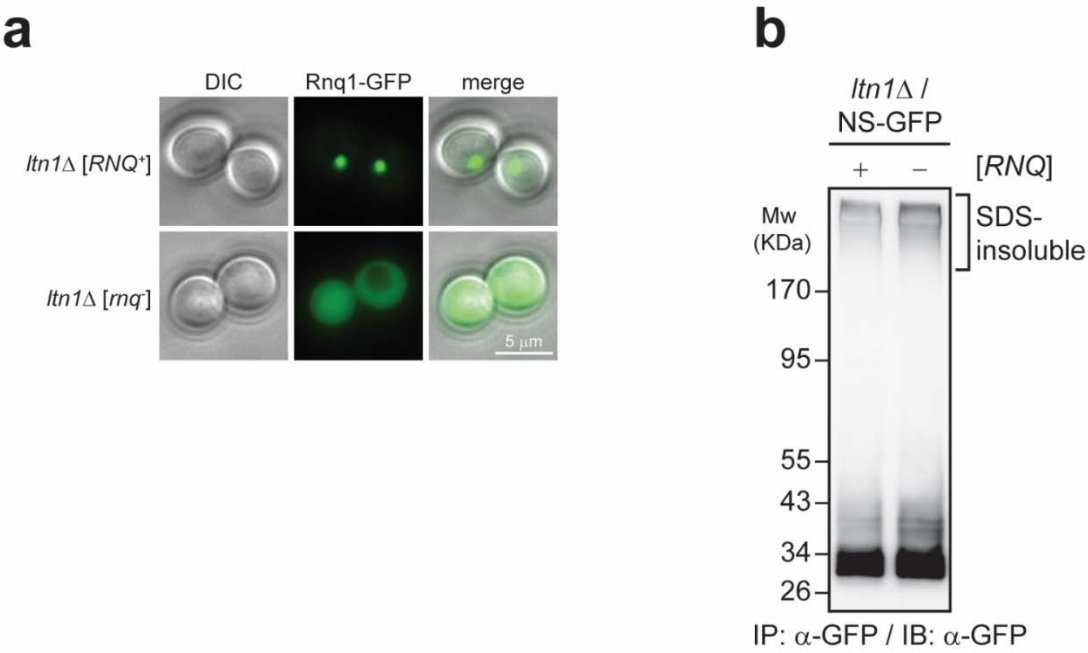

Fig. III.4: Aggregation of NS-GFP in *ltn1*Δ cells is independent of the *RNQ* prion status. (a) Rnq1p-GFP was expressed in *ltn1*Δ cells with the [*RNQ*$^+$] or the [*rnq*$^-$] phenotype. Scale bar, 5 µm. (b) NS-GFP was immunoprecipitated from *ltn1*Δ cells with the [*RNQ*$^+$] or the [*rnq*$^-$] phenotype and detected by immunoblotting against GFP. Figure modified from (Choe, Park *et al.* 2016).

III.2 Aggregation of polybasic proteins

Since translation of the poly(A) tail of a NS-mRNA leads to C-terminal extension of the nascent chain with a polylysine tract, reporter constructs with C-terminal polylysine sequences were generated in order to investigate the role of polybasic sequences in ribosomal stalling and nascent chain aggregation. Since poly(A) tails are of variable length (median of 27 nt in yeast, corresponding to 9 lysines), polylysine tracts consisting of either 12 or 20 lysines were added (Subtelny, Eichhorn *et al.* 2014). In addition, two alternative spacer sequences of 134 or 53 amino acids length were placed between the GFP moiety and the polybasic tract in order to ensure that the N-terminal GFP domain can completely leave the ribosomal exit channel and fold into its native structure before ribosomal stalling occurs. Surprisingly, a clear correlation between the

length of the polylysine stretch and aggregation propensity of the respective construct was observable: whereas expression of GFP-s-K12 resulted in 11 % of all cells carrying an inclusion, more than every second cell was showing visible aggregates upon expression of the construct coding for 20 lysines (Fig. III.5). This is consistent with the finding that expression of NS-GFP, which presumably contains a C-terminal extension of roughly 10 lysines, in *ltn1*Δ cells leads to visible inclusions in approximately 17 % of all cells (Fig. III.1b). Moreover, aggregation did not depend on the sequence of the spacer used and did not occur when GFP was fused to either of the spacer sequences, indicating that aggregation is indeed mediated by the polybasic tract (Fig. III.5). Interestingly, even expression of the reporter construct coding for 20 lysines did not lead to the formation of inclusions in WT cells, suggesting that inclusion formation is not mediated directly by the polylysine tract, but instead via an indirect effect such as ribosomal stalling, which would trigger rapid degradation of the reporter construct in cells with a functional RQC system (Fig. III.5).

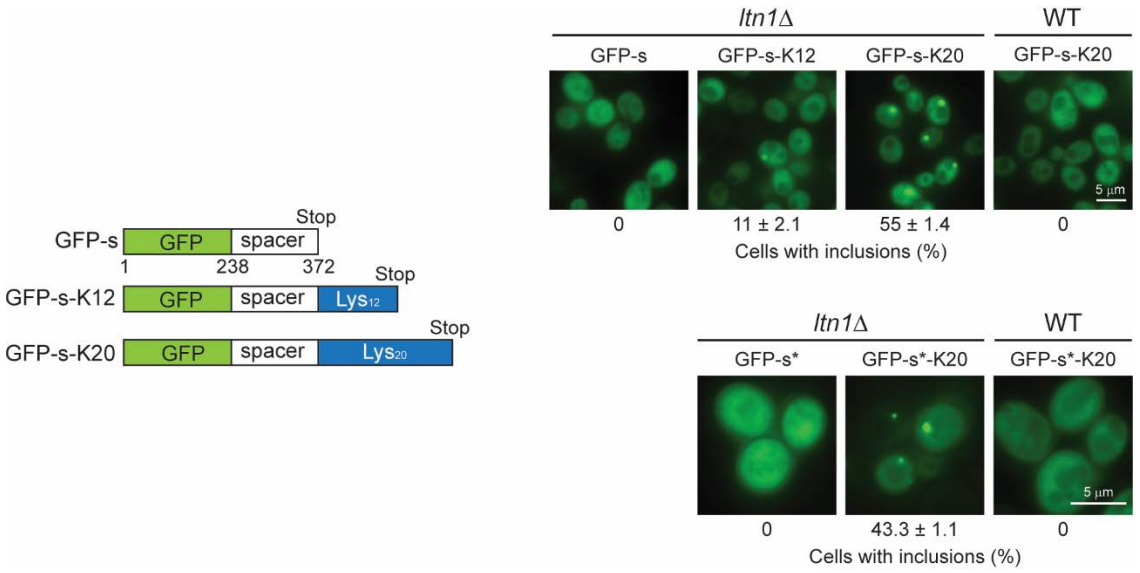

Fig. III.5: Effect of polybasic sequences on aggregation. GFP fusion constructs containing a spacer derived from the naturally unstructured, but aggregation-resistant M domain of Sup35p (s) or from the disordered region of Hsp82p (s*) and a polylysine tract of the indicated length were expressed in WT and *ltn1*Δ cells (Krishnan and Lindquist 2005). Cells containing visible inclusions were counted and expressed as a fraction of total (standard deviation from 3 independent experiments). Scale bar, 5 µm. Figure modified from (Choe, Park *et al.* 2016).

Since translation of a polylysine-encoding stretch *per se* may induce ribosomal stalling, it remained unclear whether the aggregation of NS-proteins and polylysine-encoding reporter constructs was a result of ribosomal stalling or the accumulation of nascent chains with polybasic tracts. To resolve this issue, a new series of reporter constructs with internal polyarginine stretches were employed that can be used to modulate ribosomal stalling via frequent (AGA) or rare (CGA) arginine codons (Fig. III.6a). If aggregation is simply a result of the physical properties of a protein containing a polybasic tract, then expression of GFP-s-R20$_{FREQ}$-mCh (construct #4) in *ltn1*Δ cells should lead to the formation of visible inclusions in a large number of cells, comparable to the result observed with the GFP-s-K20 construct (Fig. III.5). Surprisingly, GFP-s-R20$_{FREQ}$-mCh was efficiently translated even in *ltn1*Δ cells, as judged by the presence of a strong band corresponding to the full-length protein, mCherry fluorescence and the absence of visible inclusions in the cell (Fig. III.6b, c). Furthermore, no SDS-resistant high molecular weight species were detectable upon immunoblotting, indicating that a polybasic tract alone is also not sufficient to induce the formation of oligomeric species (Fig. III.6b). Conversely, expression of constructs coding for 4 or 20 rare arginine codons (constructs #3 and #5, respectively) in *ltn1*Δ cells resulted in the formation of SDS-resistant high molecular weight species and only small or even undetectable amounts of full-length protein, indicating that ribosomal stalling is already induced by a repeat of 4 rare arginine codons and leads to the formation of SDS-insoluble aggregates upon RQC deficiency (Fig. III.6b). Strikingly, even expression of GFP-s-R20$_{RARE}$-mCh, which is supposed to strongly induce ribosomal stalling, did not lead to the formation of visible inclusions in *ltn1*Δ cells, proving that ribosomal stalling *per se* is also not sufficient to induce the formation of visible aggregates (Fig. III.6c). Upon expression of a fusion construct coding for a non-stalling polybasic tract followed by a stalling motif (construct #6) in *ltn1*Δ cells, however, visible inclusions in approximately 23 % of all cells could be observed, demonstrating that the formation of visible aggregates requires both a polybasic sequence and ribosomal stalling (Fig. III.6c). Moreover, almost no high molecular weight smear could be detected by immunoblotting upon expression of GFP-s-R20$_{FREQ}$-R4$_{RARE}$-mCh in *ltn1*Δ cells, thereby providing further evidence that SDS-resistant species might resemble oligomeric aggregates that are distinct from observable inclusions (Fig. III.6b). Consistent with this hypothesis, analysis of *ltn1*Δ cell extracts by SDD-

AGE revealed that GFP-s-R20$_{FREQ}$-R4$_{RARE}$-mCh formed aggregates substantially larger in size than the ones observed upon expression of GFP-s-R4$_{RARE}$-mCh or GFP-s-R20$_{RARE}$-mCh (Fig. III.6d).

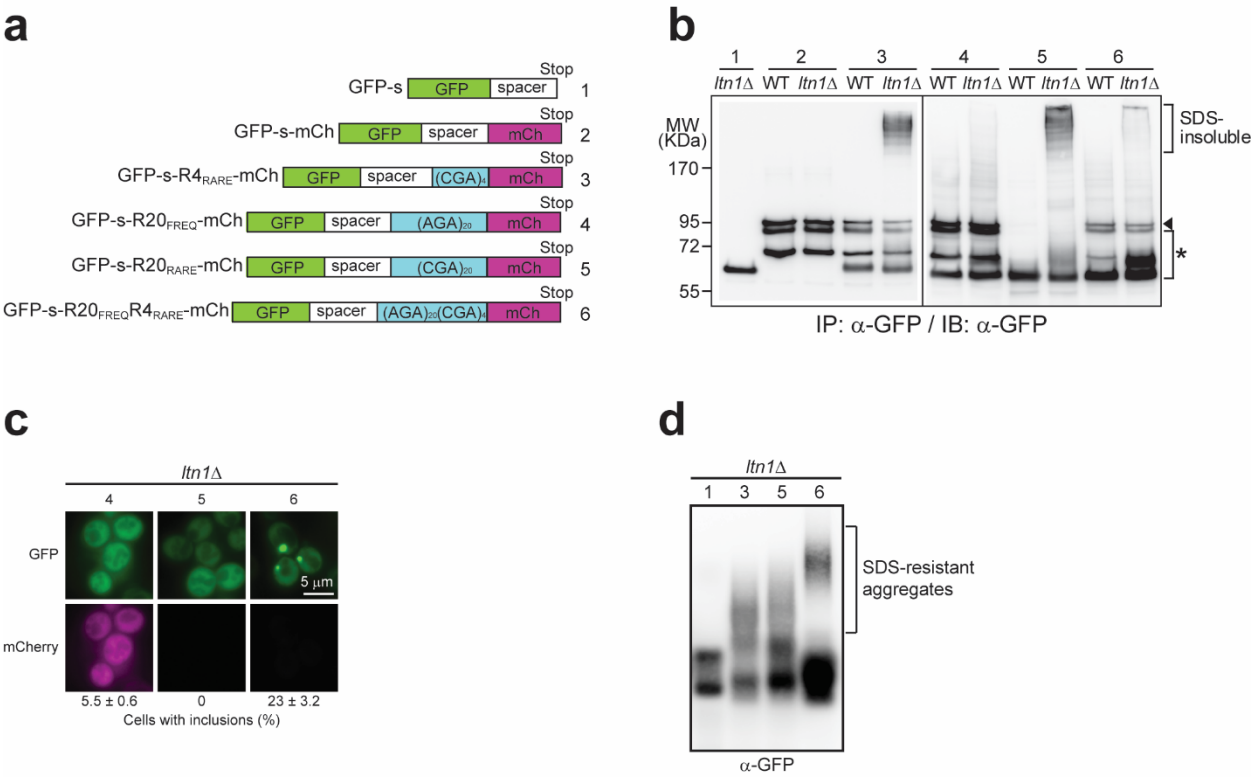

Fig. III.6: Modulation of aggregation propensity of polybasic constructs by codon usage. (a) GFP fusion constructs containing a spacer and a C-terminal mCherry domain were generated. Where indicated, stretches of frequent (AGA) or rare (CGA) codons coding for arginine were inserted upstream of the mCherry domain. (b) Fusion constructs shown in (a) were expressed in WT and *ltn1*Δ cells, immunoprecipitated and detected by immunoblotting. Arrow, full-length product. Asterisk, stalled truncation products and proteolytic fragments. (c) *ltn1*Δ cells expressing the indicated constructs were analyzed for GFP and mCherry fluorescence. Scale bar, 5 μm. (d) Extracts of *ltn1*Δ cells expressing the indicated constructs were prepared, resolved by SDD-AGE and subjected to immunoblotting. Only 25% of lysate from cells expressing construct 1 were applied to prevent overloading. Figure modified from (Choe, Park *et al.* 2016).

In summary, these findings provide evidence that ribosomal stalling *per se* is already sufficient to induce the formation of SDS-resistant oligomeric species in the absence of Ltn1p. The ability to form visible inclusions, however, requires the additional presence of a polybasic tract.

III.3 The role of Rqc2p in the aggregation of stalled nascent chains

Whereas Rqc1p is thought to be involved in the Cdc48p-mediated extraction of the ubiquitinated nascent chain, Rqc2 was shown to bind to 60S-peptidyl-tRNA complexes (Defenouillere, Yao *et al.* 2013, Lyumkis, Oliveira dos Passos *et al.* 2014). Consistent with Rqc1p and Rqc2p being key players of the RQC pathway, deletion of the respective genes resulted in accumulation of NS-GFP to a similar extent as observed in *ltn1*Δ cells (Fig. III.7a). Deletion of *RQC1*, but not of *RQC2*, led to the formation of SDS-resistant aggregates and visible inclusions (Fig. III.7a, b). Additional deletion of *RQC2* in cells lacking Ltn1p or Rqc1p abolished formation of both SDS-resistant aggregates and visible inclusions, despite even higher steady-state levels of NS-GFP than in any of the single deletion mutants (Fig. III.7a, b). Suppression of inclusion body formation in all strains lacking *RQC2* was accompanied by accumulation of significant amounts of NS-GFP in the nucleus (Fig. III.7b).

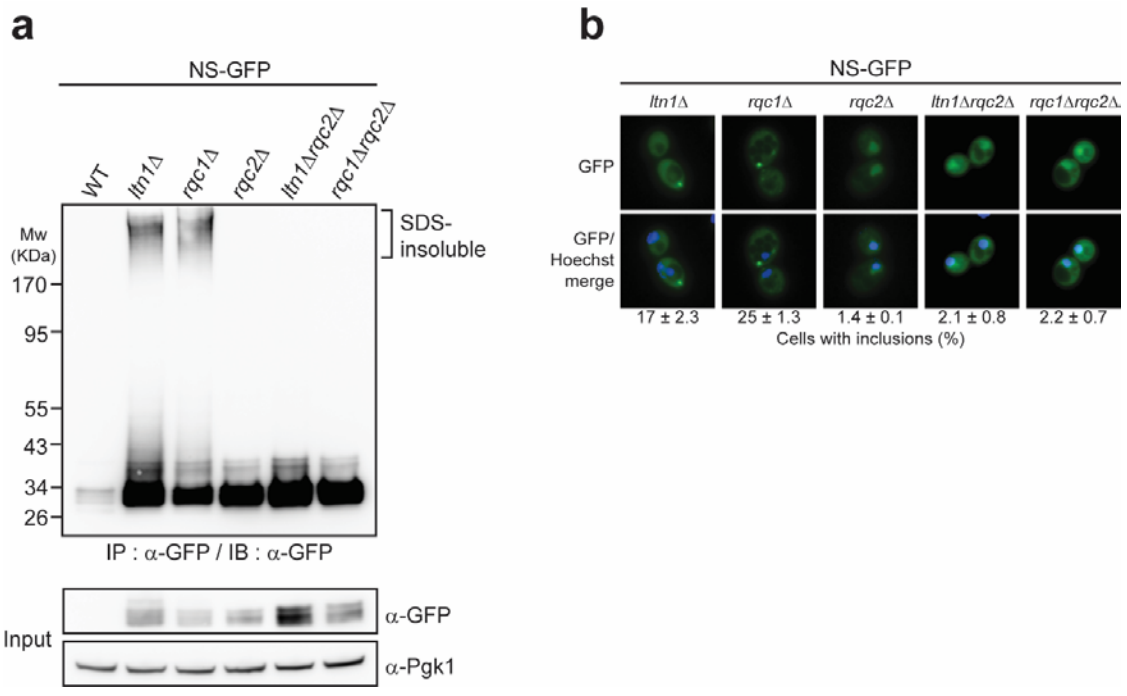

Fig. III.7: Role of RQC components on the formation of SDS-resistant aggregates and visible inclusions. (a) NS-GFP was expressed in WT or RQC mutant strains, immunoprecipitated, and detected via

immunoblotting. Pgk1p served as a loading control. (b) RQC mutant cells expressing NS-GFP were analyzed by fluorescence microscopy. Hoechst 33342 was used for nuclear staining. Scale bar, 5 μm. Figure modified from (Choe, Park *et al.* 2016).

Since it has previously been shown that Rqc2p plays a role upstream of Rqc1p and Ltn1p by providing a binding platform for the latter, it was reasoned that deletion of *RQC2* leads to inefficient recognition of 60S-peptidyl-tRNA complexes and only small amounts of free stalled nascent chains. Surprisingly, the vast majority of NS-GFP was efficiently released from the ribosome, thereby demonstrating that suppression of aggregation in an *RQC2* deletion background is not due to the nascent chain being protected by the ribosome (Fig. III.8).

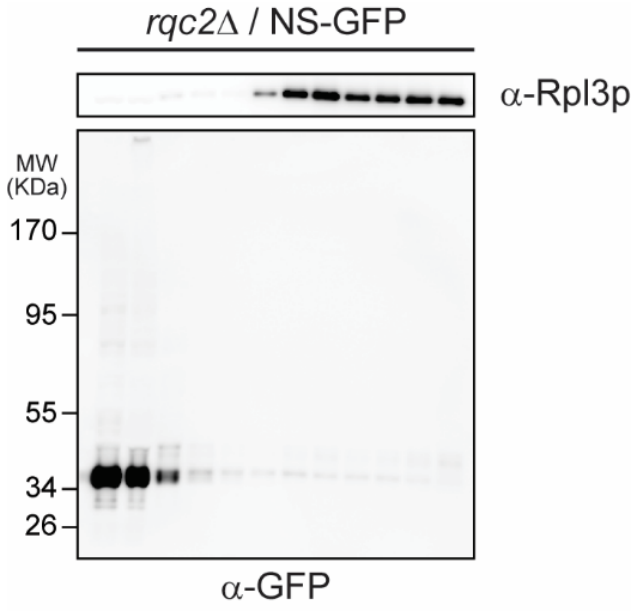

Fig. III.8: NS-proteins are efficiently released from the ribosome in the absence of Rqc2p. NS-GFP was expressed in *rqc2*Δ cells and clarified lysate was subjected to sucrose density gradient centrifugation. After centrifugation, the gradient was fractionated, and equal amounts of every fraction were analyzed by immunoblotting against GFP. Rpl3p served as a marker for the 60S subunit, 80S ribosomes and polysomes. Figure modified from (Choe, Park *et al.* 2016).

In order to exclude the possibility that deletion of *RQC2* leads to an impairment in depositing aggregation-prone proteins in intracellular inclusions, the ability of the prion protein Rnq1p to form aggregates was tested in *rqc2*Δ and *ltn1*Δ*rqc2*Δ cells. Analysis by fluorescence microscopy revealed that Rnq1p forms visible inclusions in the absence of Rqc2p, thereby showing that the general ability to form aggregate deposits is not affected (Fig. III.9).

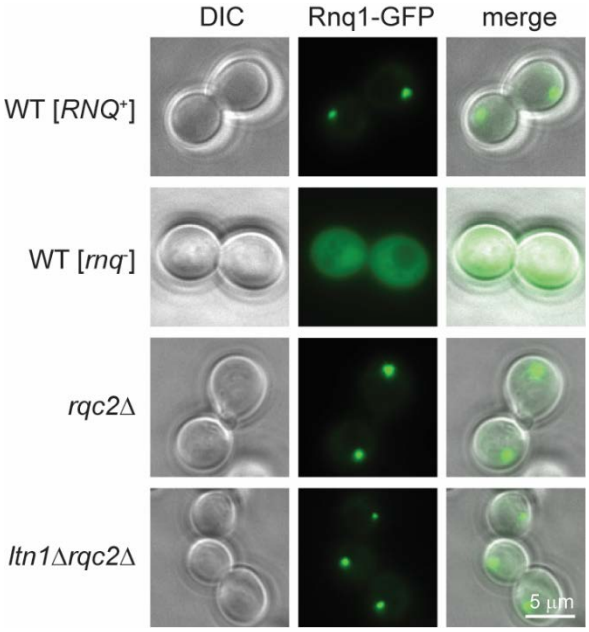

Fig. III.9: Suppression of nascent chain aggregation upon deletion of *RQC2* is not due to a general defect in aggregate deposition. Rnq1p-GFP was expressed in WT cells with the [*RNQ*$^+$] or [*rnq*$^-$] phenotype as well as in *rqc2*Δ or *ltn1*Δ*rqc2*Δ cells. Scale bar, 5 µm. Figure modified from (Choe, Park *et al.* 2016).

It has recently been shown that Rqc2p is able to mediate a template-free C-terminal extension of the nascent chain with alanine and threonine residues, thereby generating so-called CAT tails (Shen, Park *et al.* 2015). Since these CAT tails might confer the ability to form aggregates due to their mildly hydrophobic nature, it was suggested that aggregation of stalled nascent chains in the absence of Ltn1p might be dependent on these CAT tails. Western blot analysis revealed the presence of a faint smear above the truncated protein that disappears upon deletion of *RQC2*, suggesting that these stalled nascent chains might be subject to a C-terminal extension

mediated by Rqc2p (Fig. III.10a). Indeed, the absence of the observed smear in *ltn1*Δ*rqc2*Δ cells expressing GFP-s-R20$_{FREQ}$-R4$_{RARE}$-mCh was accompanied by efficient suppression of inclusion body formation, indicating that CAT tails might play a role in aggregation of stalled nascent chains (Fig. III.10b).

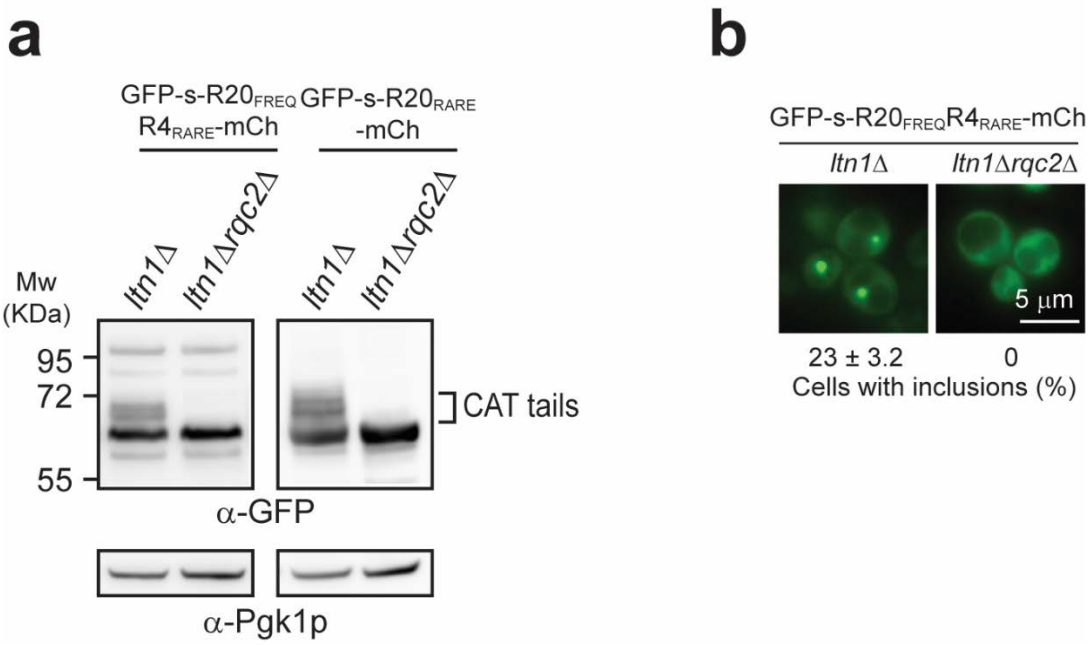

Fig. III.10: C-terminal extension and aggregation of stalled nascent chains is dependent on Rqc2p. (a) Extracts of *ltn1*Δ or *ltn1*Δ*rqc2*Δ cells expressing the indicated constructs were prepared and subjected to immunoblotting against GFP. Pgk1p served as a loading control. (b) *ltn1*Δ or *ltn1*Δ*rqc2*Δ cells expressing GFP-s-R20$_{FREQ}$-R4$_{RARE}$-mCh were analyzed by fluorescence microscopy. Scale bar, 5 μm. Figure modified from (Choe, Park *et al.* 2016).

A recent study identified three key residues (D9, D98, and R99) in the N-terminal domain of Rqc2p that might be involved in the recognition of tRNA molecules, which bind to the A-site of the 60S-peptidyl-tRNA complex in order to deliver alanine and threonine residues for CAT tail extension (Shen, Park *et al.* 2015). Mutation of these residues to alanine gave rise to a variant that is deficient in CAT tail synthesis, but is still able to bind to 60S-peptidyl-tRNA complexes and to provide a binding platform for Ltn1p (Shen, Park *et al.* 2015). In order to evaluate whether the

aggregation of stalled nascent chains is mediated by the ability of Rqc2p to synthesize CAT tails, a stalling reporter construct and either WT Rqc2p or the CAT tail-deficient mutant rqc2$_{aaa}$ were coexpressed in *rqc2*Δ or *ltn1*Δ*rqc2*Δ cells, respectively. Indeed, overexpression of WT Rqc2p, but not of rqc2$_{aaa}$, restored the ability to form aggregates as shown by the presence of SDS-resistant high molecular weight species of NS-GFP and visible inclusions of GFP-s-K20, respectively (Fig. III.11a, b). Interestingly, overexpression of either of the Rrqc2p variants led to reduced levels of NS-GFP in the *rqc2*Δ background, indicating that prevention of reassociation of the 60S-peptidyl-tRNA complex with the 40S subunit by Rqc2p might represent a rate-limiting step in the degradation pathway of NS-proteins (Fig. III.11a).

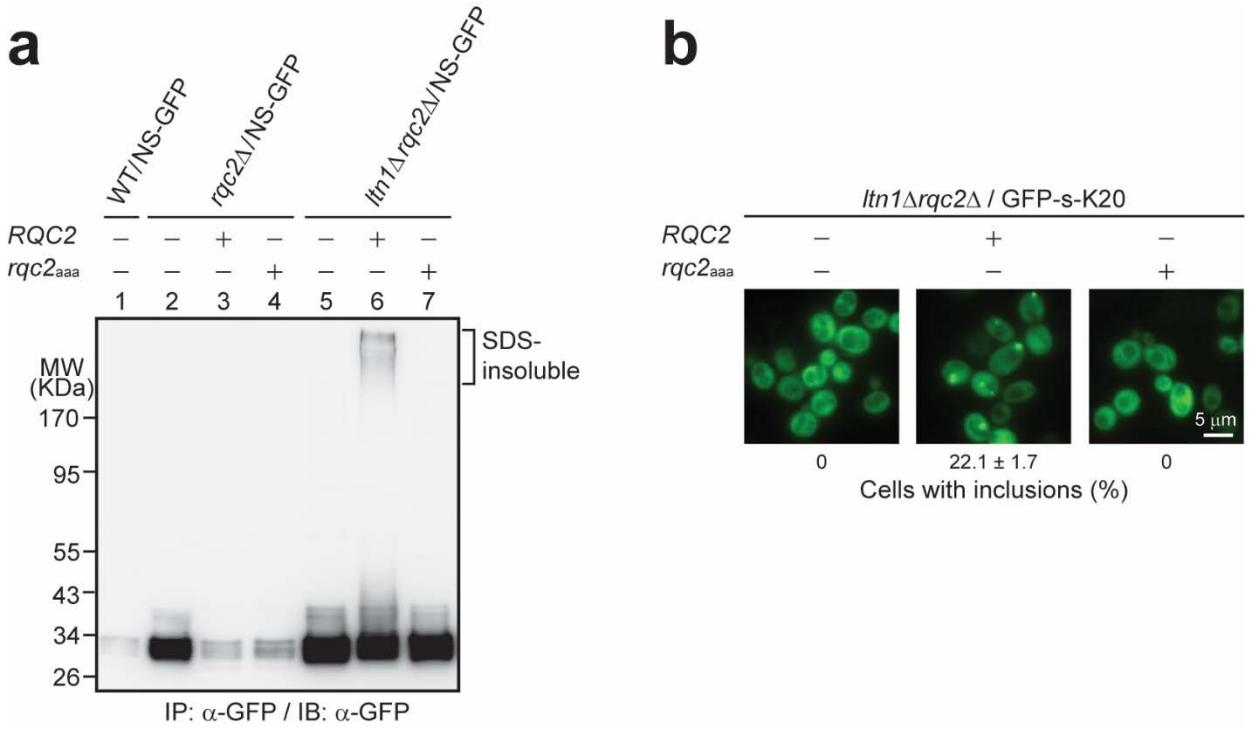

Fig. III.11: Aggregation of NS-GFP and GFP-s-K20 is CAT tail-dependent. (a) NS-GFP was immunoprecipitated from WT, *rqc2*Δ or *ltn1*Δ*rqc2*Δ cells expressing either WT *RQC2* or the CAT tail-deficient *rqc2*$_{aaa}$ mutant, and subjected to immunoblotting against GFP. (b) *ltn1*Δ*rqc2*Δ cells expressing GFP-s-K20 and either WT *RQC2* or the CAT tail-deficient *rqc2*$_{aaa}$ mutant were analyzed by fluorescence microscopy. Scale bar, 5 μm. Figure modified from (Choe, Park *et al.* 2016).

To provide further evidence that nascent chain aggregation is mediated by Rqc2p-dependent addition of CAT tails, a set of reporter constructs with polybasic tracts and artificial C-terminal extensions consisting of alternating alanine and threonine or glycine and serine residues was established (Fig. III.12a). *ltn1*Δ*hel2*Δ was used as a host strain since it has previously been shown that deletion of *HEL2*, which codes for a ribosome-associated E3 ligase, markedly enhances read-through efficiency for polybasic and other stalling sequences (Brandman, Stewart-Ornstein *et al.* 2012). Indeed, expression of a reporter construct containing an internal sequence coding for 20 consecutive lysines was efficiently translated in this strain as judged by the appearance of a strong band corresponding to full-length protein (Fig. III.12b). Interestingly, expression of neither GFP-s-K20 nor GFP-s-(AT)6 resulted in the formation of visible inclusions, indicating that a polybasic tract or a CAT tail alone is not sufficient for nascent chain aggregation (Fig. III.12a). Conversely, expression of GFP-s-K20-(AT)6 led to large amounts of cells carrying visible aggregates, whereas expression of GFP-s-K20-(GS)6 only weakly induced inclusion body formation (Fig. III12a).

Taken together, our results show that the ability of stalled nascent chains to form SDS-resistant aggregates and visible inclusions is dependent on the Rqc2p-mediated addition of CAT tails. Moreover, the absence of visible inclusions of GFP-s-K20 in *ltn1*Δ*hel2*Δ cells provides additional evidence that both a polybasic tract and ribosomal stalling are required for the formation of enhanced aggregates. Visible inclusions reappeared after addition of an encoded CAT tail, indicating that these C-terminal extensions are usually added as a result of ribosomal stalling.

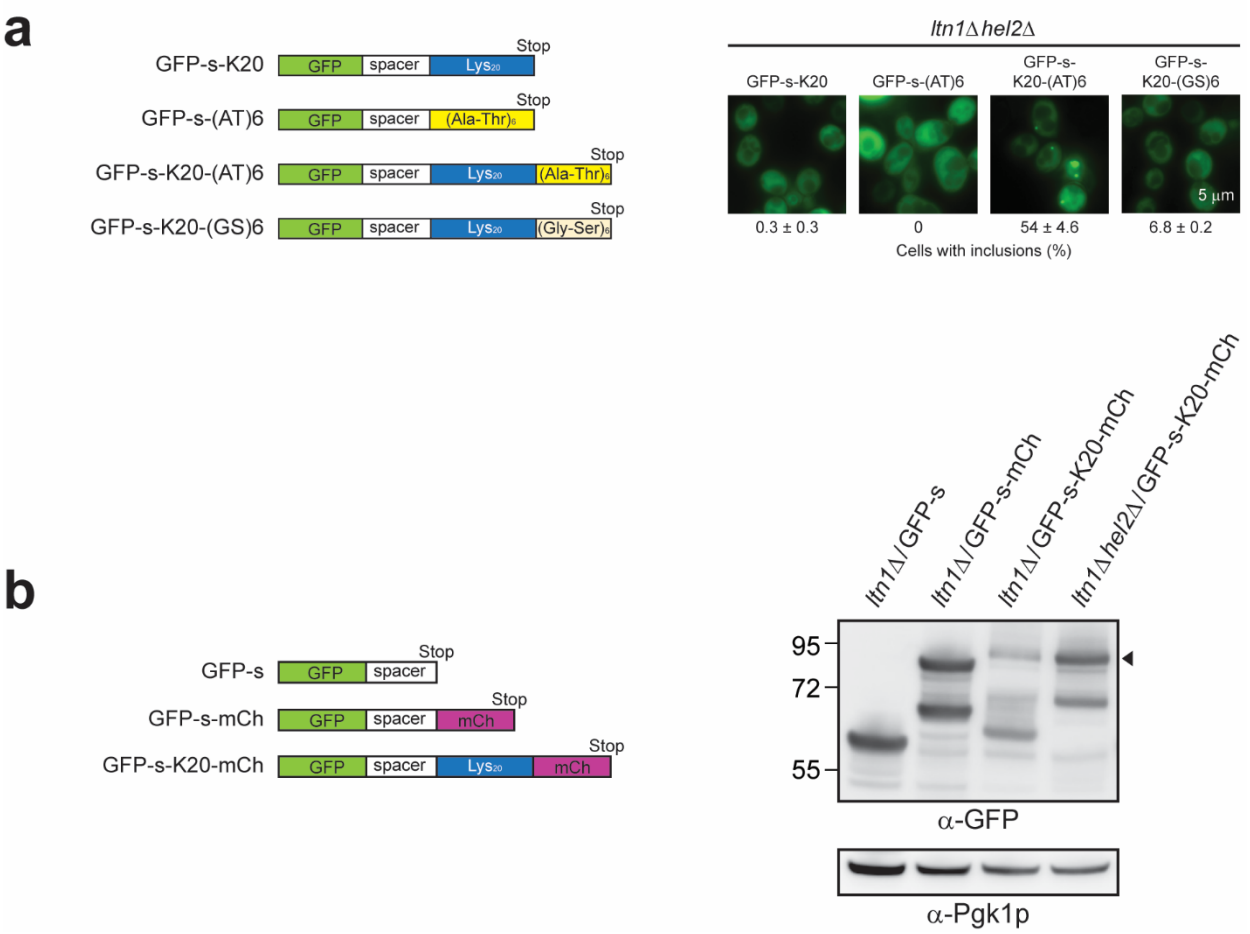

Fig. III.12: Formation of visible inclusions is dependent on CAT tails and polybasic tracts. (a) *ltn1Δhel2Δ* cells expressing the indicated reporter constructs were analyzed by fluorescence microscopy. Scale bar, 5 μm. (b) Extracts were prepared from *ltn1Δ* or *ltn1Δhel2Δ* cells expressing the indicated reporter constructs, and subjected to immunoblotting against GFP. Arrow, full-length product. Figure modified from (Choe, Park *et al.* 2016).

III.4 Non-stop protein aggregates sequester chaperones

Since the formation of visible inclusions and SDS-resistant aggregates has previously been associated with the sequestration of various cytosolic factors such as molecular chaperones, we reasoned that NS-GFP might also form aberrant interactions with components of the proteostasis network upon aggregation in the absence of Ltn1p (Olzscha, Schermann *et al.* 2011, Park, Kukushkin *et al.* 2013). To this end, a quantitative proteomics approach was used to determine the interactome of NS-GFP in *ltn1*Δ cells, with the interactomes of NS-GFP in WT cells and GFP in *ltn1*Δ cells serving as background controls, respectively (Fig. III.13). Interestingly, the Hsp40, Sis1p, an essential cochaperone of Hsp70 that has previously been shown to be sequestered by amyloid-forming polyQ proteins and artificial β-sheet polypeptides, was found to be a very strong interactor of NS-GFP (Fig. III.13) (Olzscha, Schermann *et al.* 2011, Park, Kukushkin *et al.* 2013). Besides Sis1p, a plethora of other molecular chaperones were identified as NS-GFP interactors, including the small Hsps, Hsp42 and Hsp26, the amyloid-targeting cochaperone Sgt2p, the Hsp90 cochaperones Cns1 and Sti1, and several Hsp70s and Hsp90s (Fig. III.13). Consistent with these results, Sis1p was found to physically interact with both visible inclusions and SDS-insoluble aggregates of NS-GFP in *ltn1*Δ cells (Fig. III.14a, b).

Interestingly, deletion of *RQC2* in WT, *ltn1*Δ or *rqc1*Δ cells suppressed Sis1p interaction with NS-GFP, indicating that Rqc2p-mediated aggregation of stalled nascent chains is a prerequisite for Sis1p sequestration. Indeed, Sis1p coaggregation with NS-GFP was reconstituted by expression of wildtype Rqc2p, but not of the CAT tail-deficient rqc2$_{aaa}$ mutant, in *ltn1*Δ*rqc2*Δ cells, indicating that Sis1p sequestration is dependent on CAT tail-mediated aggregation (Fig. III.15).

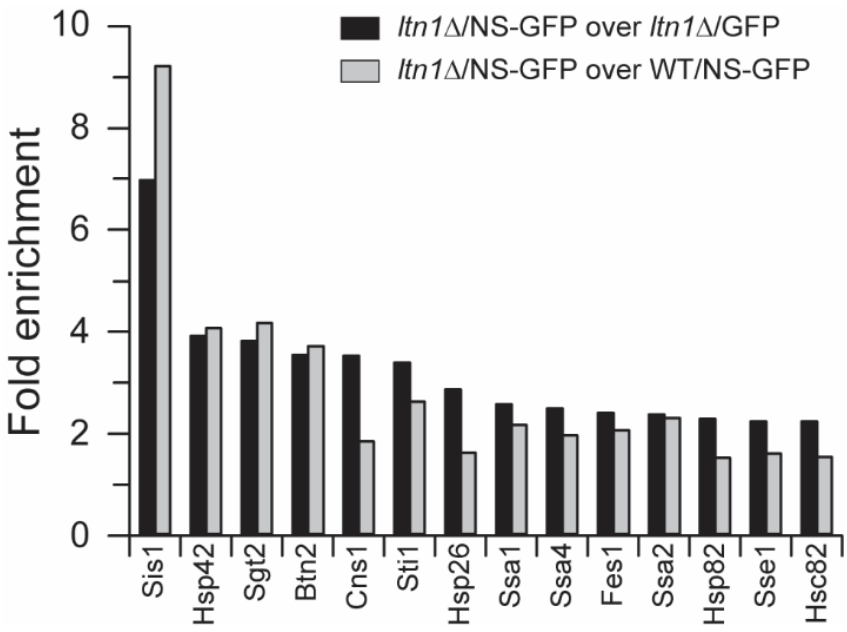

Fig. III.13: Interactome of NS-GFP in *ltn1*Δ cells. Molecular chaperones identified as interactors of NS-GFP in the absence of Ltn1p. Black bars, fold enrichment over GFP in *ltn1*Δ cells. Grey bars, fold enrichment over NS-GFP in WT cells. Figure modified from (Choe, Park *et al.* 2016).

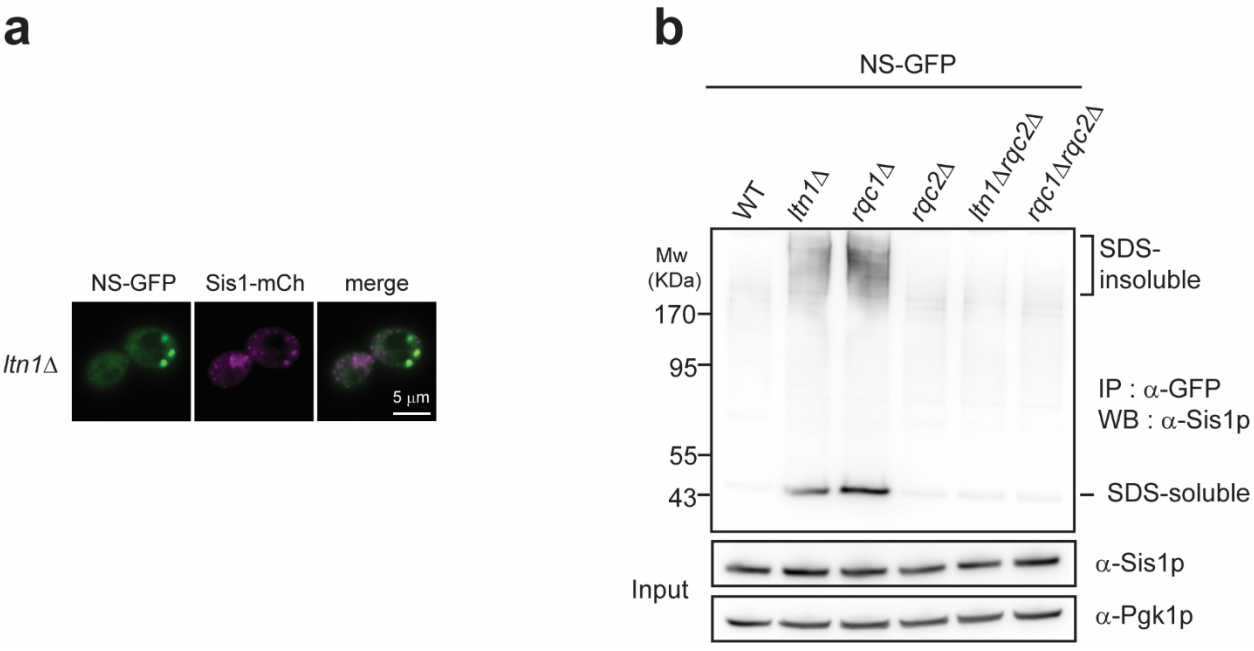

Fig. III.14: Sis1p and NS-GFP interact in *ltn1*Δ cells. (a) *ltn1*Δ cells with *SIS1*-mCh integrated at the *SIS1* locus expressing NS-GFP were analyzed by fluorescence microscopy. Scale bar, 5 μm. (b) NS-GFP was

expressed in WT or RQC mutant strains, immunoprecipitated, and Sis1p was detected via immunoblotting. Pgk1p served as a loading control. Figure modified from (Choe, Park *et al.* 2016).

To test whether the ability of NS-GFP aggregates to sequester Sis1p is specific for NS-proteins or rather a generic feature of stalled polypeptides, GFP-s-R4$_{RARE}$-mCh, which induces ribosomal stalling but lacks a polybasic sequence, was expressed in WT, *ltn1*Δ and *ltn1*Δ*rqc2*Δ cells. Again, a strong interaction between Sis1p and this construct was observed in *ltn1*Δ, but not in *ltn1*Δ*rqc2*Δ cells, indicating that sequestration of Sis1p indeed relies on aggregation of stalled nascent chains and is independent of the type of stalling (Fig. III.16).

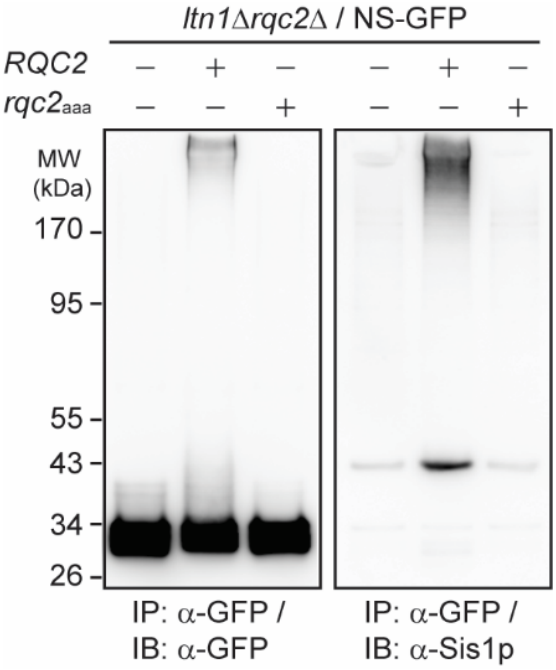

Fig. III.15: Interaction of Sis1p with NS-GFP is CAT tail-dependent. (a) NS-GFP was immunoprecipitated from *ltn1*Δ*rqc2*Δ cells expressing either wildtype *RQC2* or the CAT tail-deficient *rqc2*$_{aaa}$ mutant, and subjected to immunoblotting against GFP and Sis1p, respectively. Figure modified from (Choe, Park *et al.* 2016).

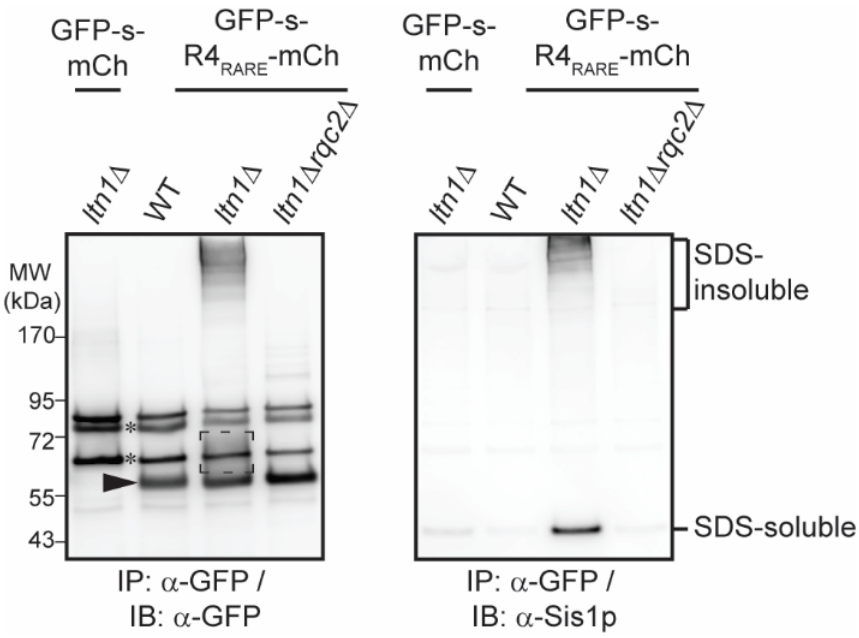

Fig. III.16: Sis1p interacts with stalled nascent chains in the absence of Ltn1p. (a) GFP-s-mCh or GFP-s-R4RARE-mCh were expressed in WT, *ltn1*Δ and *ltn1*Δ*rqc2*Δ cells, immunoprecipitated, and subjected to immunodetection for GFP and Sis1p, respectively. Arrowhead, stalled truncation product; asterisks, proteolytic fragments; dashed box, CAT tails. Figure modified from (Choe, Park *et al.* 2016).

Since the RQC pathway is highly conserved from yeast to mammals, we assumed that cells are constantly challenged by stalled nascent chains that must be efficiently recognized and degraded to maintain proteome integrity. Consistent with this notion, Sis1p was found to form high molecular weight, SDS-resistant aggregates in *ltn1*Δ and *rqc1*Δ cells, even without expression of a stalling reporter construct (Fig. III.17a, b). Again, deletion of RQC2 completely abolished Sis1p aggregation, indicating that aggregation of endogenous stalled nascent chains and thus aggregation of Sis1p is CAT tail-dependent (Fig. III.17a, b). Furthermore, the fraction of cells carrying visible Sis1p-positive inclusions was markedly enhanced in the absence of Ltn1p, suggesting that endogenous stalled polypeptides can form both SDS-resistant oligomers and visible inclusions (Fig. III.17c).

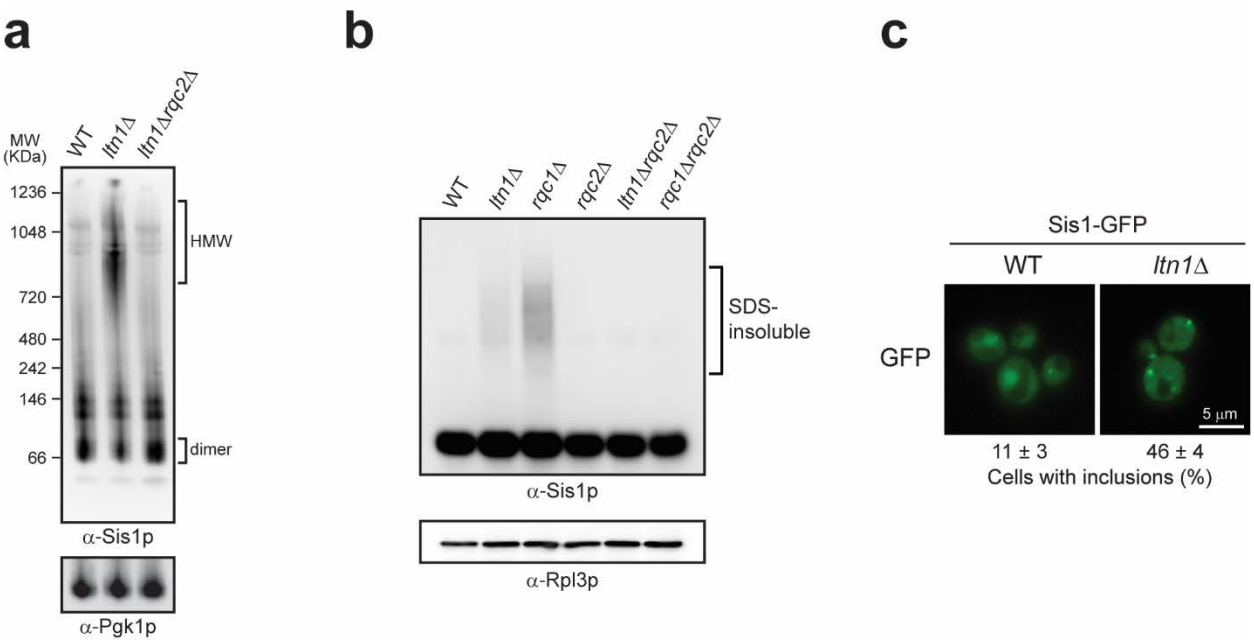

Fig. III.17: Sis1p forms SDS-resistant aggregates and visible inclusions in *ltn1*Δ cells. (a) Cell extracts of WT, *ltn1*Δ and *ltn1*Δ*rqc2*Δ cells were prepared, resolved by Blue Native-PAGE, and subjected to immunodetection for Sis1p. Pgk1p served as a loading control. HMW, high molecular weight species. (b) Cell extracts of a WT and the indicated RQC mutant strains were prepared and resolved by SDD-AGE. Sis1p was detected by immunoblotting. Rpl3p served as a loading control. (c) Fluorescence microscopy of WT and *ltn1*Δ cells carrying the *SIS1-GFP* allele at the chromosomal *SIS1* locus. Cells containing visible fluorescent inclusions were counted and expressed as a fraction of total (standard deviation from 3 independent experiments). Scale bar, 5 μm. Figure modified from (Choe, Park *et al.* 2016).

In summary, it was shown that stalled nascent polypeptides such as NS-proteins or nascent chains with internal stalling sequences interact with various cellular components, especially molecular chaperones. The Hsp40 Sis1p was found to be recruited to both SDS-resistant aggregates and visible inclusions of NS-GFP, and also interacted with a stalling reporter lacking a polybasic stretch. Similar to aggregation of stalled nascent polypeptides, coaggregation with Sis1p was dependent on Rqc2p-mediated CAT tail synthesis. Moreover, Sis1p forms both SDS-resistant aggregates and visible inclusions in *ltn1*Δ cells even in the absence of a stalling reporter, indicating that cells accumulate considerable amounts of endogenous stalled nascent chains upon failure of the RQC pathway.

III.5 Impairment of ribosomal quality control induces proteotoxic stress

Since Sis1p sequestration by amyloid aggregates has been shown to perturb the proteostasis network by interfering with nuclear transport of polypeptides targeted for proteasomal degradation, it was assumed that deletion of *LTN1* might result in proteostasis stress as well (Park, Kukushkin *et al.* 2013). The terminally misfolded reporter protein cytosolic carboxypeptidase Y (CPY*), whose transport to the nucleus for degradation is known to depend on Sis1p, was fused to mCherry (CmCh*) and expressed in WT, *ltn1*Δ and *ltn1*Δ*rqc2*Δ cells. Alternatively, CPY* fused to GFP (CG*) was expressed in *ltn1*Δ cells with or without additional overexpression of HA-Sis1p. After global translation shutdown by addition of cycloheximide, both CmCh* and CG* were rapidly degraded in WT cells, but strongly accumulated in *ltn1*Δ cells, indicating a general failure of cytosolic protein quality control upon impairment of the RQC pathway (Fig. III.18a, b). Furthermore, degradation of both reporters was restored by additional deletion of *RQC2* or overexpression of Sis1p, consistent with depletion of Sis1p due to coaggregation with endogenous stalled nascent chains in an Rqc2p-dependent manner (Fig. III.18a, b).

To rule out the possibility that deletion of the E3 ligase *LTN1* leads to lower levels of ubiquitination of CPY* and thus to delayed degradation, the ubiquitination status of CmCh* was compared in WT and *ltn1*Δ cells. As expected for a ribosome-associated E3 ligase such as Ltn1p, which is mainly responsible for the ubiquitination of stalled nascent chains, deletion of *LTN1* did not affect ubiquitination of CmCh* (Fig. III.19).

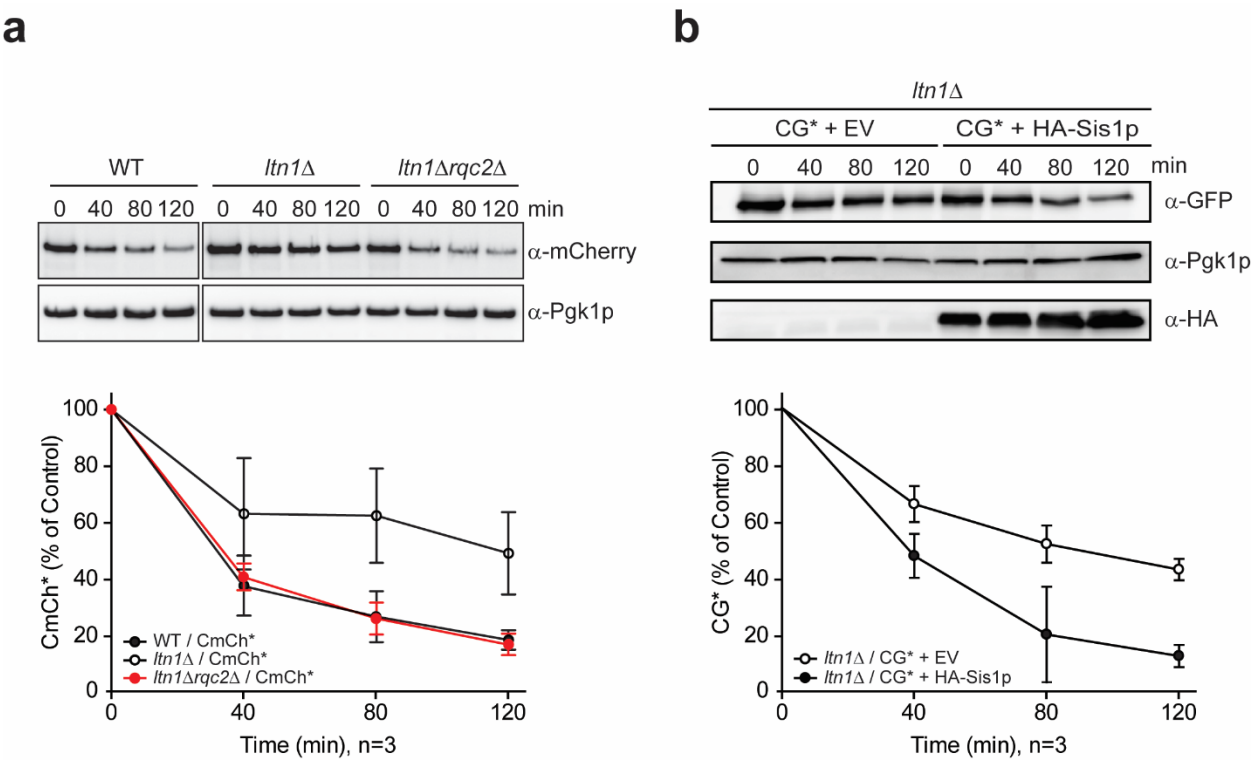

Fig. III.18: Degradation of a terminally misfolded reporter is markedly delayed in *ltn1Δ* cells. (a) CmCh* was expressed in WT, *ltn1*Δ and *ltn1*Δ*rqc2*Δ cells, and degradation was followed by cycloheximide chase. CmCh* levels were detected via immunoblotting against CPY and quantified by densitometry. Pgk1p served as a loading control. Error bars represent standard deviation from three independent experiments. (b) CG* was expressed in *ltn1*Δ with or without additional overexpression of HA-Sis1p, and degradation was followed by cycloheximide chase. CG* levels were detected via immunoblotting against GFP and quantified by densitometry. Pgk1p served as a loading control. Expression of HA-Sis1p was confirmed by immunoblotting against the HA tag. Error bars represent standard deviation from three independent experiments. Figure modified from (Choe, Park *et al.* 2016).

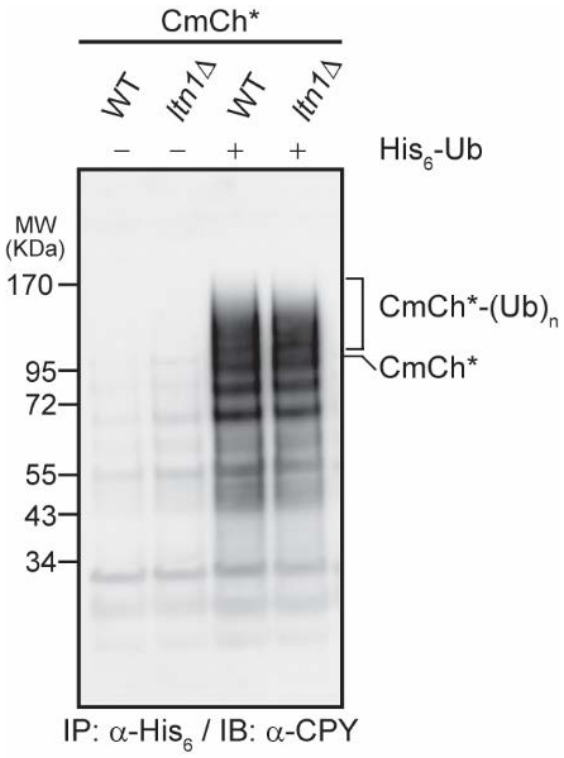

Fig. III.19: Terminally misfolded proteins are efficiently ubiquitinated in *ltn1*Δ cells. (a) CmCh* was coexpressed with or without His_6-tagged ubiquitin in WT and *ltn1*Δ cells. His_6-ubiquitinated proteins were immunoprecipitated and CmCh* was detected via immunoblotting for CPY. Figure modified from (Choe, Park *et al.* 2016).

Although considerable amounts of Sis1p are sequestrated by aggregates of endogenous stalled nascent chains, deletion of *LTN1* or *RQC1* alone did not lead to a measurable growth defect (Fig. III.20a). However, the presence of low amounts of Hygromycin B, an antibiotic that reduces translational fidelity and thus leads to enhanced production of non-stop proteins, was highly toxic for cells lacking functional Ltn1p or Rqc1p, and strongly increased the amount of visible Sis1p-positive foci in *ltn1*Δ cells (Fig. III.20a, b). Again, this phenotype was rescued by additional deletion of *RQC2*, indicating that the growth defect was caused by aggregation of stalled nascent chains (Fig. III.20a).

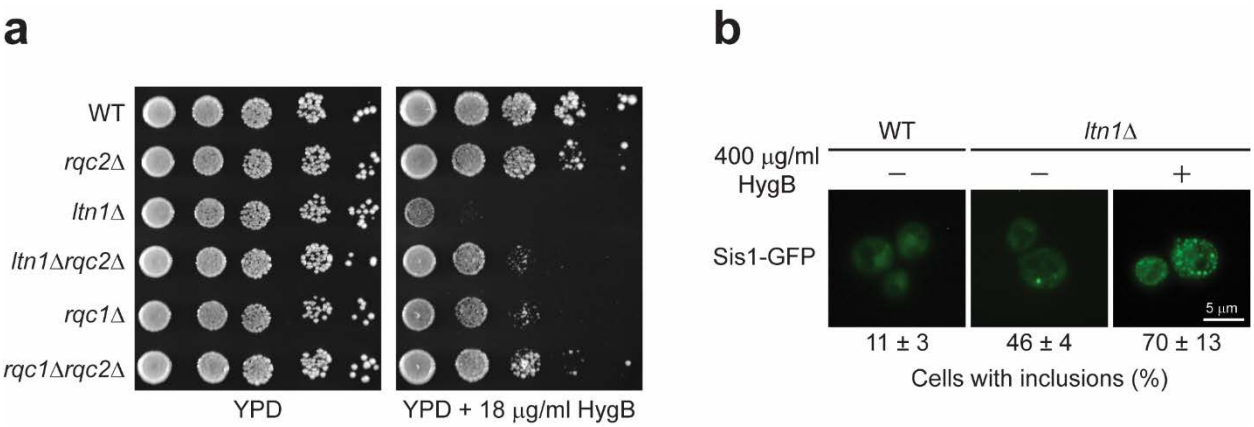

Fig. III.20: RQC-deficient cells are hypersensible to translational stress. (a) WT and RQC mutant strains were grown to mid-log phase in YPD medium, serial dilutions were spotted onto YPD plates with or without Hygromycin B (HygB), and plates were incubated for 2-3 days at 37 °C. (b) WT or *ltn1*Δ cells carrying the *SIS1*-GFP allele at the chromosomal *SIS1* locus were grown in YPD medium with or without HygB and analyzed by fluorescence microscopy. Scale bar, 5 μm. Figure modified from (Choe, Park *et al.* 2016).

Taken together, these results implicate that RQC impairment *per se*, although leading to a general defect in protein quality control, does not exert a cytotoxic effect on cells. Upon additional proteostasis stress such as the presence of Hygromycin B in combination with mild heat stress, however, a defect in the RQC pathway causes a strong defect in cell growth.

III.6 *In vitro* aspects of CAT tail- and polybasic stretch-dependent aggregation

In order to elucidate the mechanisms of CAT tail- and polybasic stretch-induced aggregation, studies were performed *in vitro* with purified proteins containing encoded polylysine tracts and CAT tails (Fig. III.21a). Constructs were N-terminally fused to the highly soluble glutathione-S-transferase (GST) domain for purification and to prevent aggregation, a strategy that has previously been used for *in vitro* aggregation studies with polyQ proteins (Muchowski, Schaffar

et al. 2000, Haacke, Broadley *et al.* 2006, Haacke, Hartl *et al.* 2007). In addition, a PreScission protease cleavage site was inserted between the GST and GFP domains to allow for proteolytic removal of the GST domain (Fig. III.21a). Aggregation was then induced by incubation with PreScission Protease for 16 hours at 30 °C, which led to efficient cleavage of the GST tag (Fig. III.21b). The faint band corresponding to cleaved GFP-s-K_{20}-$(AT)_{10}$ indicates that only a small fraction of this construct remains SDS-soluble after proteolytic removal of the GST moiety, presumably because the aggregates formed by this construct are too large to migrate into the gel and thus are retained in the well, where they escape Coomassie staining (Fig. III.21b).

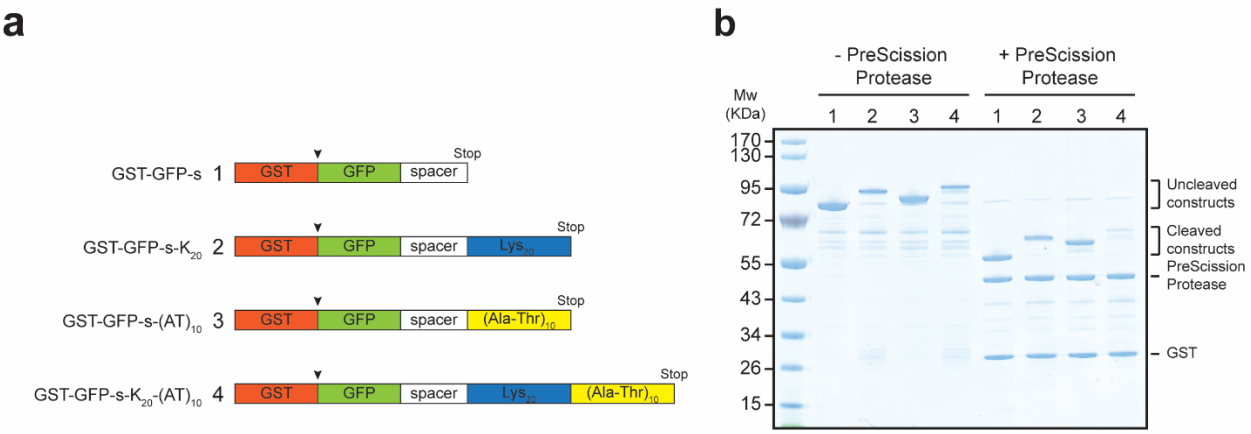

Fig. III.21: GST fusion proteins are efficiently cleaved by PreScission Protease *in vitro*. (a) GFP-spacer constructs with or without a polylysine stretch and an encoded CAT tail were N-terminally fused to a cleavable GST domain and purified from *E. coli*. Arrowhead, PreScission Protease cleavage site. (b) Constructs indicated in (a) were subjected to incubation for 16 hours at 30 °C with buffer or PreScission Protease, and analyzed by SDS-PAGE.

Following proteolytic removal of the GST moiety, a filter retardation assay was used to detect SDS-resistant aggregates. Consistent with previous results obtained *in vivo*, both a polybasic stretch and a CAT tail are required for efficient formation of SDS-resistant aggregates *in vitro* (Fig. III.22). Interestingly, a polylysine tract alone was sufficient to induce mild aggregation, but the presence of a CAT tail *per se* did not induce the formation of SDS-resistant aggregates large enough to be retained by the filter (pore size 0.2 μm) (Fig. III.22). These results

indicate that the aggregation process is mainly driven by stretches of polybasic residues, probably by the formation of amyloid-like β-sheet fibrils. CAT tails could support this process by facilitating the formation of SDS-soluble, prefibrillar oligomers due to their mildly hydrophobic nature.

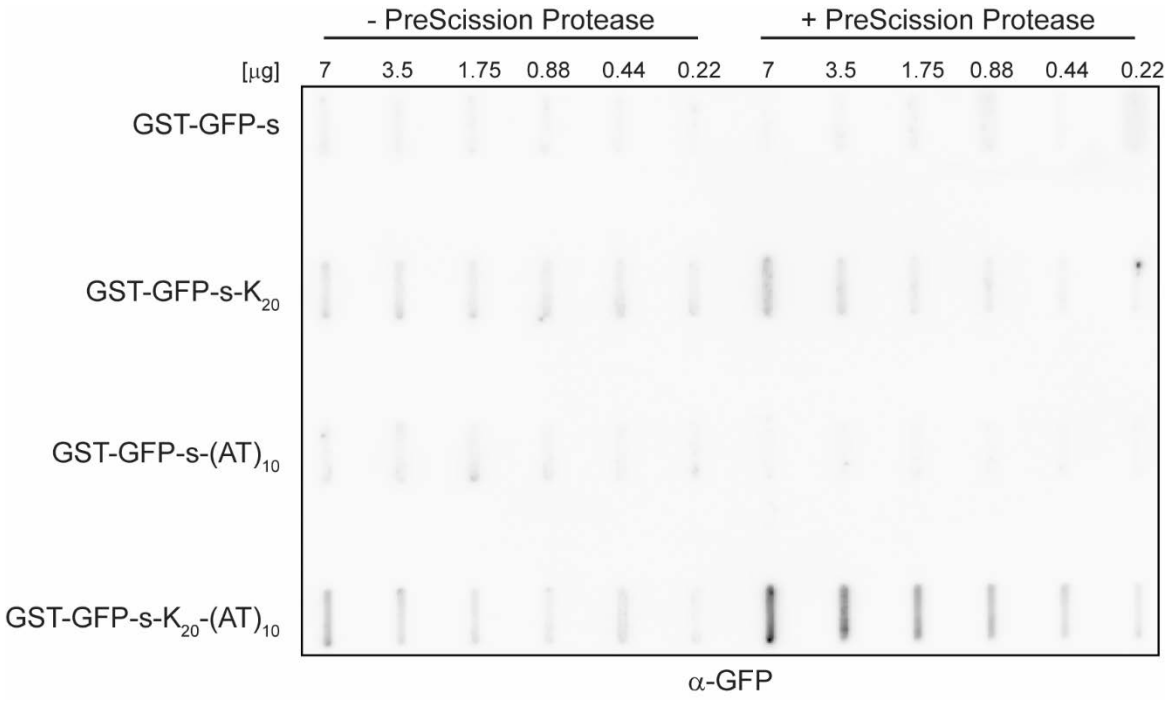

Fig. III.22: Both a polybasic stretch and a CAT tail are required for efficient aggregation *in vitro*. Purified constructs were incubated with buffer or PreScission protease, and indicated amounts were analyzed by a filter retardation assay. SDS-resistant aggregates were detected by immunoblotting against GFP.

III.7 Proteotoxicity of stalled nascent chains is suppressed by the limited capacity of Rqc2p to synthesize CAT tails

The aggregation of stalled nascent chains has been shown to be dependent on the Rqc2p-mediated addition of CAT tails; however, failure of ribosomal quality control and the accumulation of aberrant polypeptides *per se* did not exert a general proteotoxic effect. We reasoned that overexpression of a stalling reporter construct might exceed the capacity of the RQC pathway, resulting in a significant amount of nascent chains escaping CAT tail addition, rendering them less aggregation-prone than their CAT-tailed counterparts. The toxicity of aberrant polypeptides carrying CAT tails could therefore be limited by the availability of Rqc2p under physiological conditions.

To test whether overexpression of a reporter construct containing an internal stalling sequence exceeds the capacity of endogenous Rqc2p to add CAT tails, FLAG-tagged Rqc2p or the CAT tail-defective mutant rqc2$_{aaa}$ were additionally overexpressed in WT and *ltn1*Δ cells. Indeed, overexpression of wildtype Rqc2p and a stalling reporter resulted in a strong growth defect in *ltn1*Δ cells, whereas overexpression of mutant rqc2$_{aaa}$ did not exert a toxic effect (Fig. III.23a). Conversely, overexpression of Rqc2p in WT cells did not lead to a measurable growth defect, consistent with efficient degradation of stalled nascent polypeptides (Fig. III.23a). Interestingly, toxicity of the stalled reporter construct in the presence of excess amounts of Rqc2p was dependent on the presence of a stalling sequence, but not on its length (Fig. III.23b).

Since the Rqc2p-dependent addition of CAT tails was shown to be necessary for aggregation of stalled nascent chains, it seemed possible that overexpression of Rqc2p would lead to strongly enhanced aggregation of stalling reporter constructs. Indeed, overexpression of wildtype Rqc2p, but not of mutant rqc2$_{aaa}$, resulted in strong aggregation of GFP-s-R20$_{RARE}$-mCh in *ltn1*Δ cells, as judged by the appearance of SDS-resistant aggregates and visible inclusions (Fig. III.24a, b). In contrast, overexpression of wildtype Rqc2p in WT cells had no effect on the

aggregation behavior of GFP-s-R20RARE-mCh, consistent with these cells showing no measurable growth defect (Fig. III.23a and III.24a, b).

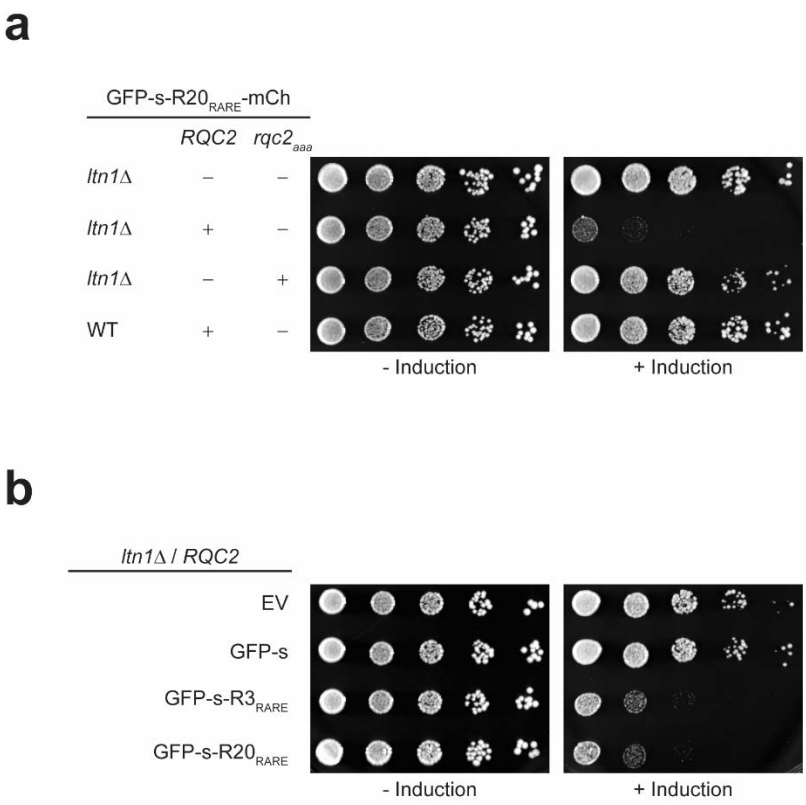

Fig. III.23: Rqc2p becomes the limiting factor upon overexpression of stalling reporter constructs. (a) WT and *ltn1*Δ cells expressing GFP-s-R20RARE-mCh and either empty vector (EV), WT Rqc2p or mutant rqc2aaa under control of the *GAL1* promoter were grown to mid-log phase in Raffinose medium, and serial dilutions were spotted onto dropout plates supplied with Glucose (- Induction) or Raffinose and Galactose (+ Induction). Plates were incubated for 2-3 days at 30 °C. (b) *ltn1*Δ cells expressing wildtype Rqc2p and either empty vector (EV) or one of the indicated reporter constructs were grown to mid-log phase in Raffinose medium and processed as described in (a). Data obtained in collaboration with Dr. Young-Jun Choe.

In summary, these results suggest that upon overexpression of stalled nascent chains in the absence of *LTN1*, only a fraction of aberrant translation products are elongated with CAT tails due to the low abundance of endogenous Rqc2p. Upon additional overexpression of Rqc2p,

however, the majority of aberrant polypeptides receives CAT tails, which results in strongly enhanced aggregation and proteotoxicity.

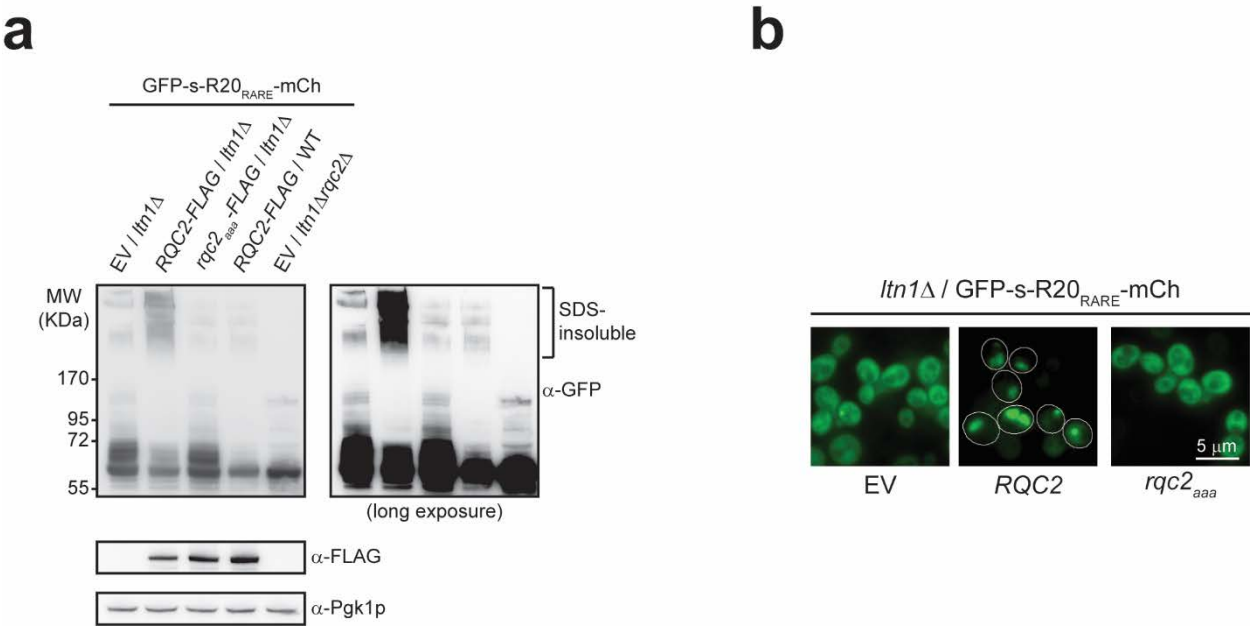

Fig. III.24: Overexpression of RQC2, but not of rqc2$_{aaa}$, leads to enhanced formation of SDS-resistant aggregates and visible inclusions in *ltn1*Δ cells. (a) Cell extracts were prepared from WT, *ltn1*Δ, and *ltn1*Δ*rqc2*Δ cells expressing GFP-s-R20$_{RARE}$-mCh and either empty vector (EV), WT Rqc2p or mutant rqc2$_{aaa}$ and subjected to immunoblotting against GFP. Expression of Rqc2p variants was confirmed by immunoblotting against the FLAG epitope. Pgk1p served as a loading control. (b) *ltn1*Δ cells expressing GFP-s-R20$_{RARE}$-mCh and either empty vector (EV), WT Rqc2p or mutant rqc2$_{aaa}$ were analyzed by fluorescence microscopy. Scale bar, 5 μm. Data obtained in collaboration with Dr. Young-Jun Choe.

III.8 Stalling mRNAs are preferentially degraded via the SKI complex-exosome pathway

Ribosomal stalling has been shown to induce endonucleolytic cleavage of the aberrant transcript by a yet unknown endonuclease, giving rise to two mRNA fragments that can be degraded from the 5′ or the 3′ end by Xrn1p or the cytosolic SKI complex-exosome pathway, respectively (Doma

and Parker 2006, Van Hoof and Wagner 2011, Shoemaker and Green 2012). Previous studies have shown that the adaptor protein Ski7p, which mediates contact between the SKI complex and the cytosolic exosome, plays a role in NSD (Frischmeyer, van Hoof *et al.* 2002, van Hoof, Frischmeyer *et al.* 2002). Overexpression of Rqc2p and the stalling reporter GFP-s-R3$_{RARE}$ resulted in a strong growth defect in cells lacking *LTN1* and the SKI complex helicase *SKI2*, but not in cells lacking the exonuclease *XRN1* (Fig. III.25). This suggests that aberrant recombinant transcripts are preferentially degraded via the cytosolic SKI complex-exosome pathway, and that failure of this branch of mRNA surveillance leads to accumulation of faulty transcripts and thus to repeated rounds of translation and production of toxic aberrant polypeptides. This was further supported by the notion that overexpression of Rqc2p alone was already sufficient to cause a strong growth defect in *ltn1*Δ*ski2*Δ cells, indicating that endogenous aberrant mRNAs are also preferentially degraded from their 3' end and accumulate to toxic levels upon failure of the SKI complex-exosome pathway (Fig. III.25).

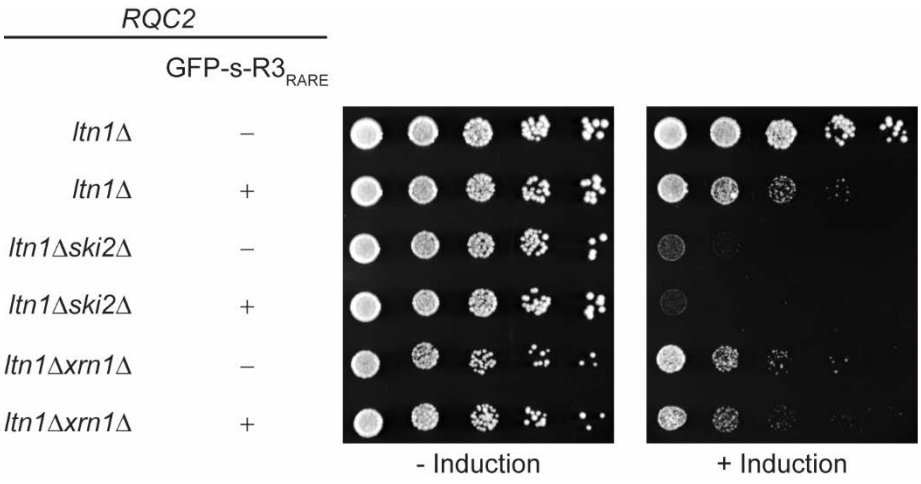

Fig. III.25: Both recombinant and endogenous faulty mRNAs are preferentially degraded via the cytosolic SKI complex-exosome pathway. Indicated strains expressing Rqc2p and either an empty vector control or GFP-s-R3$_{RARE}$ were grown to mid-log phase in Raffinose medium, and serial dilutions were spotted onto dropout plates supplied with Glucose (- Induction) or Raffinose and Galactose (+ Induction). Plates were incubated for 2-3 days at 30 °C. Data obtained in collaboration with Dr. Young-Jun Choe.

To further confirm that the growth defect observed in *ltn1*Δ*ski2*Δ cells was caused by impairment of the SKI complex-exosome machinery and not due to a SKI complex-independent effect caused by deletion of *SKI2*, mutant strains lacking each of the components of the SKI complex, i.e. Ski3p, Ski7p and Ski8p, were generated. As expected, all strains showed a strong growth defect upon overexpression of Rqc2p, accompanied by an enhanced formation of SDS-resistant, Sis1p-positive aggregates (Fig. III.26a, b). Protein aggregation is a concentration-dependent process, and thus larger Sis1p aggregates reflect more abundant stalled chains in *ltn1*Δ*ski7*Δ and *ltn1*Δ*ski2*Δ cells (Fig. III. 26b). Conversely, overexpression of Rqc2p in *ltn1*Δ*xrn1*Δ cells did not cause a measurable growth defect and even resulted in slightly reduced levels of Sis1p aggregation when compared to *ltn1*Δ cells (Fig. III.26a, b). It is notable that the level of overexpressed Rqc2p is lower in *ltn1*Δ*ski7*Δ and *ltn1*Δ*ski2*Δ cells, indicating that there was a negative selection pressure due to a strong toxicity of Rqc2p in these cells (Fig. III.26b).

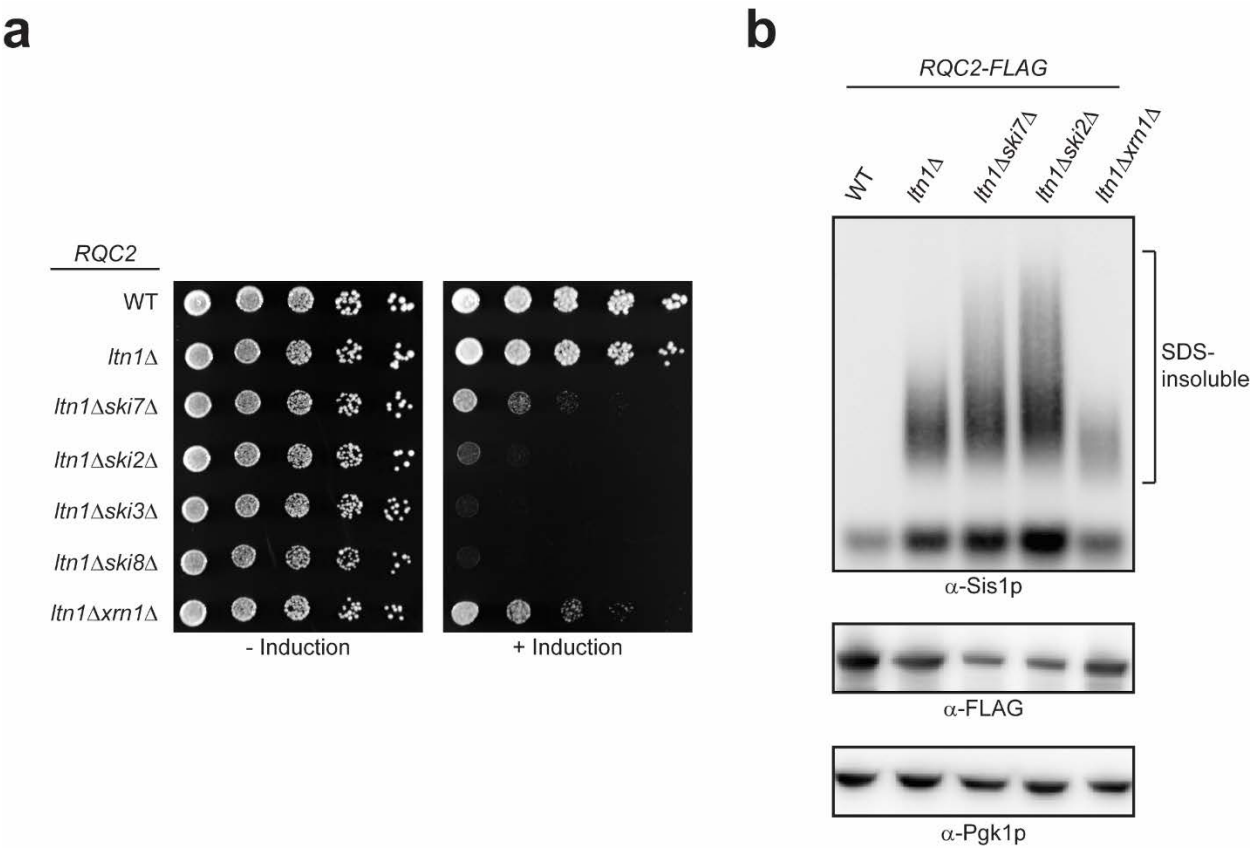

Fig. III.26: Overexpression of Rqc2p causes toxic aggregation of Sis1p in cells lacking a functional RQC and exosome pathway. (a) Rqc2p was expressed in the indicated strains, cells were grown to mid-log phase in Raffinose medium, and serial dilutions were spotted onto dropout plates supplied with Glucose (- Induction) or Raffinose and Galactose (+ Induction). Plates were incubated for 2-3 days at 30 °C. Data obtained in collaboration with Dr. Young-Jun Choe. (b) Cell extracts were prepared from the indicated strains expressing Rqc2p and resolved by SDD-AGE and SDS-PAGE, followed by immunoblotting against Sis1p. Expression of Rqc2p was confirmed by immunoblotting against the FLAG epitope. Pgk1p served as a loading control.

RQC assembly (and thus elongation of stalled nascent chains with CAT tails) requires dissociation of the stalled ribosome by the Dom34p/Hbs1p machinery. Therefore, deletion of *DOM34* and *HBS1* was expected to reduce the amount of RQC substrates, thereby reducing both cytotoxicity and aggregation of Sis1p. Indeed, deletion of either of the genes in an *ltn1*Δ*ski7*Δ background efficiently suppressed the growth defect and reduced the amount of Sis1p-positive aggregates caused by Rqc2p overexpression (Fig. III.27a, b).

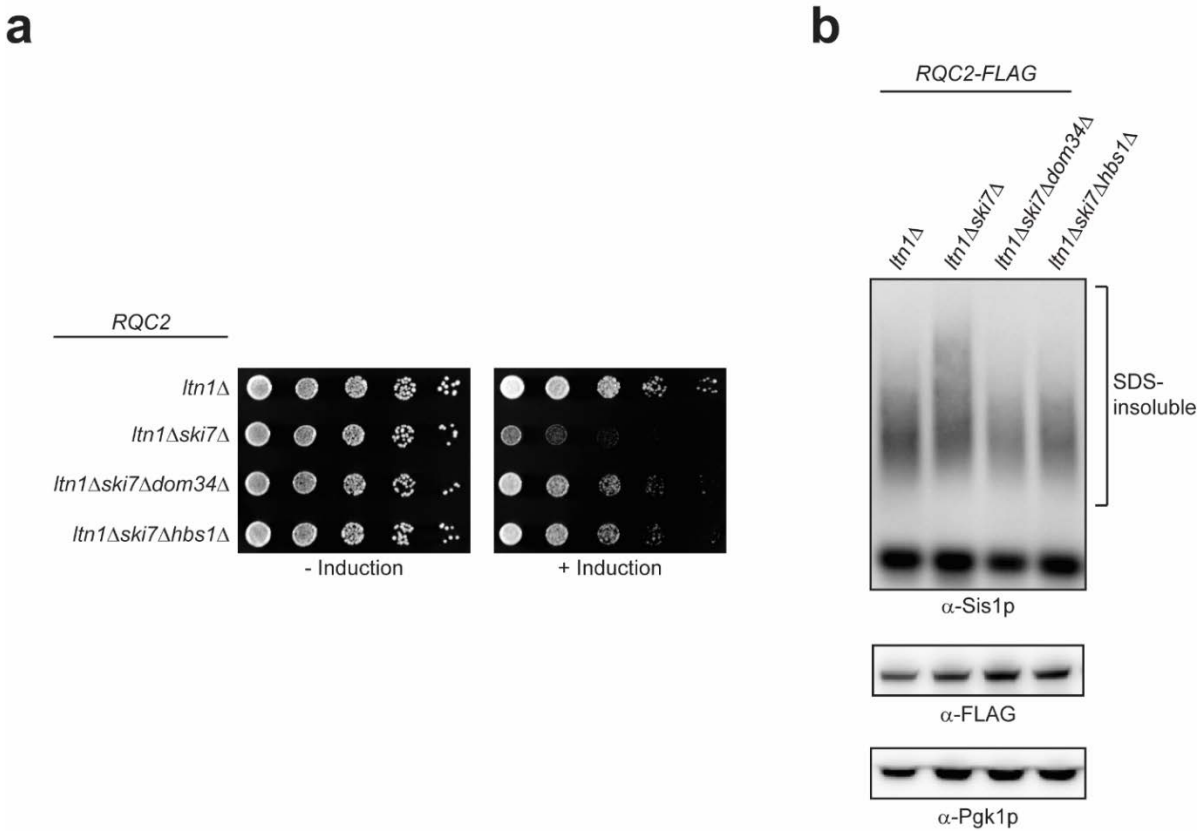

Fig. III.27: Inhibition of dissociation of stalled ribosomes efficiently suppresses toxic effects caused by Rqc2p overexpression. (a) Rqc2p was expressed in the indicated strains, cells were grown to mid-log phase in Raffinose medium, and serial dilutions were spotted onto dropout plates supplied with Glucose (- Induction) or Raffinose and Galactose (+ Induction). Plates were incubated for 2-3 days at 30 °C. Data obtained in collaboration with Dr. Young-Jun Choe. (b) Cell extracts were prepared from the indicated strains expressing Rqc2p and resolved by SDD-AGE and SDS-PAGE, followed by immunoblotting against Sis1p. Expression of Rqc2p was confirmed by immunoblotting against the FLAG epitope. Pgk1p served as a loading control.

Taken together, simultaneous impairment of RNA and ribosomal protein quality control results in massive accumulation of aberrant polypeptides due to repeated rounds of translation of faulty transcripts. However, due to the limited capacity of the RQC pathway, most stalled nascent chains escape CAT tail elongation and remain soluble, thereby preventing sequestration of essential chaperones like Sis1p to a toxic level. Overexpression of Rqc2p, however, leads to efficient CAT tail addition and thus strong aggregation of endogenous stalled polypeptides

III.9 Overexpression of Rqc2p triggers the cytosolic heat shock response

Initial studies on the RQC complex suggested a role of Rqc2p in triggering the Hsf1p-mediated heat shock response in the absence of *LTN1* (Brandman, Stewart-Ornstein *et al.* 2012). Given that the aggregation of aberrant polypeptides depends on Rqc2p-mediated CAT tail elongation and that accumulation of misfolded polypeptides *per se* can induce the cytosolic heat shock response, it seemed plausible that Hsf1p signaling could be mediated – directly or indirectly – by CAT tails.

To test this, wildtype or mutant Rqc2p variants were expressed in WT or *ltn1*Δ cells, and steady-state levels of heat shock-inducible chaperones such as Hsp104p, Sis1p, Hsp42p and Hsp26p were determined (Fig. III.28a). As expected, overexpression of wildtype Rqc2p in *ltn1*Δ cells resulted in an up to two-fold upregulation of these chaperones, whereas expression of the CAT tail-defective mutant rqc2$_{aaa}$ barely affected their steady-state levels (Fig. III.28a).

Interestingly, deletion of *LTN1* alone induced a slight upregulation of all chaperones, indicating that endogenous Rqc2p is already sufficient to elicit a mild heat shock response (Fig. III.28a). To further prove that the upregulation of the aforementioned chaperones is indeed a result of Hsf1p activation, β-galactosidase (lacZ) was expressed as a reporter under control of a heat shock-inducible promoter. Coexpression of this reporter with WT Rqc2p in *ltn1*Δ cells resulted in a two-fold increase in steady-state level and a 1.5-fold increase in activity of β-galactosidase, whereas expression of the $rqc2_{aaa}$ mutant did not affect β-galactosidase levels or activity (Fig. III.28b, c). Again, deletion of *LTN1* alone was already sufficient to cause a slight increase in β-galactosidase levels and activity (Fig. III.28b, c). These results indicate that Rqc2p, via its ability to synthesize CAT tails, activates Hsf1p and thus triggers the upregulation of heat shock-inducible chaperones.

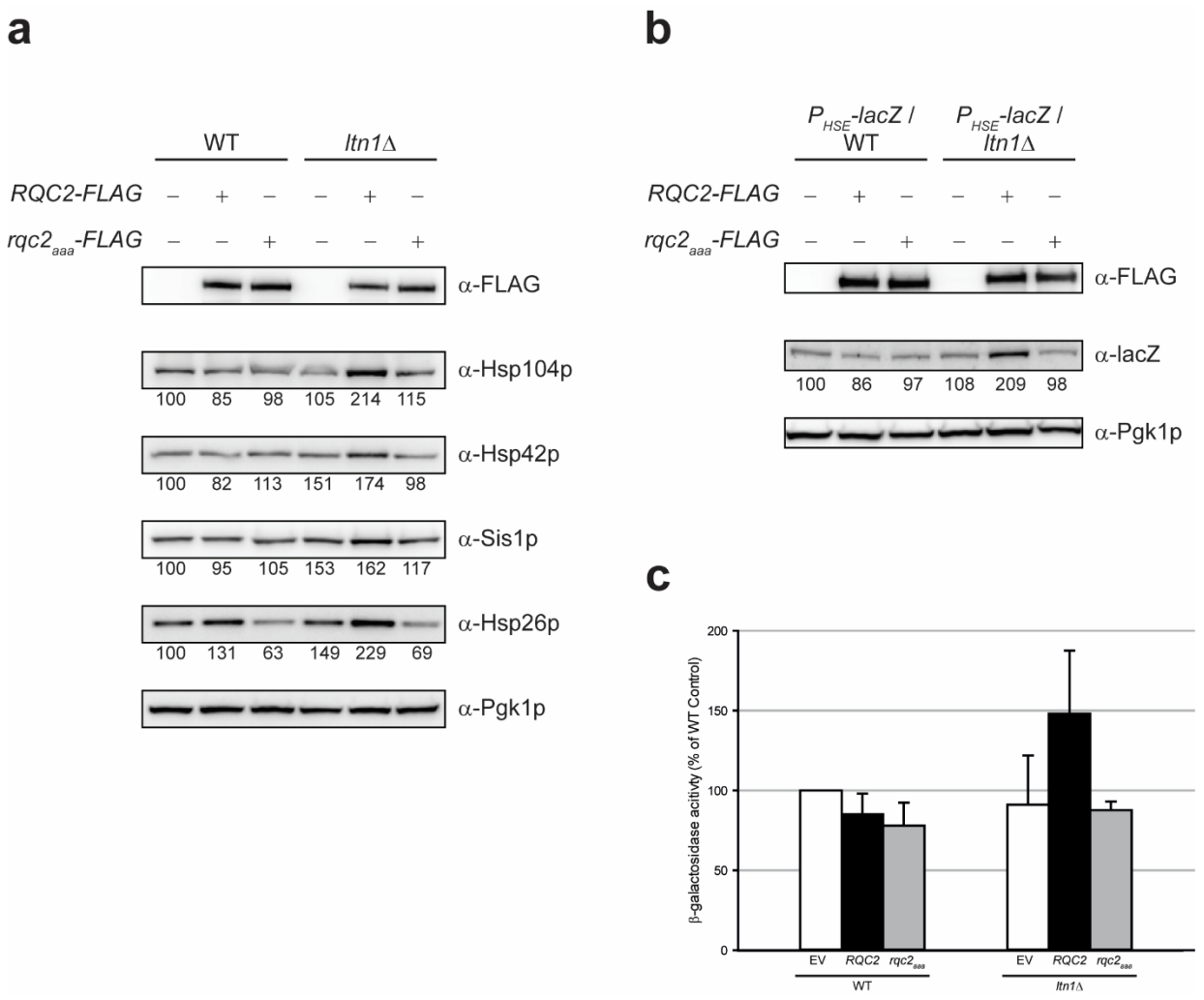

Fig. III.28: Rqc2p activates the cytosolic heat shock response in the absence of *LTN1*. (a) Cell extracts were prepared from WT and *ltn1*Δ cells expressing either empty vector (EV), wildtype Rqc2p, or mutant rqc2$_{aaa}$, and subjected to immunoblotting using the indicated antibodies. Expression of Rqc2p variants was confirmed by immunoblotting against the FLAG tag. Pgk1p served as a loading control. Band intensities were quantified by densitometry. (b) Cell extracts were prepared from WT and *ltn1*Δ cells expressing β-Galactosidase (lacZ) under control of a heat shock-inducible promoter and either empty vector (EV), wildtype Rqc2p, or mutant rqc2$_{aaa}$, and subjected to immunoblotting against β-Galactosidase. Expression of Rqc2p variants was confirmed by immunoblotting against the FLAG epitope. Pgk1p served as a loading control. Band intensities were quantified by densitometry. (c) The same cell extracts as used in (b) were assayed for β-Galactosidase activity. Error bars represent standard deviation from three independent experiments.

III.10 Identification of endogenous stalled nascent chains

In order to identify potential endogenous stalled nascent chains, we used a stable isotopic labeling with amino acids in cell culture (SILAC)-based mass spectrometry approach. To this end, we first exploited the tendency of Sis1p to coaggregate with aberrant polypeptides in order to isolate SDS-resistant aggregates by immunoprecipitation. *ltn1*Δ cells harboring an empty vector were used as a background control and labeled with light (L) lysine. In contrast, *ltn1*Δ cells or *ltn1*Δ*ski7*Δ cells overexpressing Rqc2p were labeled with medium (M) or heavy (H) lysine, respectively. Following immunoprecipitation of genomically tagged HA-Sis1p, LC-MS/MS analysis showed that 188 proteins were reproducibly enriched in SDS-resistant aggregates isolated from *ltn1*Δ*ski7*Δ cells overexpressing Rqc2p when compared to aggregates isolated from *ltn1*Δ cells harboring an empty vector (Fig. III.29). Essentially all proteins that were enriched based on their M/L and H/M SILAC ratios were also identified in the H/L dataset, suggesting a synergistic effect of quantitative CAT tail elongation and impairment of RNA quality control on the accumulation and aggregation of stalled nascent chains (Fig. III.29). The list of 188 proteins identified in this experiment should thus contain potential endogenous stalled polypeptides.

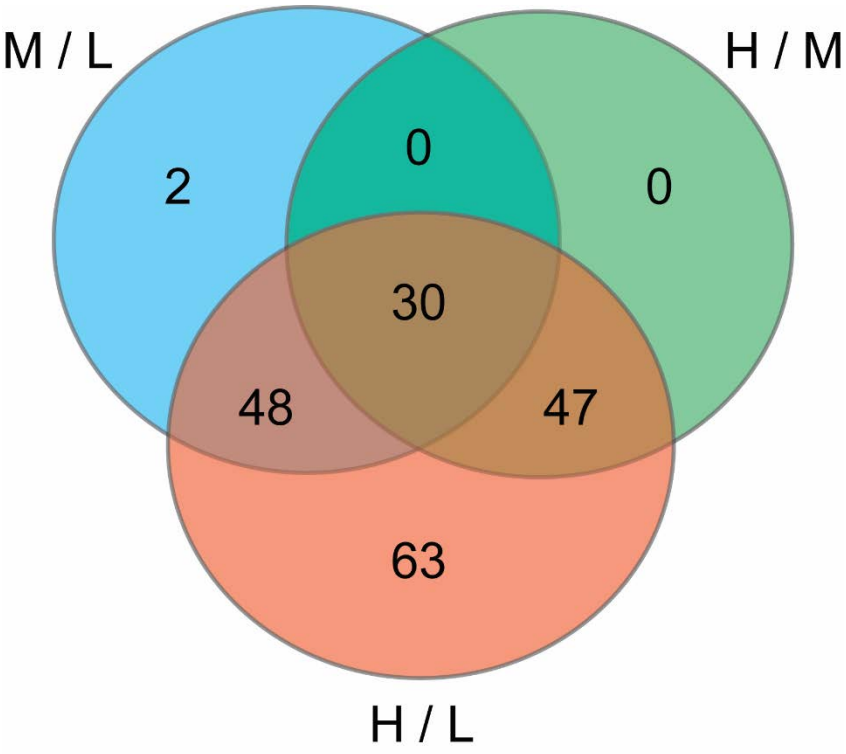

Fig. III.29: Venn diagram of proteins enriched in SDS-resistant aggregates after immunoprecipitation of genomically tagged HA-Sis1p. SILAC ratios were calculated by comparing peak intensities between proteins labeled with medium and light lysine (M/L, blue circle), heavy and medium lysine (H/M, green circle), or heavy and light lysine (H/L, red circle). Numbers indicate the amount of proteins that were enriched 2-fold or higher in at least two out of three independent experiments.

Earlier work identified four genes that produce truncated transcripts, possibly due to the existence of cryptic polyadenylation signals within the ORF: *CBP1*, *SIR3*, *AEP2*, and *RNA14* (Sparks and Dieckmann 1998). Furthermore, 127 of the 826 yeast genes deposited in the PACdb database were predicted to contain at least one internal polyadenylation signal that could also give rise to alternative 3' processing and thus truncated transcripts (Brockman, Singh *et al.* 2005). Of those, 8 proteins were also identified by mass spectrometry to be significantly enriched in SDS-resistant aggregates, suggesting that these proteins could indeed represent stalled polypeptides that arise from translation of aberrant transcripts (Tab. III.1). Although *RQC2* was predicted to contain a polyadenylation signal within its coding sequence, the massive enrichment of the corresponding protein in SDS-resistant aggregates is probably an artifact due to overexpression

of recombinant Rqc2p. Furthermore, due to its size of approximately 120 kDa, a fraction of Rqc2p might have been accidentally copurified during isolation of SDS-resistant aggregates from the gel. Immunoblotting for Rqc2p failed to detect any SDS-resistant species comigrating with aggregates of stalled nascent chains (data not shown).

Tab. III.1 List of potential endogenous stalled nascent chains. The number of predicted internal polyadenylation sites was obtained from the PACdb database (Brockman, Singh *et al.* 2005).

Gene Name	Number of predicted int. polyadenylation sites	H/L Ratio	Description
RQC2	1	29.82	Translation-associated element 2
BAP2	1	7.24	Leu/Val/Ile amino-acid permease
AEP2	?	4.67	ATPase expression protein 2, mitochondrial
ATP1	2	4.35	ATP synthase subunit alpha, mitochondrial
PGK1	2	4.35	Phosphoglycerate kinase
RNA14	?	4.20	mRNA 3-end-processing protein RNA14
SAH1	1	3.87	Adenosylhomocysteinase
CPR6	1	3.19	Peptidyl-prolyl cis-trans isomerase CPR6

IV. Discussion

This study presents evidence that yeast cells with defective ribosome quality control (RQC) produce aberrant polypeptides from mRNAs that stall during translation. Stalling can be induced by stretches encoding polybasic sequences, the presence of multiple rare codons, or the absence of an in-frame stop codon. Translation of these faulty messages leads to an irreversible block of translation elongation or termination known as ribosomal stalling, and to synthesis of aberrant polypeptides, which are mostly non-functional and can pose a serious threat to proteome integrity due to their propensity to form aggregates and to sequester various key proteostasis factors. In healthy cells, stalled ribosomes are efficiently recognized and aberrant nascent chains targeted for proteasomal degradation by the RQC system. Failure of this pathway, however, results in accumulation of these nascent chains in SDS-resistant aggregates.

Besides binding at the subunit interface of the stalled 60S-peptidyl-tRNA complex and recruiting Ltn1p, Rqc2p was recently shown to mediate the template-independent elongation of stalled nascent chains with alanine and threonine residues (so-called CAT tails) (Shen, Park *et al.* 2015). During the course of this study, it was shown that aggregation of stalled aberrant polypeptides depends on the presence of these CAT tails, in a manner comparable to aggregation caused by the polyalanine repeats of certain disease proteins (Forood, Perez-Paya *et al.* 1995, Amiel, Trochet *et al.* 2004). In line with previous studies on polyQ and artificial β-sheet proteins, the aggregated nascent chains sequester various cellular proteostasis factors such as the essential Hsp40 chaperone Sis1p, thereby interfering with general protein quality control and leading to proteotoxic stress (Olzscha, Schermann *et al.* 2011, Park, Kukushkin *et al.* 2013). Interestingly, the additional impairment of exosome-mediated RNA quality control resulted in massive accumulation of aberrant polypeptides and a strong growth defect, but only when Rqc2p was overexpressed. This provides evidence that, under normal conditions, the potentially toxic nature of CAT tails is suppressed by the low abundance of endogenous Rqc2p and thus its limited capacity to quantitatively elongate stalled nascent chains.

IV.1 Failure of RQC leads to the formation of SDS-resistant aggregates

During translation of a truncated transcript, ribosomes stall at the 3' end of the mRNA due to the absence of a codon in the ribosomal A-site (Fig. IV.1, upper panel). Following dissociation of the stalled ribosome by the Dom34p/Hbs1p complex and mRNA decay, the RQC complex engages the stalled 60S-peptidyl-tRNA complex and mediates CAT tail elongation of the stalled nascent chain via its component Rqc2p (Fig. IV.1, upper panel). When the RQC system is compromised, as in the absence of Ltn1p, nascent chains are released from the ribosome in a nonubiquitinated form, and CAT tails mediate the formation of SDS-resistant oligomeric aggregates that sequester various chaperones, including the Hsp40 Sis1p, which in turn results in proteotoxic stress (Fig. IV.1, upper panel). Translation of mRNAs lacking an in-frame stop codon, however, leads to elongation of the nascent chain with a polylysine stretch due to the poly(A) tail being interpreted as part of the ORF (Fig. IV.1, bottom panel). Following ribosome dissociation, CAT tail elongation, and release of the nascent chain, the formation of SDS-resistant oligomeric aggregates is again mediated by the hydrophobic nature of CAT tails (Fig. IV.1, bottom panel). Formation of visible inclusions may then be mediated by the polybasic tracts of NS-proteins, consistent with earlier observations of polylysine being able to form amyloid-like β-sheet fibrils at high pH (Fig. IV.1, bottom panel) (Fandrich and Dobson 2002). At physiological pH, negatively charged molecules such as polyphosphate or nucleic acids could aid in overcoming charge repulsion effects (Gray, Wholey *et al.* 2014). Again, NS-protein aggregates sequester various proteostasis factors, but the exact role of CAT tails in this process remains to be elucidated (Fig. IV.1, bottom panel). Similar to polyalanine repeats in certain disease proteins, the ability of polybasic sequences to form toxic aggregates has been described, e.g. in the case of Gly-Arg or Pro-Arg dipeptide repeats in mutant *C9orf72* genes associated with amyotrophic lateral sclerosis and frontotemporal dementia (Mori, Weng *et al.* 2013, Zu, Liu *et al.* 2013). Despite the absence of a clear growth defect upon RQC impairment, the aggregation of stalled nascent chains interferes with general protein quality control pathways and has the potential to cause chronic proteotoxic stress by inducing a vicious cycle of upregulation and depletion of essential

proteostasis factors (Hipp, Park *et al.* 2014, Roth, Hutt *et al.* 2014). Strikingly, failure of the RQC system is highly toxic and results in a severe growth defect when cells are exposed to additional proteostasis stress, such as elevated temperatures, expression of misfolding proteins, or drugs that decrease translational fidelity. Since aging also represents a challenge to the proteostasis network, it is tempting to speculate that aggregation of stalled polypeptides contributes to the neurodegenerative phenotype observed in Listerin-deficient mice (Chu, Hong *et al.* 2009).

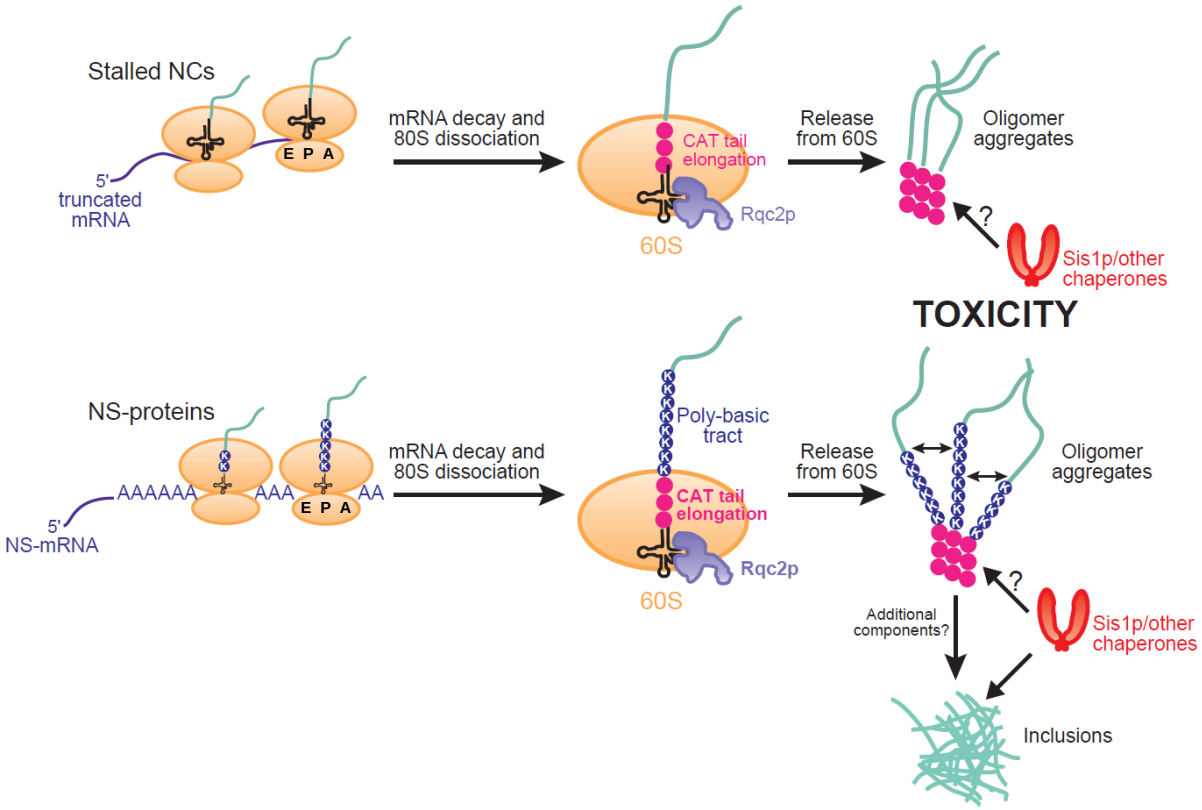

Fig. IV.1: Mechanism of aggregate formation upon failure of RQC. Translation of aberrant mRNAs leads to ribosomal stalling in the 3' region of the transcript. Following ribosome dissociation and RQC assembly at the 60S-peptidyl-tRNA complex, Rqc2p mediates elongation of the stalled nascent polypeptide with CAT tails. Release of the modified nascent chain in a nonubiquitinated state (i.e. in the absence of Ltn1p) results in CAT tail-mediated aggregation and the formation of SDS-resistant oligomers that sequester key proteostasis players such as the Hsp40 Sis1p. In case of NS-mRNAs, stalled polypeptides carry an additional polylysine tract as a result of translation of the poly(A) tail. Following CAT tail-dependent oligomerization, polybasic stretches might aid in the formation of visible inclusions due to their ability to fold into highly stable amyloid-like β-sheet fibrils. E, P, A, ribosomal E-/P-/A-sites. Figure modified from (Choe, Park *et al.* 2016).

IV.2 The biological role of CAT tail addition

Given that the aggregation of aberrant nascent chains leads to proteotoxic stress, an important question concerns the biological role of CAT tails. Under normal conditions, ubiquitination of stalled polypeptides by Ltn1p would result in their rapid degradation by the proteasome, thereby preventing CAT tail-mediated aggregation. One possible function of CAT tails could be that of a spacer peptide, which serves to push the C-terminal part of the stalled nascent chain out of the ribosomal exit channel. This in turn could facilitate ubiquitination of lysine residues in the nascent chain by Ltn1p, especially in case of non-stop proteins which contain a C-terminal polylysine tract due to translation of the poly(A) tail of the aberrant transcript (Brandman and Hegde 2016). Furthermore, the addition of CAT tails might serve in overcoming electrostatic interactions between polybasic stretches of non-stop proteins and the negatively charged ribosomal exit channel, thus facilitating Cdc48p-dependent extraction of the stalled nascent chain. Another hypothesis is that the ability of Rqc2p to elicit an Hsf1p-dependent heat shock response (HSR) is mediated by CAT tails, which would be consistent with the *rqc2*$_{aaa}$ mutant not being able to induce upregulation of various molecular chaperones when ribosome stalling occurs (Shen, Park *et al.* 2015, Brandman and Hegde 2016). However, it remains to be determined whether activation of the HSR by CAT tails is mediated via a direct effect or rather indirectly, e.g. by enabling aberrant polypeptides to form aggregates that in turn cause mild proteotoxic stress and thus induce upregulation of heat shock proteins. It also remains unclear how many alanine and threonine residues are normally incorporated during the course of CAT tail elongation, and if the corresponding aminoacyl-tRNAs are recruited in a random or ordered manner. An initial study describing CAT tails characterized C-terminal elongations of up to 19 residues consisting of roughly equal amounts of alanine and threonine, but CAT tails of a much larger size and varying sequence could be possible (Shen, Park *et al.* 2015). Furthermore, the exact mechanism and the kinetics of CAT tail elongation by Rqc2p as well as its processivity still remain elusive. Since quantitative elongation of stalled nascent polypeptides with CAT tails seems to be limited by the abundance of endogenous Rqc2p, it would be interesting to determine whether

Rqc2p overexpression results in longer CAT tails or in unspecific recognition of ribosomes, e.g. ribosomes that undergo only transient translational pausing.

IV.3 Cooperation of RNA and protein quality control pathways at the ribosome

During the course of this study, it could be shown that simultaneous disruption of exosome-dependent RNA quality control and the RQC pathway leads to massive accumulation of stalled nascent chains, probably due to repeated translation of faulty transcripts. This accumulation however, proved to be highly toxic only in the context of Rqc2p overexpression, indicating that endogenous Rqc2p is insufficient to mediate quantitative elongation of aberrant polypeptides with CAT tails. This is not surprising, considering that ribosomes (≈ 200,000 molecules per cell) outnumber the components of the RQC system by a factor of up to 1,000 (Warner 1999, Ghaemmaghami, Huh *et al.* 2003). Surprisingly, mRNAs causing ribosomes to stall seem to be preferentially degraded via the SKI complex-exosome pathway, whereas abrogation of Xrn1p-dependent mRNA decay did not exhibit a toxic effect. In general, all transcripts should be degradable by both Xrn1p and the exosome after decapping or deadenylation, respectively. However, the process of deadenylation might be preferred over decapping in the case of faulty mRNAs, thereby favoring degradation of these transcripts from the 3' end via the SKI complex-exosome system. Interestingly, the adaptor protein Ski7p, which is only present in a subset of fungi, was also shown to be necessary for the degradation of aberrant mRNAs in earlier studies (Frischmeyer, van Hoof *et al.* 2002, van Hoof, Frischmeyer *et al.* 2002). Consistent with this work, deletion of *SKI7* resulted in a phenotype that was similar, albeit less pronounced, to the one observed upon direct deletion of SKI complex components. The human homolog of Ski7p has just recently been identified as a splice variant of human Hbs1p, but it remains to be determined whether this factor is also involved in the degradation of aberrant transcripts in humans (Kowalinski, Kogel *et al.* 2016). Future studies could also focus on the identification of the

endonuclease that mediates cleavage of aberrant mRNAs in the vicinity of stalled ribosomes and triggers the NGD pathway.

IV.4 Identification of endogenous stalled nascent chains

Recent studies have provided detailed insights into the molecular mechanisms of the RQC pathway and its structural basis using recombinant transcripts containing stalling features (Shao, Brown *et al.* 2015, Choe, Park *et al.* 2016, Yonashiro, Tahara *et al.* 2016). However, the identity of endogenous stalled nascent chains as well as the frequency of stalling events and the reasons for ribosomal stalling under normal conditions are still unknown. Recent work suggests that less than 5 % of all nascent chains in a cell are subject to cotranslational ubiquitination, suggesting that the amount of polypeptides that is getting ubiquitinated by Ltn1p as a result of ribosomal stalling is even lower (Duttler, Pechmann *et al.* 2013). This is consistent with ribosomes outnumbering RQC complexes by a factor of 100-1,000 in a yeast cell (Warner 1999, Ghaemmaghami, Huh *et al.* 2003). Since every transcript can potentially be subject to erroneous RNA maturation, endonucleolytic cleavage or spontaneous mutations, transcription of virtually any gene could potentially result in an aberrant mRNA. However, mRNA maturation processes such as polyadenylation are not always 100% specific and rely on conserved sequence motifs within the pre-mRNA. Thus, premature addition of a poly(A) tail can also occur due to recognition of a cryptic polyadenylation site within the coding sequence of a gene, resulting in generation of a non-stop mRNA. Whereas initial *in silico* studies showed that up to 0.8 % of yeast ORFs contain a cryptic poly(A) signal that could lead to premature polyadenylation, later work suggested an even higher number (Frischmeyer, van Hoof *et al.* 2002, Brockman, Singh *et al.* 2005). Translation of these truncated messages could possibly result in ribosomal stalling, and a defect in exosome-mediated mRNA quality control together with Rqc2p overexpression should result in strong aggregation of the respective aberrant translation products. Indeed, a SILAC-based approach led to the identification of 7 genes that not only showed strong enrichment in SDS-

resistant aggregates isolated from *ltn1*Δ*ski7*Δ cells overexpressing Rqc2p, but were also predicted to have at least one cryptic polyadenylation signal within their coding sequence. The 7 genes corresponding to these proteins are thus promising candidates for production of stalled nascent chains. However, as premature polyadenylation would only result in the production of NS-mRNAs, these candidates might only represent a subset of all endogenous aberrant polypeptides. The prediction of internal stalling features, such as stretches containing rare codons, or having a tendency to form secondary structures, is challenging. Furthermore, random events that would lead to generation of truncated mRNAs, e.g. unspecific endonucleolytic cleavage or errors during splicing, are impossible to predict. Therefore, the major causes for ribosomal stalling still remain elusive. Future studies should try to combine *in silico* and *in vivo* approaches to identify the reasons for ribosomal stalling under physiologic conditions.

In summary, the work presented here describes the mechanism of aggregation for stalled nascent polypeptides and the reasons for proteotoxicity upon RQC impairment. It could also be shown that RNA and protein quality control pathways tightly cooperate at the ribosome in order to protect cells from the deleterious effects of aberrant polypeptides. Furthermore, this study provides first evidence for the identification of endogenous stalled nascent chains, and also suggests a model for the formation of SDS-resistant aggregates *in vitro*. These findings provide novel insights into the mechanisms of protein quality control in eukaryotic cells and could possibly aid in understanding the role of protein aggregation in neurodegenerative diseases.

V. References

Akerfelt, M., R. I. Morimoto and L. Sistonen (2010). "Heat shock factors: integrators of cell stress, development and lifespan." Nat Rev Mol Cell Biol **11**(8): 545-555.

Amiel, J., D. Trochet, M. Clement-Ziza, A. Munnich and S. Lyonnet (2004). "Polyalanine expansions in human." Hum Mol Genet **13 Spec No 2**: R235-243.

Amm, I., T. Sommer and D. H. Wolf (2014). "Protein quality control and elimination of protein waste: the role of the ubiquitin-proteasome system." Biochim Biophys Acta **1843**(1): 182-196.

Anckar, J. and L. Sistonen (2011). Regulation of HSF1 function in the heat stress response: Implications in aging and disease. Annual Review of Biochemistry. **80:** 1089-1115.

Anfinsen, C. B. (1972). "The formation and stabilization of protein structure." Biochem J **128**(4): 737-749.

Anfinsen, C. B. (1973). "Principles that govern the folding of protein chains." Science **181**(4096): 223-230.

Arias, E. and A. M. Cuervo (2011). "Chaperone-mediated autophagy in protein quality control." Curr Opin Cell Biol **23**(2): 184-189.

Arndt, V., N. Dick, R. Tawo, M. Dreiseidler, D. Wenzel, M. Hesse, D. O. Furst, P. Saftig, R. Saint, B. K. Fleischmann, M. Hoch and J. Hohfeld (2010). "Chaperone-assisted selective autophagy is essential for muscle maintenance." Curr Biol **20**(2): 143-148.

Arrasate, M., S. Mitra, E. S. Schweitzer, M. R. Segal and S. Finkbeiner (2004). "Inclusion body formation reduces levels of mutant huntingtin and the risk of neuronal death." Nature **431**(7010): 805-810.

Arthur, L., S. Pavlovic-Djuranovic, K. Smith-Koutmou, R. Green, P. Szczesny and S. Djuranovic (2015). "Translational control by lysine-encoding A-rich sequences." Sci Adv **1**(6).

Arthur, L. L., J. J. Chung, P. Jankirama, K. M. Keefer, I. Kolotilin, S. Pavlovic-Djuranovic, D. L. Chalker, V. Grbic, R. Green, R. Menassa, H. L. True, J. B. Skeath and S. Djuranovic (2017). "Rapid generation of hypomorphic mutations." Nat Commun **8**: 14112.

Balch, W. E., R. I. Morimoto, A. Dillin and J. W. Kelly (2008). "Adapting proteostasis for disease intervention." Science **319**(5865): 916-919.

Balchin, D., M. Hayer-Hartl and F. U. Hartl (2016). "In vivo aspects of protein folding and quality control." Science **353**(6294): aac4354.

Barriere, H., C. Nemes, K. Du and G. L. Lukacs (2007). "Plasticity of polyubiquitin recognition as lysosomal targeting signals by the endosomal sorting machinery." Mol Biol Cell **18**(10): 3952-3965.

Baudin, A., O. Ozier-Kalogeropoulos, A. Denouel, F. Lacroute and C. Cullin (1993). "A simple and efficient method for direct gene deletion in Saccharomyces cerevisiae." Nucleic Acids Res **21**(14): 3329-3330.

Becker, T., J. P. Armache, A. Jarasch, A. M. Anger, E. Villa, H. Sieber, B. A. Motaal, T. Mielke, O. Berninghausen and R. Beckmann (2011). "Structure of the no-go mRNA decay complex Dom34-Hbs1 bound to a stalled 80S ribosome." Nature Structural and Molecular Biology **18**(6): 715-720.

Ben-Zvi, A., E. A. Miller and R. I. Morimoto (2009). "Collapse of proteostasis represents an early molecular event in Caenorhabditis elegans aging." Proceedings of the National Academy of Sciences of the United States of America **106**(35): 14914-14919.

Bengtson, M. H. and C. A. Joazeiro (2010). "Role of a ribosome-associated E3 ubiquitin ligase in protein quality control." Nature **467**(7314): 470-473.

Bernasconi, R., T. Soldà, C. Galli, T. Pertel, J. Luban and M. Molinari (2010). "Cyclosporine A-Sensitive, Cyclophilin B-Dependent endoplasmic reticulum-associated degradation." PLoS ONE **5**(9).

Boczek, E. E., L. G. Reefschläger, M. Dehling, T. J. Struller, E. Häusler, A. Seidl, V. R. I. Kaila and J. Buchner (2015). "Conformational processing of oncogenic v-Src kinase by the molecular chaperone Hsp90." Proceedings of the National Academy of Sciences of the United States of America **112**(25): E3189-E3198.

Booth, D. R., M. Sunde, V. Bellotti, C. V. Robinson, W. L. Hutchinson, P. E. Fraser, P. N. Hawkins, C. M. Dobson, S. E. Radford, C. C. Blake and M. B. Pepys (1997). "Instability, unfolding and aggregation of human lysozyme variants underlying amyloid fibrillogenesis." Nature **385**(6619): 787-793.

Brandman, O. and R. S. Hegde (2016). "Ribosome-associated protein quality control." Nat Struct Mol Biol **23**(1): 7-15.

Brandman, O., J. Stewart-Ornstein, D. Wong, A. Larson, C. C. Williams, G. W. Li, S. Zhou, D. King, P. S. Shen, J. Weibezahn, J. G. Dunn, S. Rouskin, T. Inada, A. Frost and J. S. Weissman (2012). "A ribosome-bound quality control complex triggers degradation of nascent peptides and signals translation stress." Cell **151**(5): 1042-1054.

Brandt, F., L. A. Carlson, F. U. Hartl, W. Baumeister and K. Grünewald (2010). "The Three-Dimensional Organization of Polyribosomes in Intact Human Cells." Molecular Cell **39**(4): 560-569.

Brehme, M., C. Voisine, T. Rolland, S. Wachi, J. H. Soper, Y. Zhu, K. Orton, A. Villella, D. Garza, M. Vidal, H. Ge and R. I. Morimoto (2014). "A chaperome subnetwork safeguards proteostasis in aging and neurodegenerative disease." Cell Reports **9**(3): 1135-1150.

Brockman, J. M., P. Singh, D. Liu, S. Quinlan, J. Salisbury and J. H. Graber (2005). "PACdb: PolyA Cleavage Site and 3'-UTR Database." Bioinformatics **21**(18): 3691-3693.

Brockwell, D. J. and S. E. Radford (2007). "Intermediates: ubiquitous species on folding energy landscapes?" Curr Opin Struct Biol **17**(1): 30-37.

Bucciantini, M., G. Calloni, F. Chiti, L. Formigli, D. Nosi, C. M. Dobson and M. Stefani (2004). "Prefibrillar amyloid protein aggregates share common features of cytotoxicity." J Biol Chem **279**(30): 31374-31382.

Buell, A. K., C. M. Dobson and T. P. Knowles (2014). "The physical chemistry of the amyloid phenomenon: thermodynamics and kinetics of filamentous protein aggregation." Essays Biochem **56**: 11-39.

Buhr, F., S. Jha, M. Thommen, J. Mittelstaet, F. Kutz, H. Schwalbe, M. V. Rodnina and A. A. Komar (2016). "Synonymous Codons Direct Cotranslational Folding toward Different Protein Conformations." Molecular Cell **61**(3): 341-351.

Calamini, B., M. C. Silva, F. Madoux, D. M. Hutt, S. Khanna, M. A. Chalfant, S. A. Saldanha, P. Hodder, B. D. Tait, D. Garza, W. E. Balch and R. I. Morimoto (2012). "Small-molecule proteostasis regulators for protein conformational diseases." Nature Chemical Biology **8**(2): 185-196.

Calloni, G., T. Chen, S. M. Schermann, H. C. Chang, P. Genevaux, F. Agostini, G. G. Tartaglia, M. Hayer-Hartl and F. U. Hartl (2012). "DnaK Functions as a Central Hub in the E. coli Chaperone Network." Cell Reports **1**(3): 251-264.

Carvalho, P., V. Goder and T. A. Rapoport (2006). "Distinct Ubiquitin-Ligase Complexes Define Convergent Pathways for the Degradation of ER Proteins." Cell **126**(2): 361-373.

Carvalho, P., A. M. Stanley and T. A. Rapoport (2010). "Retrotranslocation of a misfolded luminal ER protein by the ubiquitin-ligase hrd1p." Cell **143**(4): 579-591.

Chen, L., D. Muhlrad, V. Hauryliuk, Z. Cheng, M. K. Lim, V. Shyp, R. Parker and H. Song (2010). "Structure of the Dom34-Hbs1 complex and implications for no-go decay." Nat Struct Mol Biol **17**(10): 1233-1240.

Choe, Y. J., S. H. Park, T. Hassemer, R. Korner, L. Vincenz-Donnelly, M. Hayer-Hartl and F. U. Hartl (2016). "Failure of RQC machinery causes protein aggregation and proteotoxic stress." Nature **531**(7593): 191-195.

Chu, J., N. A. Hong, C. A. Masuda, B. V. Jenkins, K. A. Nelms, C. C. Goodnow, R. J. Glynne, H. Wu, E. Masliah, C. A. Joazeiro and S. A. Kay (2009). "A mouse forward genetics screen identifies LISTERIN as an E3 ubiquitin ligase involved in neurodegeneration." Proc Natl Acad Sci U S A **106**(7): 2097-2103.

Chu, J., N. A. Hong, C. A. Masuda, B. V. Jenkins, K. A. Nelms, C. C. Goodnow, R. J. Glynne, H. Wu, E. Masliah, C. A. P. Joazeiro and S. A. Kay (2009). "A mouse forward genetics screen identifies LISTERIN as an E3 ubiquitin ligase involved in neurodegeneration." Proceedings of the National Academy of Sciences of the United States of America **106**(7): 2097-2103.

Ciechanover, A. and Y. T. Kwon (2015). "Degradation of misfolded proteins in neurodegenerative diseases: Therapeutic targets and strategies." Exp. Mol. Med **47**: e147.

Claessen, J. H. L., L. Kundrat and H. L. Ploegh (2011). Trends Cell Biol.

Cohen, S. I. A., P. Arosio, J. Presto, F. R. Kurudenkandy, H. Biverstål, L. Dolfe, C. Dunning, X. Yang, B. Frohm, M. Vendruscolo, J. Johansson, C. M. Dobson, A. Fisahn, T. P. J. Knowles and S. Linse (2015). "A molecular chaperone breaks the catalytic cycle that generates toxic Aβ oligomers." Nature Structural and Molecular Biology **22**(3): 207-213.

Daggett, V. and A. R. Fersht (2003). "Is there a unifying mechanism for protein folding?" Trends Biochem Sci **28**(1): 18-25.

Defenouillere, Q., Y. H. Yao, J. Mouaikel, A. Namane, A. Galopier, L. Decourty, A. Doyen, C. Malabat, C. Saveanu, A. Jacquier and M. Fromont-Racine (2013). "Cdc48-associated complex bound to 60S particles is required for the clearance of aberrant translation products." Proceedings of the National Academy of Sciences of the United States of America **110**(13): 5046-5051.

Defenouillere, Q., E. Zhang, A. Namane, J. Mouaikel, A. Jacquier and M. Fromont-Racine (2016). "Rqc1 and Ltn1 Prevent C-terminal Alanine-Threonine Tail (CAT-tail)-induced Protein Aggregation by Efficient Recruitment of Cdc48 on Stalled 60S Subunits." J Biol Chem **291**(23): 12245-12253.

del Alamo, M., D. J. Hogan, S. Pechmann, V. Albanese, P. O. Brown and J. Frydman (2011). "Defining the specificity of cotranslationally acting chaperones by systematic analysis of mRNAs associated with ribosome-nascent chain complexes." PLoS Biology **9**(7).

DePristo, M. A., D. M. Weinreich and D. L. Hartl (2005). "Missense meanderings in sequence space: a biophysical view of protein evolution." Nat Rev Genet **6**(9): 678-687.

Dill, K. A., S. Bromberg, K. Yue, K. M. Fiebig, D. P. Yee, P. D. Thomas and H. S. Chan (1995). "Principles of protein folding--a perspective from simple exact models." Protein Sci **4**(4): 561-602.

Dill, K. A. and H. S. Chan (1997). "From Levinthal to pathways to funnels." Nat Struct Biol **4**(1): 10-19.

Dinner, A. R., A. Sali, L. J. Smith, C. M. Dobson and M. Karplus (2000). "Understanding protein folding via free-energy surfaces from theory and experiment." Trends Biochem Sci **25**(7): 331-339.

Dobson, C. M. (1999). "Protein misfolding, evolution and disease." Trends Biochem Sci **24**(9): 329-332.

Dobson, C. M. (2004). "Principles of protein folding, misfolding and aggregation." Semin Cell Dev Biol **15**(1): 3-16.

Dobson, C. M., A. Šali and M. Karplus (1998). "Protein Folding: A Perspective from Theory and Experiment." Angewandte Chemie International Edition **37**(7): 868-893.

Doma, M. K. and R. Parker (2006). "Endonucleolytic cleavage of eukaryotic mRNAs with stalls in translation elongation." Nature **440**(7083): 561-564.

Drumm, M. L., D. J. Wilkinson, L. S. Smit, R. T. Worrell, T. V. Strong, R. A. Frizzell, D. C. Dawson and F. S. Collins (1991). "Chloride conductance expressed by ΔF508 and other mutant CFTRs in Xenopus oocytes." Science **254**(5039): 1797-1799.

Duttler, S., S. Pechmann and J. Frydman (2013). "Principles of Cotranslational Ubiquitination and Quality Control at the Ribosome." Molecular Cell **50**(3): 379-393.

Ellis, R. J. (2001). "Macromolecular crowding: obvious but underappreciated." Trends Biochem Sci **26**(10): 597-604.

Ellis, R. J. and A. P. Minton (2006). "Protein aggregation in crowded environments." Biol Chem **387**(5): 485-497.

Escusa-Toret, S., W. I. M. Vonk and J. Frydman (2013). "Spatial sequestration of misfolded proteins by a dynamic chaperone pathway enhances cellular fitness during stress." Nature Cell Biology **15**(10): 1231-1243.

Etchells, S. A. and F. U. Hartl (2004). "The dynamic tunnel." Nat Struct Mol Biol **11**(5): 391-392.

Fandrich, M. and C. M. Dobson (2002). "The behaviour of polyamino acids reveals an inverse side chain effect in amyloid structure formation." EMBO J **21**(21): 5682-5690.

Finley, D. (2009). "Recognition and processing of ubiquitin-protein conjugates by the proteasome." Annu Rev Biochem **78**: 477-513.

Flick, K., I. Ouni, J. A. Wohlschlegel, C. Capati, W. H. McDonald, J. R. Yates and P. Kaiser (2004). "Proteolysis-independent regulation of the transcription factor Met4 by a single Lys 48-linked ubiquitin chain." Nat Cell Biol **6**(7): 634-641.

Forood, B., E. Perez-Paya, R. A. Houghten and S. E. Blondelle (1995). "Formation of an extremely stable polyalanine beta-sheet macromolecule." Biochem Biophys Res Commun **211**(1): 7-13.

Frischmeyer, P. A., A. van Hoof, K. O'Donnell, A. L. Guerrerio, R. Parker and H. C. Dietz (2002). "An mRNA surveillance mechanism that eliminates transcripts lacking termination codons." Science **295**(5563): 2258-2261.

Frydman, J. and F. U. Hartl (1996). "Principles of chaperone-assisted protein folding: differences between in vitro and in vivo mechanisms." Science **272**(5267): 1497-1502.

Fujiwara, K., Y. Ishihama, K. Nakahigashi, T. Soga and H. Taguchi (2010). "A systematic survey of in vivo obligate chaperonin-dependent substrates." EMBO Journal **29**(9): 1552-1564.

Gamerdinger, M., P. Hajieva, A. M. Kaya, U. Wolfrum, F. U. Hartl and C. Behl (2009). "Protein quality control during aging involves recruitment of the macroautophagy pathway by BAG3." EMBO Journal **28**(7): 889-901.

Gamerdinger, M., A. M. Kaya, U. Wolfrum, A. M. Clement and C. Behl (2011). "BAG3 mediates chaperone-based aggresome-targeting and selective autophagy of misfolded proteins." EMBO Rep **12**(2): 149-156.

Gardner, R. G., G. M. Swarbrick, N. W. Bays, S. R. Cronin, S. Wilhovsky, L. Seelig, C. Kim and R. Y. Hampton (2000). "Endoplasmic reticulum degradation requires lumen to cytosol signaling: Transmembrane control of Hrd1p by Hrd3p." Journal of Cell Biology **151**(1): 69-82.

Gasch, A. P., P. T. Spellman, C. M. Kao, O. Carmel-Harel, M. B. Eisen, G. Storz, D. Botstein and P. O. Brown (2000). "Genomic expression programs in the response of yeast cells to environmental changes." Mol Biol Cell **11**(12): 4241-4257.

Gauss, R., E. Jarosch, T. Sommer and C. Hirsch (2006). "A complex of Yos9p and the HRD ligase integrates endoplasmic reticulum quality control into the degradation machinery." Nature Cell Biology **8**(8): 849-854.

Gerber, A. P. and W. Keller (1999). "An adenosine deaminase that generates inosine at the wobble position of tRNAs." Science **286**(5442): 1146-1149.

Ghaemmaghami, S., W. K. Huh, K. Bower, R. W. Howson, A. Belle, N. Dephoure, E. K. O'Shea and J. S. Weissman (2003). "Global analysis of protein expression in yeast." Nature **425**(6959): 737-741.

Gietz, R. D. and R. A. Woods (2002). "Transformation of yeast by lithium acetate/single-stranded carrier DNA/polyethylene glycol method." Methods Enzymol **350**: 87-96.

Goetz, M. P., D. O. Toft, M. M. Ames and C. Erlichman (2003). "The Hsp90 chaperone complex as a novel target for cancer therapy." Ann Oncol **14**(8): 1169-1176.

Gray, M. J., W. Y. Wholey, N. O. Wagner, C. M. Cremers, A. Mueller-Schickert, N. T. Hock, A. G. Krieger, E. M. Smith, R. A. Bender, J. C. A. Bardwell and U. Jakob (2014). "Polyphosphate Is a Primordial Chaperone." Molecular Cell **53**(5): 689-699.

Gregersen, N., P. Bross, S. Vang and J. H. Christensen (2006). Protein misfolding and human disease. Annual Review of Genomics and Human Genetics. **7:** 103-124.

Gupta, A. J., S. Haldar, G. Miličić, F. U. Hartl and M. Hayer-Hartl (2014). "Active cage mechanism of chaperonin-assisted protein folding demonstrated at single-molecule level." Journal of Molecular Biology **426**(15): 2739-2754.

Guydosh, N. R. and R. Green (2014). "Dom34 rescues ribosomes in 3' untranslated regions." Cell **156**(5): 950-962.

Haacke, A., S. A. Broadley, R. Boteva, N. Tzvetkov, F. U. Hartl and P. Breuer (2006). "Proteolytic cleavage of polyglutamine-expanded ataxin-3 is critical for aggregation and sequestration of non-expanded ataxin-3." Hum Mol Genet **15**(4): 555-568.

Haacke, A., F. U. Hartl and P. Breuer (2007). "Calpain inhibition is sufficient to suppress aggregation of polyglutamine-expanded ataxin-3." J Biol Chem **282**(26): 18851-18856.

Hanahan, D. (1983). "Studies on transformation of Escherichia coli with plasmids." J Mol Biol **166**(4): 557-580.

Hartl, F. U. (1996). "Molecular chaperones in cellular protein folding." Nature **381**(6583): 571-579.

Hartl, F. U. and M. Hayer-Hartl (2002). "Protein folding. Molecular chaperones in the cytosol: From nascent chain to folded protein." Science **295**(5561): 1852-1858.

Hartl, F. U. and M. Hayer-Hartl (2009). "Converging concepts of protein folding in vitro and in vivo." Nat Struct Mol Biol **16**(6): 574-581.

Hayer-Hartl, M., A. Bracher and F. U. Hartl (2016). "The GroEL-GroES Chaperonin Machine: A Nano-Cage for Protein Folding." Trends in Biochemical Sciences **41**(1): 62-76.

Heck, J. W., S. K. Cheung and R. Y. Hampton (2010). "Cytoplasmic protein quality control degradation mediated by parallel actions of the E3 ubiquitin ligases Ubr1 and San1." Proc Natl Acad Sci U S A **107**(3): 1106-1111.

Helenius, A. and M. Aebi (2004). Roles of N-linked glycans in the endoplasmic reticulum. Annual Review of Biochemistry. **73:** 1019-1049.

Hershko, A. and A. Ciechanover (1992). "The ubiquitin system for protein degradation." Annu Rev Biochem **61**: 761-807.

Hipp, M. S., S. H. Park and F. U. Hartl (2014). "Proteostasis impairment in protein-misfolding and -aggregation diseases." Trends Cell Biol **24**(9): 506-514.

Hirsch, C., D. Blom and H. L. Ploegh (2003). "A role for N-glycanase in the cytosolic turnover of glycoproteins." EMBO Journal **22**(5): 1036-1046.

Hosokawa, N., I. Wada, K. Nagasawa, T. Moriyama, K. Okawa and K. Nagata (2008). "Human XTP3-B forms an endoplasmic reticulum quality control scaffold with the HRD1-SEL1L ubiquitin ligase complex and BiP." Journal of Biological Chemistry **283**(30): 20914-20924.

Huh, W. K., J. V. Falvo, L. C. Gerke, A. S. Carroll, R. W. Howson, J. S. Weissman and E. K. O'Shea (2003). "Global analysis of protein localization in budding yeast." Nature **425**(6959): 686-691.

Inada, T. (2013). "Quality control systems for aberrant mRNAs induced by aberrant translation elongation and termination." Biochimica et Biophysica Acta - Gene Regulatory Mechanisms **1829**(6-7): 634-642.

Inada, T. (2016). "The Ribosome as a Platform for mRNA and Nascent Polypeptide Quality Control." Trends Biochem Sci.

Inada, T. and H. Aiba (2005). "Translation of aberrant mRNAs lacking a termination codon or with a shortened 3′-UTR is repressed after initiation in yeast." EMBO Journal **24**(8): 1584-1595.

Ishimura, R., G. Nagy, I. Dotu, H. Zhou, X. L. Yang, P. Schimmel, S. Senju, Y. Nishimura, J. H. Chuang and S. L. Ackerman (2014). "Ribosome stalling induced by mutation of a CNS-specific tRNA causes neurodegeneration." Science **345**(6195): 455-459.

Ito-Harashima, S., K. Kuroha, T. Tatematsu and T. Inada (2007). "Translation of the poly(A) tail plays crucial roles in nonstop mRNA surveillance via translation repression and protein destabilization by proteasome in yeast." Genes Dev **21**(5): 519-524.

Izawa, T., T. Tsuboi, K. Kuroha, T. Inada, S. I. Nishikawa and T. Endo (2012). "Roles of Dom34:Hbs1 in Nonstop Protein Clearance from Translocators for Normal Organelle Protein Influx." Cell Reports **2**(3): 447-453.

Jahn, T. R. and S. E. Radford (2005). "The Yin and Yang of protein folding." FEBS J **272**(23): 5962-5970.

Juszkiewicz, S. and R. S. Hegde (2016). "Initiation of Quality Control during Poly(A) Translation Requires Site-Specific Ribosome Ubiquitination." Mol Cell.

Kaganovich, D., R. Kopito and J. Frydman (2008). "Misfolded proteins partition between two distinct quality control compartments." Nature **454**(7208): 1088-1095.

Kaiser, C. M., H. C. Chang, V. R. Agashe, S. K. Lakshmipathy, S. A. Etchells, M. Hayer-Hartl, F. U. Hartl and J. M. Barral (2006). "Real-time observation of trigger factor function on translating ribosomes." Nature **444**(7118): 455-460.

Kaiser, C. M., D. H. Goldman, J. D. Chodera, I. Tinoco Jr and C. Bustamante (2011). "The ribosome modulates nascent protein folding." Science **334**(6063): 1723-1727.

Karagöz, G. E. and S. G. D. Rüdiger (2015). "Hsp90 interaction with clients." Trends in Biochemical Sciences **40**(2): 117-125.

Kettern, N., M. Dreiseidler, R. Tawo and J. Höhfeld (2010). "Chaperone-assisted degradation: Multiple paths to destruction." Biological Chemistry **391**(5): 481-489.

Kim, Y. E., M. S. Hipp, A. Bracher, M. Hayer-Hartl and F. U. Hartl (2013). "Molecular chaperone functions in protein folding and proteostasis." Annu Rev Biochem **82**: 323-355.

Kirkwood, T. B. (1977). "Evolution of ageing." Nature **270**(5635): 301-304.

Klauer, A. A. and A. van Hoof (2012). "Degradation of mRNAs that lack a stop codon: A decade of nonstop progress." Wiley Interdisciplinary Reviews: RNA **3**(5): 649-660.

Knowles, T. P., M. Vendruscolo and C. M. Dobson (2014). "The amyloid state and its association with protein misfolding diseases." Nat Rev Mol Cell Biol **15**(6): 384-396.

Knowles, T. P. J., C. A. Waudby, G. L. Devlin, S. I. A. Cohen, A. Aguzzi, M. Vendruscolo, E. M. Terentjev, M. E. Welland and C. M. Dobson (2009). "An analytical solution to the kinetics of breakable filament assembly." Science **326**(5959): 1533-1537.

Kobayashi, K., I. Kikuno, K. Kuroha, K. Saito, K. Ito, R. Ishitani, T. Inada and O. Nureki (2010). "Structural basis for mRNA surveillance by archaeal Pelota and GTP-bound EF1α complex." Proceedings of the National Academy of Sciences of the United States of America **107**(41): 17575-17579.

Kopito, R. R. (2000). "Aggresomes, inclusion bodies and protein aggregation." Trends Cell Biol **10**(12): 524-530.

Kowalinski, E., A. Kogel, J. Ebert, P. Reichelt, E. Stegmann, B. Habermann and E. Conti (2016). "Structure of a Cytoplasmic 11-Subunit RNA Exosome Complex." Mol Cell **63**(1): 125-134.

Kowalinski, E., A. Schuller, R. Green and E. Conti (2015). "Saccharomyces cerevisiae Ski7 Is a GTP-Binding Protein Adopting the Characteristic Conformation of Active Translational GTPases." Structure **23**(7): 1336-1343.

Krishnan, R. and S. L. Lindquist (2005). "Structural insights into a yeast prion illuminate nucleation and strain diversity." Nature **435**(7043): 765-772.

Kryndushkin, D. S., I. M. Alexandrov, M. D. Ter-Avanesyan and V. V. Kushnirov (2003). "Yeast [PSI+] prion aggregates are formed by small Sup35 polymers fragmented by Hsp104." J Biol Chem **278**(49): 49636-49643.

Labbadia, J. and R. I. Morimoto (2015). The biology of proteostasis in aging and disease. Annual Review of Biochemistry. **84:** 435-464.

LaRiviere, F. J., S. E. Cole, D. J. Ferullo and M. J. Moore (2006). "A late-acting quality control process for mature eukaryotic rRNAs." Molecular Cell **24**(4): 619-626.

Lee, B. H., M. J. Lee, S. Park, D. C. Oh, S. Elsasser, P. C. Chen, C. Gartner, N. Dimova, J. Hanna, S. P. Gygi, S. M. Wilson, R. W. King and D. Finley (2010). "Enhancement of proteasome activity by a small-molecule inhibitor of USP14." Nature **467**(7312): 179-184.

Lee, J. W., K. Beebe, L. A. Nangle, J. Jang, C. M. Longo-Guess, S. A. Cook, M. T. Davisson, J. P. Sundberg, P. Schimmel and S. L. Ackerman (2006). "Editing-defective tRNA synthetase causes protein misfolding and neurodegeneration." Nature **443**(7107): 50-55.

Lee, R. J., C. W. Liu, C. Harty, A. A. McCracken, M. Latterich, K. Römisch, G. N. DeMartino, P. J. Thomas and J. L. Brodsky (2004). "Uncoupling retro-translocation and degradation in the ER-associated degradation of a soluble protein." EMBO Journal **23**(11): 2206-2215.

Leitner, A., L. A. Joachimiak, A. Bracher, L. Mönkemeyer, T. Walzthoeni, B. Chen, S. Pechmann, S. Holmes, Y. Cong, B. Ma, S. Ludtke, W. Chiu, F. U. Hartl, R. Aebersold and J. Frydman (2012). "The molecular architecture of the eukaryotic chaperonin TRiC/CCT." Structure **20**(5): 814-825.

Letzring, D. P., K. M. Dean and E. J. Grayhack (2010). "Control of translation efficiency in yeast by codon-anticodon interactions." RNA **16**(12): 2516-2528.

Letzring, D. P., A. S. Wolf, C. E. Brule and E. J. Grayhack (2013). "Translation of CGA codon repeats in yeast involves quality control components and ribosomal protein L1." RNA **19**(9): 1208-1217.

Li, M. Z. and S. J. Elledge (2007). "Harnessing homologous recombination in vitro to generate recombinant DNA via SLIC." Nat Methods **4**(3): 251-256.

Li, W., M. H. Bengtson, A. Ulbrich, A. Matsuda, V. A. Reddy, A. Orth, S. K. Chanda, S. Batalov and C. A. Joazeiro (2008). "Genome-wide and functional annotation of human E3 ubiquitin ligases identifies MULAN, a mitochondrial E3 that regulates the organelle's dynamics and signaling." PLoS One **3**(1): e1487.

Lopez, T., K. Dalton and J. Frydman (2015). "The Mechanism and Function of Group II Chaperonins." Journal of Molecular Biology **427**(18): 2919-2930.

Lord, J. M., L. M. Roberts and W. I. Lencer (2006). Entry of protein toxins into mammalian cells by crossing the endoplasmic reticulum membrane: Co-opting basic mechanisms of endoplasmic reticulum-associated degradation. Current Topics in Microbiology and Immunology. **300:** 149-168.

Losson, R. and F. Lacroute (1979). "Interference of nonsense mutations with eukaryotic messenger RNA stability." Proceedings of the National Academy of Sciences of the United States of America **76**(10): 5134-5137.

Lu, J. and C. Deutsch (2005). "Folding zones inside the ribosomal exit tunnel." Nat Struct Mol Biol **12**(12): 1123-1129.

Lu, J., W. R. Kobertz and C. Deutsch (2007). "Mapping the Electrostatic Potential within the Ribosomal Exit Tunnel." Journal of Molecular Biology **371**(5): 1378-1391.

Lykke-Andersen, S. and T. H. Jensen (2015). "Nonsense-mediated mRNA decay: An intricate machinery that shapes transcriptomes." Nature Reviews Molecular Cell Biology **16**(11): 665-677.

Lyumkis, D., S. K. Doamekpor, M. H. Bengtson, J. W. Lee, T. B. Toro, M. D. Petroski, C. D. Lima, C. S. Potter, B. Carragher and C. A. P. Joazeiro (2013). "Single-particle EM reveals extensive conformational variability of the Ltn1 E3 ligase." Proceedings of the National Academy of Sciences of the United States of America **110**(5): 1702-1707.

Lyumkis, D., D. Oliveira dos Passos, E. B. Tahara, K. Webb, E. J. Bennett, S. Vinterbo, C. S. Potter, B. Carragher and C. A. Joazeiro (2014). "Structural basis for translational surveillance by the large ribosomal subunit-associated protein quality control complex." Proc Natl Acad Sci U S A **111**(45): 15981-15986.

Marcuccilli, C. J., S. K. Mathur, R. I. Morimoto and R. J. Miller (1996). "Regulatory differences in the stress response of hippocampal neurons and glial cells after heat shock." J Neurosci **16**(2): 478-485.

Mathur, S. K., L. Sistonen, I. R. Brown, S. P. Murphy, K. D. Sarge and R. I. Morimoto (1994). "Deficient induction of human hsp70 heat shock gene transcription in Y79 retinoblastoma cells despite activation of heat shock factor 1." Proc Natl Acad Sci U S A **91**(18): 8695-8699.

Mayer, M. P. (2013). "Hsp70 chaperone dynamics and molecular mechanism." Trends in Biochemical Sciences **38**(10): 507-514.

Mbonye, U. R., M. Wada, C. J. Rieke, H. Y. Tang, D. L. DeWitt and W. L. Smith (2006). "The 19-amino acid cassette of cyclooxygenase-2 mediates entry of the protein into the endoplasmic reticulum-associated degradation system." Journal of Biological Chemistry **281**(47): 35770-35778.

Meaux, S. and A. Van Hoof (2006). "Yeast transcripts cleaved by an internal ribozyme provide new insight into the role of the cap and poly(A) tail in translation and mRNA decay." RNA **12**(7): 1323-1337.

Merret, R., V. K. Nagarajan, M. C. Carpentier, S. Park, J. J. Favory, J. Descombin, C. Picart, Y. Y. Charng, P. J. Green, J. M. Deragon and C. Bousquet-Antonelli (2015). "Heat-induced ribosome pausing triggers mRNA co-translational decay in Arabidopsis thaliana." Nucleic Acids Research **43**(8): 4121-4132.

Mogk, A., E. Kummer and B. Bukau (2015). "Cooperation of hsp70 and hsp100 chaperone Machines in protein disaggregation." Front Mol Biosci **2**: 22.

Mori, K., S. M. Weng, T. Arzberger, S. May, K. Rentzsch, E. Kremmer, B. Schmid, H. A. Kretzschmar, M. Cruts, C. Van Broeckhoven, C. Haass and D. Edbauer (2013). "The C9orf72 GGGGCC Repeat Is Translated into Aggregating Dipeptide-Repeat Proteins in FTLD/ALS." Science **339**(6125): 1335-1338.

Morimoto, R. I. (2008). "Proteotoxic stress and inducible chaperone networks in neurodegenerative disease and aging." Genes Dev **22**(11): 1427-1438.

Muchowski, P. J., G. Schaffar, A. Sittler, E. E. Wanker, M. K. Hayer-Hartl and F. U. Hartl (2000). "Hsp70 and hsp40 chaperones can inhibit self-assembly of polyglutamine proteins into amyloid-like fibrils." Proc Natl Acad Sci U S A **97**(14): 7841-7846.

Nakatsukasa, K., G. Huyer, S. Michaelis and J. L. Brodsky (2008). "Dissecting the ER-Associated Degradation of a Misfolded Polytopic Membrane Protein." Cell **132**(1): 101-112.

Neudegger, T., J. Verghese, M. Hayer-Hartl, F. U. Hartl and A. Bracher (2016). "Structure of human heat-shock transcription factor 1 in complex with DNA." Nat Struct Mol Biol **23**(2): 140-146.

Nilsson, O. B., R. Hedman, J. Marino, S. Wickles, L. Bischoff, M. Johansson, A. Müller-Lucks, F. Trovato, J. D. Puglisi, E. P. O'Brien, R. Beckmann and G. von Heijne (2015). "Cotranslational Protein Folding inside the Ribosome Exit Tunnel." Cell Reports **12**(10): 1533-1540.

O'Brien, E. P., J. Christodoulou, M. Vendruscolo and C. M. Dobson (2011). "New scenarios of protein folding can occur on the ribosome." Journal of the American Chemical Society **133**(3): 513-526.

Oda, Y., N. Hosokawa, I. Wada and K. Nagata (2003). "EDEM as an acceptor of terminally misfolded glycoproteins released from calnexin." Science **299**(5611): 1394-1397.

Okuda-Shimizu, Y. and L. M. Hendershot (2007). "Characterization of an ERAD Pathway for Nonglycosylated BiP Substrates, which Require Herp." Molecular Cell **28**(4): 544-554.

Olzscha, H., S. M. Schermann, A. C. Woerner, S. Pinkert, M. H. Hecht, G. G. Tartaglia, M. Vendruscolo, M. Hayer-Hartl, F. U. Hartl and R. M. Vabulas (2011). "Amyloid-like aggregates sequester numerous metastable proteins with essential cellular functions." Cell **144**(1): 67-78.

Ozsolak, F., P. Kapranov, S. Foissac, S. W. Kim, E. Fishilevich, A. P. Monaghan, B. John and P. M. Milos (2010). "Comprehensive polyadenylation site maps in yeast and human reveal pervasive alternative polyadenylation." Cell **143**(6): 1018-1029.

Park, S. H., Y. Kukushkin, R. Gupta, T. Chen, A. Konagai, M. S. Hipp, M. Hayer-Hartl and F. U. Hartl (2013). "PolyQ proteins interfere with nuclear degradation of cytosolic proteins by sequestering the Sis1p chaperone." Cell **154**(1): 134-145.

Parker, R. (2012). "RNA degradation in Saccharomyces cerevisae." Genetics **191**(3): 671-702.

Pechmann, S., J. W. Chartron and J. Frydman (2014). "Local slowdown of translation by nonoptimal codons promotes nascent-chain recognition by SRP in vivo." Nature Structural and Molecular Biology **21**(12): 1100-1105.

Pechmann, S. and J. Frydman (2013). "Evolutionary conservation of codon optimality reveals hidden signatures of cotranslational folding." Nat Struct Mol Biol **20**(2): 237-243.

Pisareva, V. P., M. A. Skabkin, C. U. Hellen, T. V. Pestova and A. V. Pisarev (2011). "Dissociation by Pelota, Hbs1 and ABCE1 of mammalian vacant 80S ribosomes and stalled elongation complexes." EMBO J **30**(9): 1804-1817.

Polo, S., S. Sigismund, M. Faretta, M. Guidi, M. R. Capua, G. Bossi, H. Chen, P. De Camilli and P. P. Di Fiore (2002). "A single motif responsible for ubiquitin recognition and monoubiquitination in endocytic proteins." Nature **416**(6879): 451-455.

Powers, E. T., R. I. Morimoto, A. Dillin, J. W. Kelly and W. E. Balch (2009). Biological and chemical approaches to diseases of proteostasis deficiency. Annual Review of Biochemistry. **78:** 959-991.

Prakash, S. and A. Matouschek (2004). "Protein unfolding in the cell." Trends Biochem Sci **29**(11): 593-600.

Pratt, W. B., J. E. Gestwicki, Y. Osawa and A. P. Lieberman (2015). Targeting Hsp90/Hsp70-based protein quality control for treatment of adult onset neurodegenerative diseases. Annual Review of Pharmacology and Toxicology. **55:** 353-371.

Preissler, S. and E. Deuerling (2012). "Ribosome-associated chaperones as key players in proteostasis." Trends in Biochemical Sciences **37**(7): 274-283.

Rampelt, H., J. Kirstein-Miles, N. B. Nillegoda, K. Chi, S. R. Scholz, R. I. Morimoto and B. Bukau (2012). "Metazoan Hsp70 machines use Hsp110 to power protein disaggregation." EMBO Journal **31**(21): 4221-4235.

Ravid, T., S. G. Kreft and M. Hochstrasser (2006). "Membrane and soluble substrates of the Doa10 ubiquitin ligase are degraded by distinct pathways." EMBO Journal **25**(3): 533-543.

Röhl, A., J. Rohrberg and J. Buchner (2013). "The chaperone Hsp90: Changing partners for demanding clients." Trends in Biochemical Sciences **38**(5): 253-262.

Roth, D. M., D. M. Hutt, J. Tong, M. Bouchecareilh, N. Wang, T. Seeley, J. F. Dekkers, J. M. Beekman, D. Garza, L. Drew, E. Masliah, R. I. Morimoto and W. E. Balch (2014). "Modulation of the maladaptive stress response to manage diseases of protein folding." PLoS Biol **12**(11): e1001998.

Sahni, N., S. Yi, M. Taipale, J. I. Fuxman Bass, J. Coulombe-Huntington, F. Yang, J. Peng, J. Weile, G. I. Karras, Y. Wang, I. A. Kovács, A. Kamburov, I. Krykbaeva, M. H. Lam, G. Tucker, V. Khurana, A. Sharma, Y. Y. Liu, N. Yachie, Q. Zhong, Y. Shen, A. Palagi, A. San-Miguel, C. Fan, D. Balcha, A. Dricot, D. M. Jordan, J. M. Walsh, A. A. Shah, X. Yang, A. K. Stoyanova, A. Leighton, M. A. Calderwood, Y. Jacob, M. E. Cusick, K. Salehi-Ashtiani, L. J. Whitesell, S. Sunyaev, B. Berger, A. L. Barabási, B. Charloteaux, D. E. Hill, T. Hao, F. P. Roth, Y. Xia, A. J. M. Walhout, S. Lindquist and M. Vidal (2015). "Widespread macromolecular interaction perturbations in human genetic disorders." Cell **161**(3): 647-660.

Sauna, Z. E. and C. Kimchi-Sarfaty (2011). "Understanding the contribution of synonymous mutations to human disease." Nature Reviews Genetics **12**(10): 683-691.

Scazzari, M., I. Amm and D. H. Wolf (2015). "Quality control of a cytoplasmic protein complex: chaperone motors and the ubiquitin-proteasome system govern the fate of orphan fatty acid synthase subunit Fas2 of yeast." J Biol Chem **290**(8): 4677-4687.

Schaffar, G., P. Breuer, R. Boteva, C. Behrends, N. Tzvetkov, N. Strippel, H. Sakahira, K. Siegers, M. Hayer-Hartl and F. U. Hartl (2004). "Cellular toxicity of polyglutamine expansion proteins: Mechanism of transcription factor deactivation." Molecular Cell **15**(1): 95-105.

Scheper, G. C., M. S. Van Der Knaap and C. G. Proud (2007). "Translation matters: Protein synthesis defects in inherited disease." Nature Reviews Genetics **8**(9): 711-723.

Scherzinger, E., R. Lurz, M. Turmaine, L. Mangiarini, B. Hollenbach, R. Hasenbank, G. P. Bates, S. W. Davies, H. Lehrach and E. E. Wanker (1997). "Huntingtin-encoded polyglutamine expansions form amyloid-like protein aggregates in vitro and in vivo." Cell **90**(3): 549-558.

Schmidt, C., E. Kowalinski, V. Shanmuganathan, Q. Defenouillere, K. Braunger, A. Heuer, M. Pech, A. Namane, O. Berninghausen, M. Fromont-Racine, A. Jacquier, E. Conti, T. Becker and R. Beckmann (2016). "The cryo-EM structure of a ribosome-Ski2-Ski3-Ski8 helicase complex." Science **354**(6318): 1431-1433.

Schubert, U., L. C. Anton, J. Gibbs, C. C. Norbury, J. W. Yewdell and J. R. Bennink (2000). "Rapid degradation of a large fraction of newly synthesized proteins by proteasomes." Nature **404**(6779): 770-774.

Schuck, S., W. A. Prinz, K. S. Thorn, C. Voss and P. Walter (2009). "Membrane expansion alleviates endoplasmic reticulum stress independently of the unfolded protein response." J Cell Biol **187**(4): 525-536.

Schulz, A. M. and C. M. Haynes (2015). "UPRmt-mediated cytoprotection and organismal aging." Biochimica et Biophysica Acta - Bioenergetics **1847**(11): 1448-1456.

Shalgi, R., J. A. Hurt, I. Krykbaeva, M. Taipale, S. Lindquist and C. B. Burge (2013). "Widespread Regulation of Translation by Elongation Pausing in Heat Shock." Molecular Cell **49**(3): 439-452.

Shao, S., A. Brown, B. Santhanam and R. S. Hegde (2015). "Structure and assembly pathway of the ribosome quality control complex." Mol Cell **57**(3): 433-444.

Shao, S. and R. S. Hegde (2014). "Reconstitution of a minimal ribosome-associated ubiquitination pathway with purified factors." Mol Cell **55**(6): 880-890.

Shao, S., K. von der Malsburg and R. S. Hegde (2013). "Listerin-dependent nascent protein ubiquitination relies on ribosome subunit dissociation." Mol Cell **50**(5): 637-648.

Sharma, S. K., P. De Los Rios, P. Christen, A. Lustig and P. Goloubinoff (2010). "The kinetic parameters and energy cost of the Hsp70 chaperone as a polypeptide unfoldase." Nature Chemical Biology **6**(12): 914-920.

Shearer, A. G. and R. Y. Hampton (2005). "Lipid-mediated, reversible misfolding of a sterol-sensing domain protein." EMBO Journal **24**(1): 149-159.

Shen, P. S., J. Park, Y. Qin, X. Li, K. Parsawar, M. H. Larson, J. Cox, Y. Cheng, A. M. Lambowitz, J. S. Weissman, O. Brandman and A. Frost (2015). "Protein synthesis. Rqc2p and 60S ribosomal subunits mediate mRNA-independent elongation of nascent chains." Science **347**(6217): 75-78.

Shevchenko, A., M. Wilm, O. Vorm and M. Mann (1996). "Mass spectrometric sequencing of proteins silver-stained polyacrylamide gels." Anal Chem **68**(5): 850-858.

Shi, Y., D. D. Mosser and R. I. Morimoto (1998). "Molecular chaperones as HSF1-specific transcriptional repressors." Genes Dev **12**(5): 654-666.

Shoemaker, C. J., D. E. Eyler and R. Green (2010). "Dom34:Hbs1 promotes subunit dissociation and peptidyl-tRNA drop-off to initiate no-go decay." Science **330**(6002): 369-372.

Shoemaker, C. J. and R. Green (2011). "Kinetic analysis reveals the ordered coupling of translation termination and ribosome recycling in yeast." Proc Natl Acad Sci U S A **108**(51): E1392-1398.

Shoemaker, C. J. and R. Green (2012). "Translation drives mRNA quality control." Nat Struct Mol Biol **19**(6): 594-601.

Sikorski, R. S. and P. Hieter (1989). "A system of shuttle vectors and yeast host strains designed for efficient manipulation of DNA in Saccharomyces cerevisiae." Genetics **122**(1): 19-27.

Simms, C. L., E. N. Thomas and H. S. Zaher (2017). "Ribosome-based quality control of mRNA and nascent peptides." Wiley Interdiscip Rev RNA **8**(1).

Smith, M. H., H. L. Ploegh and J. S. Weissman (2011). "Road to ruin: targeting proteins for degradation in the endoplasmic reticulum." Science **334**(6059): 1086-1090.

Sontag, E. M., W. I. M. Vonk and J. Frydman (2014). "Sorting out the trash: The spatial nature of eukaryotic protein quality control." Current Opinion in Cell Biology **26**(1): 139-146.

Sorger, P. K. and H. C. Nelson (1989). "Trimerization of a yeast transcriptional activator via a coiled-coil motif." Cell **59**(5): 807-813.

Sparks, K. A. and C. L. Dieckmann (1998). "Regulation of poly(A) site choice of several yeast mRNAs." Nucleic Acids Res **26**(20): 4676-4687.

Subtelny, A. O., S. W. Eichhorn, G. R. Chen, H. Sive and D. P. Bartel (2014). "Poly(A)-tail profiling reveals an embryonic switch in translational control." Nature **508**(7494): 66-71.

Swanson, R., M. Locher and M. Hochstrasser (2001). "A conserved ubiquitin ligase of the nuclear envelope/endoplasmic reticulum that functions in both ER-associated and Matα2 repressor degradation." Genes and Development **15**(20): 2660-2674.

Tabas, I. and D. Ron (2011). "Integrating the mechanisms of apoptosis induced by endoplasmic reticulum stress." Nat Cell Biol **13**(3): 184-190.

Taipale, M., I. Krykbaeva, M. Koeva, C. Kayatekin, K. D. Westover, G. I. Karras and S. Lindquist (2012). "Quantitative analysis of Hsp90-client interactions reveals principles of substrate recognition." Cell **150**(5): 987-1001.

Taipale, M., G. Tucker, J. Peng, I. Krykbaeva, Z. Y. Lin, B. Larsen, H. Choi, B. Berger, A. C. Gingras and S. Lindquist (2014). "A quantitative chaperone interaction network reveals the architecture of cellular protein homeostasis pathways." Cell **158**(2): 434-448.

Taylor, R. C. and A. Dillin (2011). "Aging as an event of proteostasis collapse." Cold Spring Harbor perspectives in biology **3**(5).

Treweek, T. M., S. Meehan, H. Ecroyd and J. A. Carver (2015). "Small heat-shock proteins: Important players in regulating cellular proteostasis." Cellular and Molecular Life Sciences **72**(3): 429-451.

Trinklein, N. D., J. I. Murray, S. J. Hartman, D. Botstein and R. M. Myers (2004). "The role of heat shock transcription factor 1 in the genome-wide regulation of the mammalian heat shock response." Mol Biol Cell **15**(3): 1254-1261.

Tsaytler, P., H. P. Harding, D. Ron and A. Bertolotti (2011). "Selective inhibition of a regulatory subunit of protein phosphatase 1 restores proteostasis." Science **332**(6025): 91-94.

Tsuboi, T., K. Kuroha, K. Kudo, S. Makino, E. Inoue, I. Kashima and T. Inada (2012). "Dom34:hbs1 plays a general role in quality-control systems by dissociation of a stalled ribosome at the 3' end of aberrant mRNA." Mol Cell **46**(4): 518-529.

Turner, G. C. and A. Varshavsky (2000). "Detecting and measuring cotranslational protein degradation in vivo." Science **289**(5487): 2117-2120.

Ushioda, R., J. Hoseki, K. Araki, G. Jansen, D. Y. Thomas and K. Nagata (2008). "ERdj5 is required as a disulfide reductase for degradation of misfolded proteins in the ER." Science **321**(5888): 569-572.

Vabulas, R. M. and F. U. Hartl (2005). "Cell biology: Protein synthesis upon acute nutrient restriction relies on proteasome function." Science **310**(5756): 1960-1963.

Vabulas, R. M., S. Raychaudhuri, M. Hayer-Hartl and F. U. Hartl (2010). "Protein folding in the cytoplasm and the heat shock response." Cold Spring Harb Perspect Biol **2**(12): a004390.

van Hoof, A., P. A. Frischmeyer, H. C. Dietz and R. Parker (2002). "Exosome-mediated recognition and degradation of mRNAs lacking a termination codon." Science **295**(5563): 2262-2264.

Van Hoof, A. and E. J. Wagner (2011). "A brief survey of mRNA surveillance." Trends in Biochemical Sciences **36**(11): 585-592.

Verma, R., R. S. Oania, N. J. Kolawa and R. J. Deshaies (2013). "Cdc48/p97 promotes degradation of aberrant nascent polypeptides bound to the ribosome." Elife **2**: e00308.

Walter, P. and D. Ron (2011). "The unfolded protein response: From stress pathway to homeostatic regulation." Science **334**(6059): 1081-1086.

Wang, T., K. Birsoy, N. W. Hughes, K. M. Krupczak, Y. Post, J. J. Wei, E. S. Lander and D. M. Sabatini (2015). "Identification and characterization of essential genes in the human genome." Science **350**(6264): 1096-1101.

Warner, J. R. (1999). "The economics of ribosome biosynthesis in yeast." Trends Biochem Sci **24**(11): 437-440.

Willmund, F., M. Del Alamo, S. Pechmann, T. Chen, V. Albanèse, E. B. Dammer, J. Peng and J. Frydman (2013). "The cotranslational function of ribosome-associated Hsp70 in eukaryotic protein homeostasis." Cell **152**(1-2): 196-209.

Wilson, D. N. and R. Beckmann (2011). "The ribosomal tunnel as a functional environment for nascent polypeptide folding and translational stalling." Current Opinion in Structural Biology **21**(2): 274-282.

Wilson, M. A., S. Meaux and A. van Hoof (2007). "A genomic screen in yeast reveals novel aspects of nonstop mRNA metabolism." Genetics **177**(2): 773-784.

Wisniewski, J. R., D. F. Zielinska and M. Mann (2011). "Comparison of ultrafiltration units for proteomic and N-glycoproteomic analysis by the filter-aided sample preparation method." Anal Biochem **410**(2): 307-309.

Woerner, A. C., F. Frottin, D. Hornburg, L. R. Feng, F. Meissner, M. Patra, J. Tatzelt, M. Mann, K. F. Winklhofer, F. U. Hartl and M. S. Hipp (2016). "Cytoplasmic protein aggregates interfere with nucleocytoplasmic transport of protein and RNA." Science **351**(6269): 173-176.

Wolf, A. S. and E. J. Grayhack (2015). "Asc1, homolog of human RACK1, prevents frameshifting in yeast by ribosomes stalled at CGA codon repeats." RNA **21**(5): 935-945.

Wu, C. (1995). "Heat shock transcription factors: structure and regulation." Annu Rev Cell Dev Biol **11**: 441-469.

Yonashiro, R., E. B. Tahara, M. H. Bengtson, M. Khokhrina, H. Lorenz, K. C. Chen, Y. Kigoshi-Tansho, J. N. Savas, J. R. Yates, S. A. Kay, E. A. Craig, A. Mogk, B. Bukau and C. A. Joazeiro (2016). "The Rqc2/Tae2 subunit of the ribosome-associated quality control (RQC) complex marks ribosome-stalled nascent polypeptide chains for aggregation." Elife **5**.

Zhou, M., J. Guo, J. Cha, M. Chae, S. Chen, J. M. Barral, M. S. Sachs and Y. Liu (2013). "Non-optimal codon usage affects expression, structure and function of clock protein FRQ." Nature **495**(7439): 111-115.

Zhuravleva, A. and L. M. Gierasch (2015). "Substrate-binding domain conformational dynamics mediate Hsp70 allostery." Proceedings of the National Academy of Sciences of the United States of America **112**(22): E2865-E2873.

Zu, T., Y. Liu, M. Banez-Coronel, T. Reid, O. Pletnikova, J. Lewis, T. M. Miller, M. B. Harms, A. E. Falchook, S. H. Subramony, L. W. Ostrow, J. D. Rothstein, J. C. Troncoso and L. P. Ranum (2013). "RAN proteins and RNA foci from antisense transcripts in C9ORF72 ALS and frontotemporal dementia." Proc Natl Acad Sci U S A **110**(51): E4968-4977.

VI. Appendix

Tab. VI.1: Interactors of Sis-HA. Interactors sorted according to their enrichment in SDS-resistant aggregates from high to low values (M/L ratio corresponding to Sis1-HA in *ltn1*Δ cells overexpressing Rqc2p compared to Sis1-HA in *ltn1*Δ cells harboring an empty vector; H/M ratio corresponding to Sis1-HA in *ltn1*Δ*ski7*Δ cells overexpressing Rqc2p compared to Sis1-HA in *ltn1*Δ cells overexpressing Rqc2p; H/L ratio corresponding to Sis1-HA in *ltn1*Δ*ski7*Δ cells overexpressing Rqc2p compared to Sis1-HA in *ltn1*Δ cells harboring an empty vector). Ratios represent the median of three independent experiments. Listed are proteins that were enriched 2-fold or more in at least 2 out of 3 independent experiments. MW, molecular weight; -/-, SILAC ratio not determined. Potential endogenous stalled polypeptides are highlighted in blue.

Protein ID	Gene Name	Description	MW (kDa)	M/L Ratio	H/M Ratio	H/L Ratio
Q12532	RQC2	Translation-associated element 2	119,1	28,32	-/-	29,82
Q12127; Q7LHD1	CCW12	Covalently-linked cell wall protein 12	13,1	10,42	2,68	24,73
P48510	DSK2	Ubiquitin domain-containing protein DSK2	39,3	6,95	2,33	17,13
P40956	GTS1	Protein GTS1	44,4	5,21	3,07	16,34
Q07442	BDF2	Bromodomain-containing factor 2	72,5	-/-	12,64	16,01
P32478	HSP150	Cell wall mannoprotein HSP150	41,1	6,68	2,18	15,59
P40529	AGE2	ADP-ribosylation factor GTPase-activating protein effector protein 2	32,6	6,69	-/-	13,04
P38011	ASC1	Guanine nucleotide-binding protein subunit beta-like protein	34,8	3,49	4,17	12,65
Q12118	SGT2	Small glutamine-rich tetratricopeptide repeat-containing protein 2	37,2	6,22	2,06	12,07
P22202; P09435	SSA4; SSA3	Heat shock protein SSA4; Heat shock protein SSA3	69,7	3,90	2,35	11,55
Q04964	SML1	Ribonucleotide reductase inhibitor protein SML1	11,8	5,36	-/-	11,34
O14467	MBF1	Multiprotein-bridging factor 1	16,4	4,19	2,69	11,01
Q07655	WHI4	Protein WHI4	70,7	2,79	3,12	9,67
P36102	PAN3	PAB-dependent poly(A)-specific ribonuclease subunit PAN3	76,5	5,12	2,51	8,92
P07213	TOM70	Mitochondrial import receptor subunit TOM70	70,1	2,36	3,13	8,69
Q08925	MRN1	RNA-binding protein MRN1	68,7	-/-	5,08	8,68
P38225	FAT1	Very long-chain fatty acid transport protein	77,1	-/-	4,86	8,50
P09436	ILS1	Isoleucine--tRNA ligase, cytoplasmic	123,0	-/-	4,50	8,41
P32618	YEL043W	Uncharacterized protein YEL043W	106,1	3,76	2,93	8,28

P32909	SMY2	Protein SMY2	81,4	4,64	2,77	7,95
P06169; P26263; P16467	PDC1	Pyruvate decarboxylase isozyme 1	61,5	2,16	3,73	7,67
P00359; P00358	TDH3; TDH2	Glyceraldehyde-3-phosphate dehydrogenase 3; Glyceraldehyde-3-phosphate dehydrogenase 2	35,7	2,90	2,72	7,46
P38084	BAP2	Leu/Val/Ile amino-acid permease	67,8	-/-	4,15	7,24
P19358	SAM2	S-adenosylmethionine synthase 2	42,3	4,04	-/-	7,12
P40185	MMF1	Protein MMF1, mitochondrial	15,9	2,83	-/-	7,08
P09950	HEM1	5-aminolevulinate synthase, mitochondrial	59,4	2,05	3,14	7,03
P07246	ADH3	Alcohol dehydrogenase 3, mitochondrial	40,4	-/-	3,91	7,01
P35191	MDJ1	DnaJ homolog 1, mitochondrial	55,6	-/-	3,32	6,95
P41338	ERG10	Acetyl-CoA acetyltransferase	41,7	3,11	-/-	6,94
P05694	MET6	5-methyltetrahydropteroyltriglutamate--homocysteine methyltransferase	85,9	-/-	3,81	6,92
P35997; P38711	RPS27A; RPS27B	40S ribosomal protein S27-A; 40S ribosomal protein S27-B	8,9	2,80	2,46	6,88
P19414; P39533	ACO1	Aconitate hydratase, mitochondrial	85,4	-/-	3,81	6,83
P21954; P53982	IDP1	Isocitrate dehydrogenase [NADP], mitochondrial	48,2	-/-	4,78	6,66
P14540	FBA1	Fructose-bisphosphate aldolase	39,6	2,21	2,39	6,65
Q07959	IZH3	ADIPOR-like receptor IZH3	62,6	2,61	2,58	6,48
P48527	MSY1	Tyrosine--tRNA ligase, mitochondrial	55,3	-/-	4,72	6,43
P13663	HOM2	Aspartate-semialdehyde dehydrogenase	39,5	-/-	-/-	6,40
P54115	ALD6	Magnesium-activated aldehyde dehydrogenase, cytosolic	54,4	2,41	2,46	6,29
P25560	RER1	Protein RER1	22,3	-/-	5,79	6,25
P35197	GCS1	ADP-ribosylation factor GTPase-activating protein GCS1	39,3	-/-	2,83	6,16
P23254	TKL1	Transketolase 1	73,8	3,52	-/-	6,04
P04387	GAL80	Galactose/lactose metabolism regulatory protein GAL80	48,3	-/-	4,40	5,93
P14907	NSP1	Nucleoporin NSP1	86,5	3,91	-/-	5,92
Q08280	BSC6	Bypass of stop codon protein 6	55,1	-/-	3,57	5,88
P00830	ATP2	ATP synthase subunit beta, mitochondrial	54,8	-/-	2,59	5,85
P34761	WHI3	Protein WHI3	71,3	2,81	2,80	5,80
P32476	ERG1	Squalene monooxygenase	55,1	-/-	3,55	5,70
P07257	QCR2	Cytochrome b-c1 complex subunit 2, mitochondrial	40,5	-/-	3,60	5,57

P15019	TAL1	Transaldolase	37,0	2,48	2,23	5,43
P40516	SEE1	N-lysine methyltransferase SEE1	28,7	2,90	-/-	5,42
P43616	DUG1	Cys-Gly metallodipeptidase DUG1	52,9	-/-	3,30	5,37
P37292	SHM1	Serine hydroxymethyltransferase, mitochondrial	53,7	-/-	3,30	5,31
P40341	YTA12	Mitochondrial respiratory chain complexes assembly protein YTA12	93,3	-/-	2,90	5,29
P08417	FUM1	Fumarate hydratase, mitochondrial	53,2	-/-	3,40	5,26
P33307	CSE1	Importin alpha re-exporter	109,4	-/-	-/-	5,25
P40047	ALD5	Aldehyde dehydrogenase 5, mitochondrial	56,7	-/-	3,68	5,22
P32767	KAP122	Importin beta-like protein KAP122	123,5	-/-	-/-	5,14
P12709	PGI1	Glucose-6-phosphate isomerase	61,3	2,55	2,56	5,14
P40531	GVP36	Protein GVP36	36,7	2,23	2,24	5,10
P00942	TPI1	Triosephosphate isomerase	26,8	2,03	2,24	4,97
P39743	RVS167	Reduced viability upon starvation protein 167	52,8	3,98	-/-	4,95
P41940	PSA1	Mannose-1-phosphate guanyltransferase	39,6	2,06	-/-	4,90
P00924	ENO1	Enolase 1	46,8	2,76	-/-	4,85
P54885	PRO2	Gamma-glutamyl phosphate reductase	49,7	2,25	2,04	4,83
P07245	ADE3	C-1-tetrahydrofolate synthase, cytoplasmic; Methylenetetrahydrofolate dehydrogenase; Methenyltetrahydrofolate cyclohydrolase; Formyltetrahydrofolate synthetase	102,2	-/-	-/-	4,75
P38879	EGD2	Nascent polypeptide-associated complex subunit alpha	18,7	2,32	2,23	4,68
P22136	AEP2	ATPase expression protein 2, mitochondrial	67,5	-/-	4,36	4,67
Q05016	YMR226C	Uncharacterized oxidoreductase YMR226C	29,2	2,64	-/-	4,63
P07262; P39708	GDH1; GDH3	NADP-specific glutamate dehydrogenase 1; NADP-specific glutamate dehydrogenase 2	49,6	4,17	-/-	4,62
P05626	ATP4	ATP synthase subunit 4, mitochondrial	26,9	-/-	-/-	4,57
P25039	MEF1	Elongation factor G, mitochondrial	84,6	-/-	2,94	4,51
P32582	CYS4	Cystathionine beta-synthase	56,0	2,82	2,01	4,51
Q03648	YMR209C	Uncharacterized protein YMR209C	52,2	2,78	-/-	4,47
P06168	ILV5	Ketol-acid reductoisomerase, mitochondrial	44,4	-/-	2,60	4,47
P25340	ERG4	Delta(24(24(1)))-sterol reductase	56,0	-/-	-/-	4,42

P07256	COR1	Cytochrome b-c1 complex subunit 1, mitochondrial	50,2	-/-	2,38	4,39
P40850	MKT1	Protein MKT1	94,5	2,63	2,59	4,39
P07251	ATP1	ATP synthase subunit alpha, mitochondrial	58,6	-/-	2,12	4,35
P00560	PGK1	Phosphoglycerate kinase	44,7	2,54	2,28	4,35
P09440	MIS1	C-1-tetrahydrofolate synthase, mitochondrial; Methylenetetrahydrofolate dehydrogenase; Methenyltetrahydrofolate cyclohydrolase; Formyltetrahydrofolate synthetase	106,2	-/-	2,61	4,31
P32454	APE2	Aminopeptidase 2, mitochondrial	107,8	-/-	2,21	4,29
Q04894	ADH6	NADP-dependent alcohol dehydrogenase 6	39,6	2,22	-/-	4,28
P25298	RNA14	mRNA 3-end-processing protein RNA14	80,0	2,42	-/-	4,20
P14065	GCY1	Protein GCY	35,1	3,21	-/-	4,14
P07284	SES1	Serine--tRNA ligase, cytoplasmic	53,3	2,77	-/-	4,14
P16387	PDA1	Pyruvate dehydrogenase E1 component subunit alpha, mitochondrial	46,3	-/-	3,15	4,02
P38260	FES1	Hsp70 nucleotide exchange factor FES1	32,6	2,41	-/-	3,98
P38720; P53319	GND1	6-phosphogluconate dehydrogenase, decarboxylating 1	53,5	2,29	-/-	3,98
P38986	ASP1	L-asparaginase 1	41,4	-/-	-/-	3,95
P36060	MCR1	NADH-cytochrome b5 reductase 2; NADH-cytochrome b5 reductase p34 form; NADH-cytochrome b5 reductase p32 form	34,1	3,32	-/-	3,93
P32485	HOG1	Mitogen-activated protein kinase HOG1	48,9	3,02	-/-	3,91
P39954	SAH1	Adenosylhomocysteinase	49,1	2,41	-/-	3,87
P00925	ENO2	Enolase 2	46,9	2,31	-/-	3,83
P38323	MCX1	Mitochondrial clpX-like chaperone MCX1	57,9	-/-	-/-	3,82
P25294	SIS1	Protein SIS1	37,6	2,52	-/-	3,78
Q3E842	YMR122W-A	Uncharacterized endoplasmic reticulum membrane protein YMR122W-A	8,0	-/-	-/-	3,77
P48837	NUP57	Nucleoporin NUP57	57,5	-/-	-/-	3,70
P11986	INO1	Inositol-3-phosphate synthase	59,6	-/-	2,62	3,67
P05317	RPP0	60S acidic ribosomal protein P0	33,7	-/-	-/-	3,66
P31116	HOM6	Homoserine dehydrogenase	38,5	2,47	-/-	3,66
P32487	LYP1	Lysine-specific permease	68,1	-/-	-/-	3,62

P25379	CHA1	Catabolic L-serine/threonine dehydratase; L-serine dehydratase; L-threonine dehydratase	39,3	-/-	-/-	3,61
P34227	PRX1	Mitochondrial peroxiredoxin PRX1	29,5	-/-	2,83	3,57
P48589	RPS12	40S ribosomal protein S12	15,5	-/-	-/-	3,54
Q12166	LEU9	2-isopropylmalate synthase 2, mitochondrial	67,2	-/-	4,06	3,52
P00950	GPM1	Phosphoglycerate mutase 1	27,6	-/-	-/-	3,52
P32316	ACH1	Acetyl-CoA hydrolase	58,7	-/-	2,56	3,51
P08067	RIP1	Cytochrome b-c1 complex subunit Rieske, mitochondrial	23,4	-/-	-/-	3,48
P02992	TUF1	Elongation factor Tu, mitochondrial	48,0	-/-	2,48	3,46
P46951	YPP1	Cargo-transport protein YPP1	95,4	-/-	-/-	3,39
Q02642	EGD1	Nascent polypeptide-associated complex subunit beta-1	17,0	-/-	-/-	3,38
P53598	LSC1	Succinyl-CoA ligase [ADP-forming] subunit alpha, mitochondrial	35,0	-/-	-/-	3,37
Q06010	STE23	A-factor-processing enzyme	117,6	-/-	-/-	3,32
P12695	LAT1	Dihydrolipoyllysine-residue acetyltransferase component of pyruvate dehydrogenase complex, mitochondrial	51,8	-/-	2,20	3,31
P00817	IPP1	Inorganic pyrophosphatase	32,3	-/-	-/-	3,29
P54838	DAK1	Dihydroxyacetone kinase 1	62,2	2,59	-/-	3,28
P40474	QDR2	Quinidine resistance protein 2	59,6	-/-	2,32	3,26
P15625	FRS2	Phenylalanine--tRNA ligase alpha subunit	57,5	2,21	-/-	3,23
P02400	RPP2B	60S acidic ribosomal protein P2-beta	11,1	2,22	-/-	3,21
P38077	ATP3	ATP synthase subunit gamma, mitochondrial	34,4	-/-	2,17	3,20
Q12230	LSP1	Sphingolipid long chain base-responsive protein LSP1	38,1	-/-	-/-	3,20
P00331	ADH2	Alcohol dehydrogenase 2	36,7	-/-	2,09	3,20
P14905	CBS2	Cytochrome B translational activator protein CBS2	44,6	-/-	-/-	3,19
P53691	CPR6	Peptidyl-prolyl cis-trans isomerase CPR6	42,1	2,09	-/-	3,19
P13045	GAL3	Protein GAL3	58,1	2,20	-/-	3,14
P38196	FUI1	Uridine permease	72,2	-/-	2,44	3,12
Q02805	ROD1	Protein ROD1	92,3	2,83	-/-	3,11
P31383	TPD3	Protein phosphatase PP2A regulatory subunit A	70,9	-/-	-/-	3,06
P32263	PRO3	Pyrroline-5-carboxylate reductase	30,1	-/-	2,13	3,03
P38625	GUA1	GMP synthase [glutamine-hydrolyzing]	58,5	2,25	-/-	3,02

P26321	RPL5	60S ribosomal protein L5	33,7	-/-	-/-	2,99
P48353	HLJ1	Protein HLJ1	25,0	-/-	2,53	2,93
P18900	COQ1	Hexaprenyl pyrophosphate synthase, mitochondrial	52,6	-/-	-/-	2,92
P0CS90; P39987	SSC1	Heat shock protein SSC1, mitochondrial	70,6	-/-	-/-	2,91
Q12480	AIM45	Probable electron transfer flavoprotein subunit alpha, mitochondrial	36,8	-/-	-/-	2,86
Q05050	EIS1	Eisosome protein 1	93,3	2,36	-/-	2,85
P42943	CCT7	T-complex protein 1 subunit eta	59,7	-/-	-/-	2,85
P08018	PBS2	MAP kinase kinase PBS2	72,7	2,46	-/-	2,84
Q05468	RQC1	Uncharacterized protein YDR333C	83,4	-/-	-/-	2,83
P17505	MDH1	Malate dehydrogenase, mitochondrial	35,7	-/-	2,16	2,82
P15424	MSS116	ATP-dependent RNA helicase MSS116, mitochondrial	76,3	-/-	2,06	2,80
P43603; P32793	LSB3	LAS seventeen-binding protein 3	49,3	2,64	-/-	2,75
Q12349	ATP14	ATP synthase subunit H, mitochondrial	14,1	3,09	-/-	2,70
P37291	SHM2	Serine hydroxymethyltransferase, cytosolic	52,2	-/-	-/-	2,69
P00958	MES1	Methionine--tRNA ligase, cytoplasmic	85,7	-/-	-/-	2,66
P09624	LPD1	Dihydrolipoyl dehydrogenase, mitochondrial	54,0	-/-	-/-	2,63
P40851	AXL1	Putative protease AXL1	138,3	2,22	-/-	2,62
P53252	PIL1	Sphingolipid long chain base-responsive protein PIL1	38,3	2,01	-/-	2,58
Q12402	YOP1	Protein YOP1	20,3	-/-	-/-	2,58
P39936	TIF4632	Eukaryotic initiation factor 4F subunit p130	103,9	-/-	2,03	2,56
P06787	CMD1	Calmodulin	16,1	-/-	-/-	2,56
P39079	CCT6	T-complex protein 1 subunit zeta	59,9	-/-	2,02	2,55
P0CX53; P0CX54	RPL12A; RPL12B	60S ribosomal protein L12-A; 60S ribosomal protein L12-B	17,8	-/-	-/-	2,54
P00330	ADH1	Alcohol dehydrogenase 1	36,8	-/-	-/-	2,51
P38085	TAT1	Valine/tyrosine/tryptophan amino-acid permease 1	68,8	-/-	-/-	2,50
P15705	STI1	Heat shock protein STI1	66,3	-/-	-/-	2,44
P47143	ADO1	Adenosine kinase	36,4	-/-	-/-	2,42
P06101	CDC37	Hsp90 co-chaperone Cdc37	58,4	2,27	-/-	2,41
P33418	LOS1	Exportin-T	126,8	-/-	-/-	2,41
P32457	CDC3	Cell division control protein 3	60,1	-/-	-/-	2,41
P32353	ERG3	C-5 sterol desaturase	42,7	-/-	-/-	2,40
P53278	YGR130C	Uncharacterized protein YGR130C	92,7	2,06	-/-	2,39

P14922	CYC8	General transcriptional corepressor CYC8	107,2	2,19	-/-	2,36
P22203	VMA4	V-type proton ATPase subunit E	26,5	-/-	-/-	2,36
P29311	BMH1	Protein BMH1	30,1	-/-	-/-	2,35
P00890; P08679	CIT1	Citrate synthase, mitochondrial	53,4	2,21	-/-	2,35
P23248	RPS1B	40S ribosomal protein S1-B	28,8	-/-	-/-	2,35
P04807	HXK2	Hexokinase-2	53,9	-/-	-/-	2,34
P05319	RPP2A	60S acidic ribosomal protein P2-alpha	10,7	-/-	-/-	2,31
P40215	NDE1	External NADH-ubiquinone oxidoreductase 1, mitochondrial	62,8	-/-	-/-	2,31
P04147	PAB1	Polyadenylate-binding protein, cytoplasmic and nuclear	64,3	-/-	-/-	2,29
P19882	HSP60	Heat shock protein 60, mitochondrial	60,8	-/-	-/-	2,27
P09457	ATP5	ATP synthase subunit 5, mitochondrial	22,8	-/-	2,17	2,26
P39968	VAC8	Vacuolar protein 8	63,2	-/-	-/-	2,26
Q04947	RTN1	Reticulon-like protein 1	32,9	-/-	-/-	2,20
Q12449	AHA1	Hsp90 co-chaperone AHA1	39,4	-/-	-/-	2,18
P02829	HSP82	ATP-dependent molecular chaperone HSP82	81,4	-/-	-/-	2,18
P38217	KAP104	Importin subunit beta-2	103,7	-/-	-/-	2,17
P53276	UTP8	U3 small nucleolar RNA-associated protein 8	80,2	-/-	-/-	2,16
Q02773	RPM2	Ribonuclease P protein component, mitochondrial	139,4	-/-	-/-	2,15
P00549	CDC19	Pyruvate kinase 1	54,5	-/-	-/-	2,14
P23301; P19211	HYP2	Eukaryotic translation initiation factor 5A-1	17,1	-/-	-/-	2,13
P10592	SSA2	Heat shock protein SSA2	69,5	-/-	-/-	2,11
Q08179	MDM38	Mitochondrial distribution and morphology protein 38	65,0	-/-	2,16	2,10
P53303	ZPR1	Zinc finger protein ZPR1	55,1	-/-	-/-	2,09
P04397	GAL10	Bifunctional protein GAL10;UDP-glucose 4-epimerase; Aldose 1-epimerase	78,2	2,08	-/-	2,06
P19659	GAL11	Mediator of RNA polymerase II transcription subunit 15	120,3	2,34	-/-	2,04
Q12329	HSP42	Heat shock protein 42	42,8	-/-	-/-	2,00
P08524	ERG20	Farnesyl pyrophosphate synthase	40,5	2,43	-/-	-/-
P27472; P23337	GSY2	Glycogen [starch] synthase isoform 2	80,1	2,00	-/-	-/-